UNCLASSIFIED

AD 406 432

DEFENSE DOCUMENTATION CENTER

FOR

SCIENTIFIC AND TECHNICAL INFORMATION

CAMERON STATION, ALEXANDRIA, VIRGINIA

UNCLASSIFIED

406432

406432

63-3-6

UNIVERSITY OF SOUTHERN CALIFORNIA

SCHOOL OF ENGINEERING

RESEARCH ON RAREFIED GASDYNAMICS AND PLASMADYNAMICS

Raymond L. Chuan

USCEC Report 83-101

September 1962

This research was supported by the Mechanics Division, AFOSR, SRRM 49(638)-831

JUN 19 1963

USC Engineering Center

NOTICE: When government or other drawings, specifications or other data are used for any purpose other than in connection with a definitely related government procurement operation, the U. S. Government thereby incurs no responsibility, nor any obligation whatsoever; and the fact that the Government may have formulated, furnished, or in any way supplied the said drawings, specifications, or other data is not to be regarded by implication or otherwise as in any manner licensing the holder or any other person or corporation, or conveying any rights or permission to manufacture, use or sell any patented invention that may in any way be related thereto.

RESEARCH ON RAREFIED GASDYNAMICS AND PLASMADYNAMICS

Raymond L. Chuan

Prepared for

AIR FORCE OFFICE OF SCIENTIFIC RESEARCH
OFFICE OF AEROSPACE RESEARCH
UNITED STATES AIR FORCE

Contract AF 49(638)-831

USCEC Report 83-101

September 1962

Engineering Center
UNIVERSITY OF SOUTHERN CALIFORNIA
UNIVERSITY PARK
LOS ANGELES 7, CALIFORNIA

TABLE OF CONTENTS

LIST OF ILLUSTRATIONS

LIST OF TABLES

I. INTRODUCTION

The research activities at the University of Southern California Engineering Center in the field of rarefied gasdynamics during the period September 1960 to August 1962 are reported in summary in the present document. Most of these constitute continuation of work reported previously in Ref. 1; particularly in the experimental studies of rarefied gasdynamics, and the attendant development of equipment and experimental tools. New activities have been mainly in the general area of plasmadynamics, which is distinguished from magnetohydrodynamics (studies in which were reported in Ref. 1) in that the gas in question is only partially ionized and the electrical conductivity is far from approaching infinity. This represents a direction towards treating realistic problems, some of which are of engineering interest, such as the re-entry radio communication problem.

During the period covered by this report, the USCEC Low-Density Wind Tunnel has been placed on a routine operation basis, after considerable improvements in flow qualities have been achieved through improvements in the cryopump, in reliability of the refrigeration system and in the instrumentation. With sophistication in the conduct of experiments has come also closer examination of the basic physical mechanisms underlying the experimental conditions. Thus the low Reynolds number flow through an orifice has been studied intensively both experimentally and

theoretically. It has also become necessary to develop instrumentation systems much more sophisticated than was previously employed, in order to assure rapid and accurate acquisition of data.

Theoretical efforts in plasmadynamics have also tended to delve into more fundamental questions than previously contemplated. Out of these have come studies in the fundamental equations governing the dynamics of ionized gases and partially ionized streaming gases. Considerable improvements in conventional techniques applied to present experimental studies of plasmas have resulted in the development of very sophisticated microwave systems as well as an electrostatic probe suitable for use in a flowing gas.

Cryopumping continues to draw considerable attention, both within USCEC in striving to improve the performance of the original cryopump, and from without, due to the burgeoning development of massive space environment simulation systems. The "second generation" cryopump and allied concepts are now in general use across the country.

In the following sections are summaries of all the aspects of research conducted during the past 2 years, with references to complete reports of the various subjects investigated. The names appearing after the section titles are of the respective investigators responsible for the subjects, since such a wide range of efforts obviously cannot be those of one principal investigator. The author of the present report acts more

in the capacity of an editor, though he has been technically and administratively responsible for the overall project. To those whose names appear in this report, as well as the many others at the Engineering Center who have participated in the program, he owes much and wishes to express his gratitude.

II. EXPERIMENTAL STUDIES IN RAREFIED GASDYNAMICS

The major experiments performed have been in the study of the hypersonic viscous flow over the leading-edge region of a flat plate, and in the study of the wake behind a sphere. These studies are carried out over a Mach number range from 5.5 to 8.9, over a Reynolds number range (based on 1 cm) from 3570 to 105, and free-stream mean free path from 0.007 cm to 0.37 cm. In order to support these experiments the flows in two low-density nozzles have to be extensively surveyed and calibrated, for which it has also been necessary to develop flow-rate calibration and pressure-calibration systems for very small quantities. In the following sections are presented first the results of the leading-edge and wake experiments, followed then by sections describing the supporting investigations.

A. HYPERSONIC RAREFIED FLOW NEAR THE LEADING EDGE OF A THIN FLAT PLATE (R.L. Chuan and J.G. Everton)

The flow field near the leading edge of a flat plate may be regarded as constituting a classical problem within which it is expected that one can describe the transition from continuum gasdynamics to free molecular flow. A great deal of theoretical work exists in the literature dealing with treatments from the continuum viewpoint, such as is to be found in the various hypersonic viscous interaction theories by Lees (Ref. 2), Li and Nagamatsu (Ref. 3), Nagakura and Naruse (Ref. 4), Oguchi (Ref. 5), etc. To the authors knowledge, only one work exists which treats the problem from the kinetic viewpoint in the near free molecule regime, by Charwat (Ref. 6), although it is restricted to a highly cooled case (wall temperature much less than stream equilibrium temperature), and one work by Yang (Ref. 7) treats the problem, for the entire flow field, from the free molecular viewpoint.

The theoretical description of the problem may thus be considered as being bounded in one extreme by Yang's free molecular treatment, and in the other extreme by a weak interaction theory such as that by Lees. To form a background against which to present and discuss the experimental results of the present paper, it may be found convenient to refer to Fig. 1, in which the regions described by various theories are delineated. Far downstream of the leading edge, a boundary layer is well developed and is bounded above by an inviscid flow region which is, in turn, separated

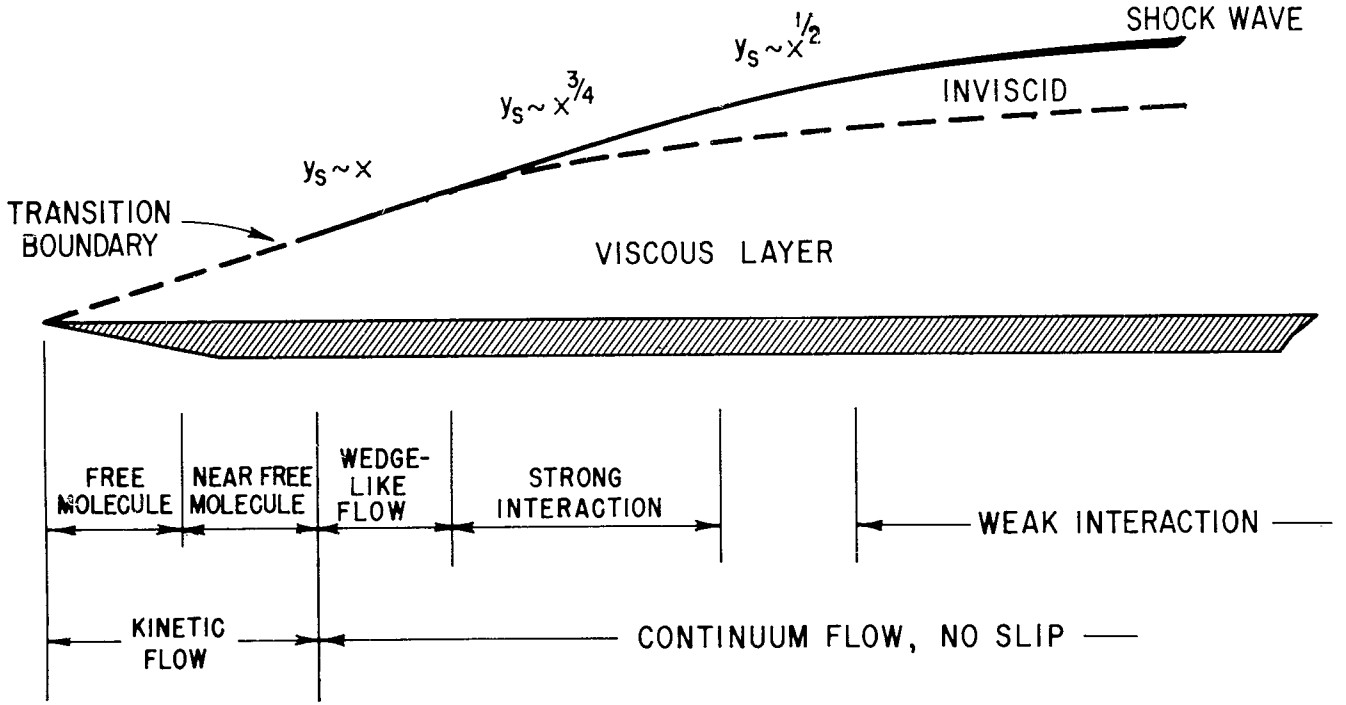

Figure 1 Flow Regimes Near A Leading Edge.

from the undisturbed flow by a thin shock wave which is curved, and is described by $y_s \sim x^{1/2}$. This is called the weak interaction region. Not as far from the leading edge is a region, called the strong interaction region, wherein the viscous region is still separated from the thin curved shock wave, characterized by $y_s \sim x^{3/4}$, by an inviscid region. In both the strong and weak interaction regions the surface pressure is higher than free-stream pressure and depends, according to theory, linearly on the hypersonic viscous interaction parameter $\chi = \frac{\sqrt{C_\infty}\, M_\infty^3}{\sqrt{Re_x}}$. Closer to the leading edge the shock wave, still thin, but straight ($y_s \sim x$), is followed immediately by the viscous region. In this region, characterized by a wedge-like flow field and called the viscous layer region, the wall pressure is predicted to attain a large constant value as compared to the free-stream pressure. Proceeding beyond this near to the leading edge — within a few mean free paths of it — kinetic descriptions of the flow field are in order. The near free molecule region is again characterized by a constant pressure, large compared to free-stream pressure. Finally, in the free molecule region of the order of a mean free path from the leading edge, theory predicts wedge-like behavior in that all flow properties are constant along straight lines emanating from the leading edge. There is, however, no thin shock wave. In the viscous layer and kinetic regions the wall pressure is not described by the hypersonic viscous interaction parameter.

The present experiments are performed with a flat plate made of an aluminum foil about 0.008 cm in thickness stretched across a low-density free jet. The arrangement is shown in Fig. 2. The experimental results may be summarized as follows:

(a) General features of the flow field and the induced surface pressure under slightly rarefied conditions — Knudsen number of the order of 10^{-3} — agree reasonably well with second order weak interaction theory (see Fig. 3).

(b) Under rarefied conditions — Knudsen number of the order of 10^{-1} — the measured flow field features and the induced surface pressure are not predicted by continuum theories either of the strong interaction type or the wedge flow type. There is no pressure plateau at χ up to 60 (see Fig. 4).

(c) Under both slightly rarefied and rarefied conditions the induced pressure is characterized not only by the hypersonic viscous interaction parameter, but also exhibits a dependence on the absolute density (see Figs. 3 and 4).

(d) The transition from the free stream to the perturbed flow downstream of the leading edge occurs along a straight line originating at the leading edge. If the maximum in the pitot-pressure profile taken at various distances from the leading edge is used to indicate such a transition, the results are as shown in Fig. 5.

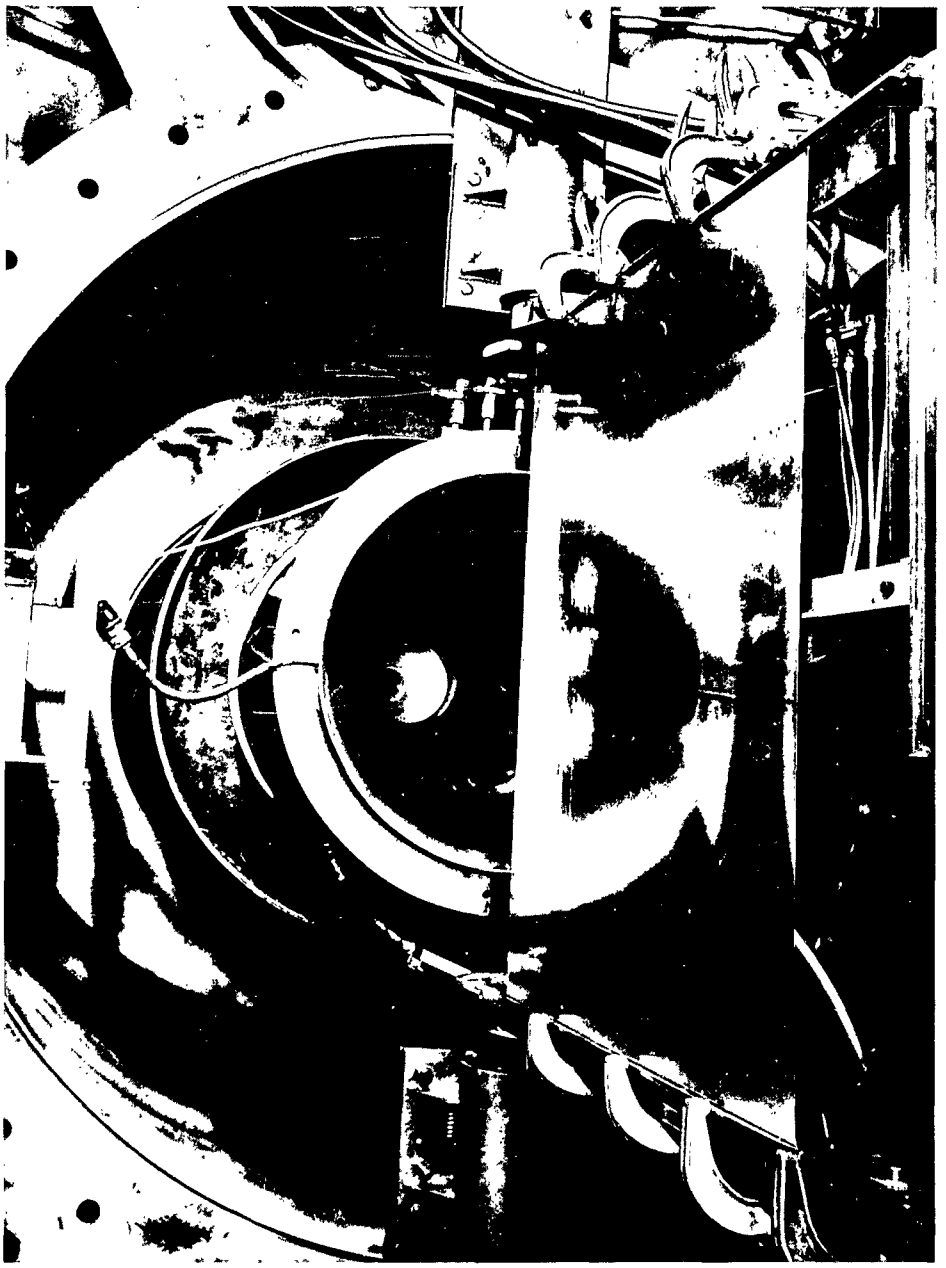

Figure 2 Flat Plate

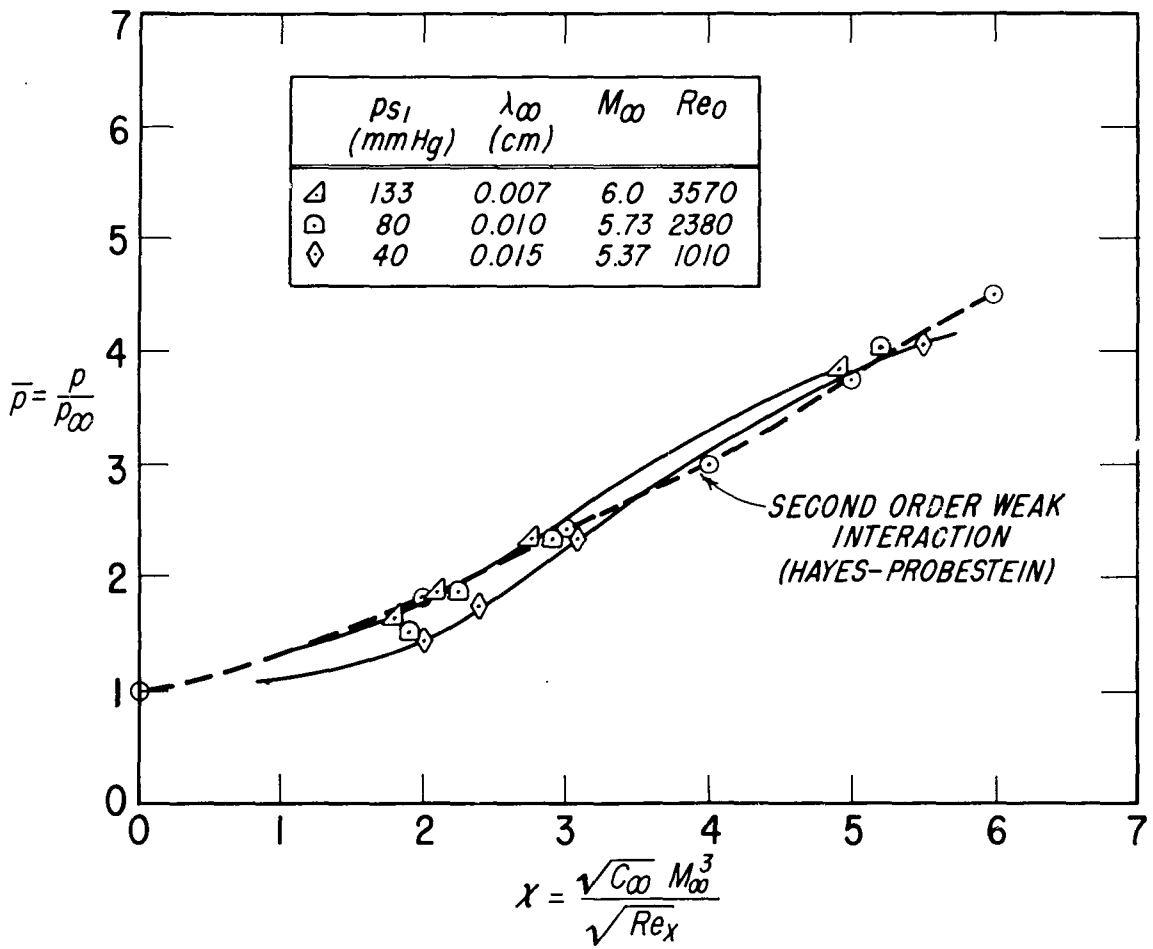

Figure 3 Induced Pressure At Mach Number 6 And Moderate Density.

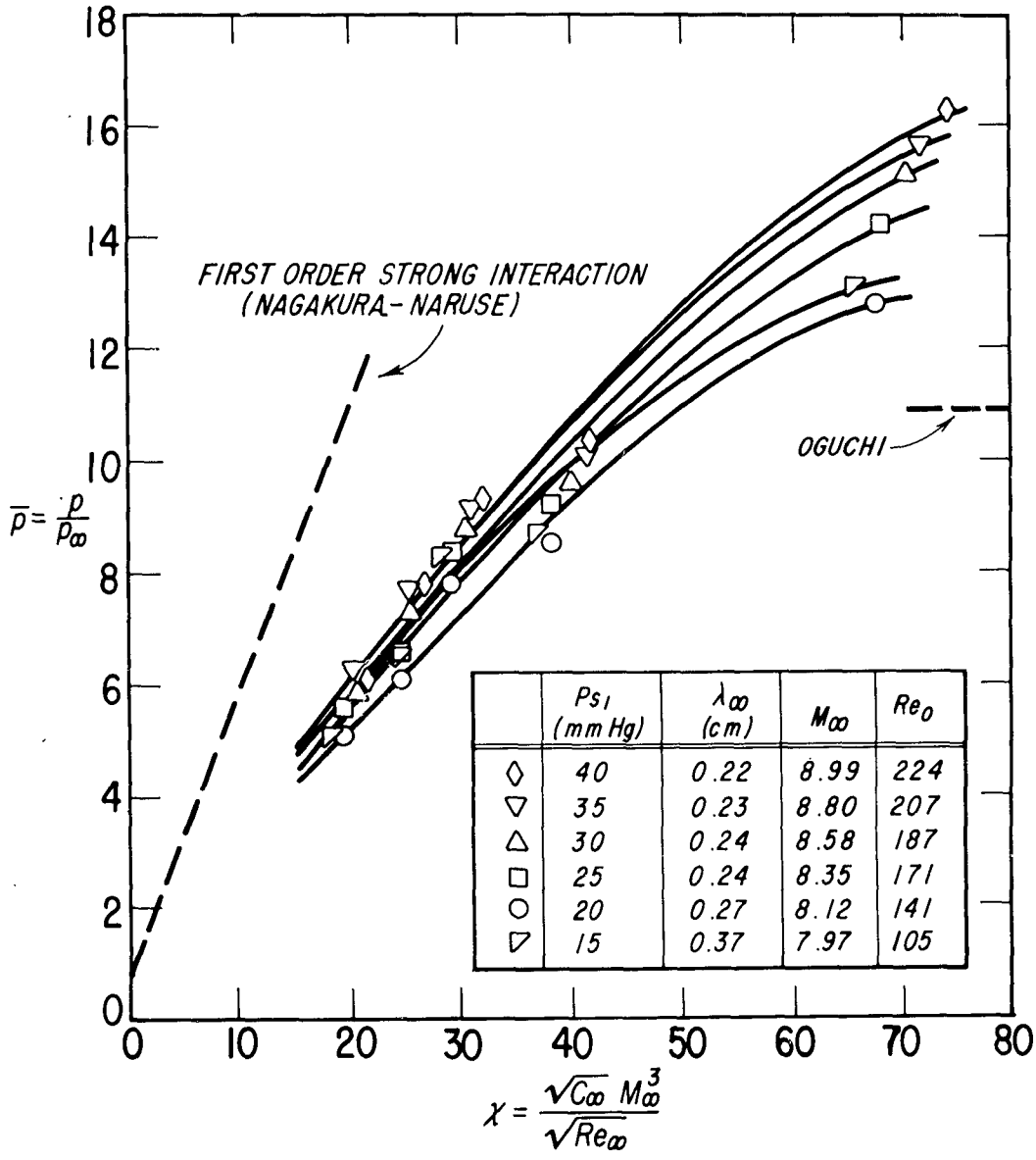

	P_{s_1} (mm Hg)	λ_∞ (cm)	M_∞	Re_0
◇	40	0.22	8.99	224
▽	35	0.23	8.80	207
△	30	0.24	8.58	187
□	25	0.24	8.35	171
○	20	0.27	8.12	141
▽	15	0.37	7.97	105

Figure 4 Induced Pressure At Mach Number 8 And Low Density.

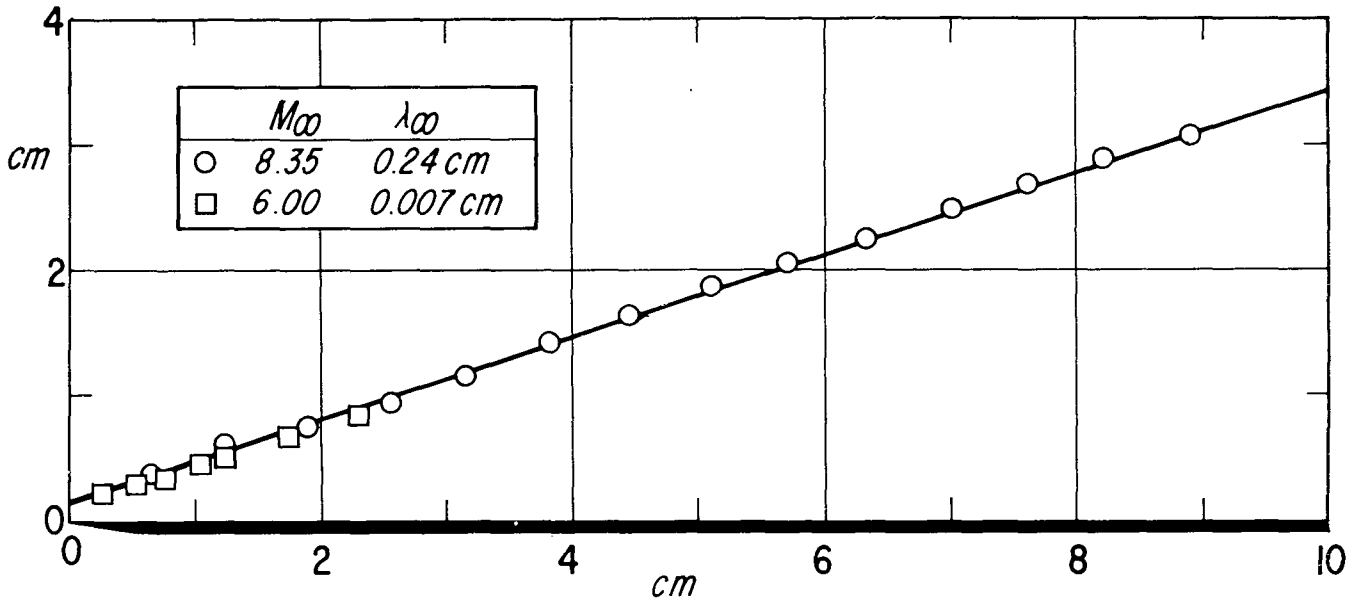

Figure 5 Location Of Transition Boundary.

(e) Velocity slip is observed at the surface, amounting to as much as 60 percent of the free-stream velocity. The results, calculated from pitot-pressure profiles, are shown in Figs. 6 and 7.

(f) The skin friction coefficient is of the same order as predicted by viscous interaction theory. The results, also calculated from pitot-pressure profiles, are shown in Fig. 8.

Further details of this study may be found in Ref. 8.

B. HYPERSONIC LOW REYNOLDS NUMBER WAKES (Chuan and Everton)

The wake behind a small sphere (diameter 0.585 cm) has been measured by means of pitot probes under two sets of conditions:
(1) moderate density, with $M = 5.5$, $Re_o = 585$ and $\lambda_\infty = 0.01$ cm;
(2) low density, with $M = 8.5$, $Re_o = 175$ and $\lambda_\infty = 0.21$ cm.

The sphere is supported by a fine wire (diameter 0.005 cm) stretched horizontally across the free jet. Pitot-pressure traverses are made in the vertical direction. No assessment has yet been made of the influence of the support wire on the structure of the wake. The results shown here must thus be regarded as preliminary.

In the moderate density case the recompression shock in the near wake is barely discernable, as is seen in Fig. 9; while under the very low-density condition, for which the Knudsen number (based on sphere diameter) is 0.35, there is no distinct shock structure at all around and behind the sphere, as shown in Fig. 10. These observations are quite

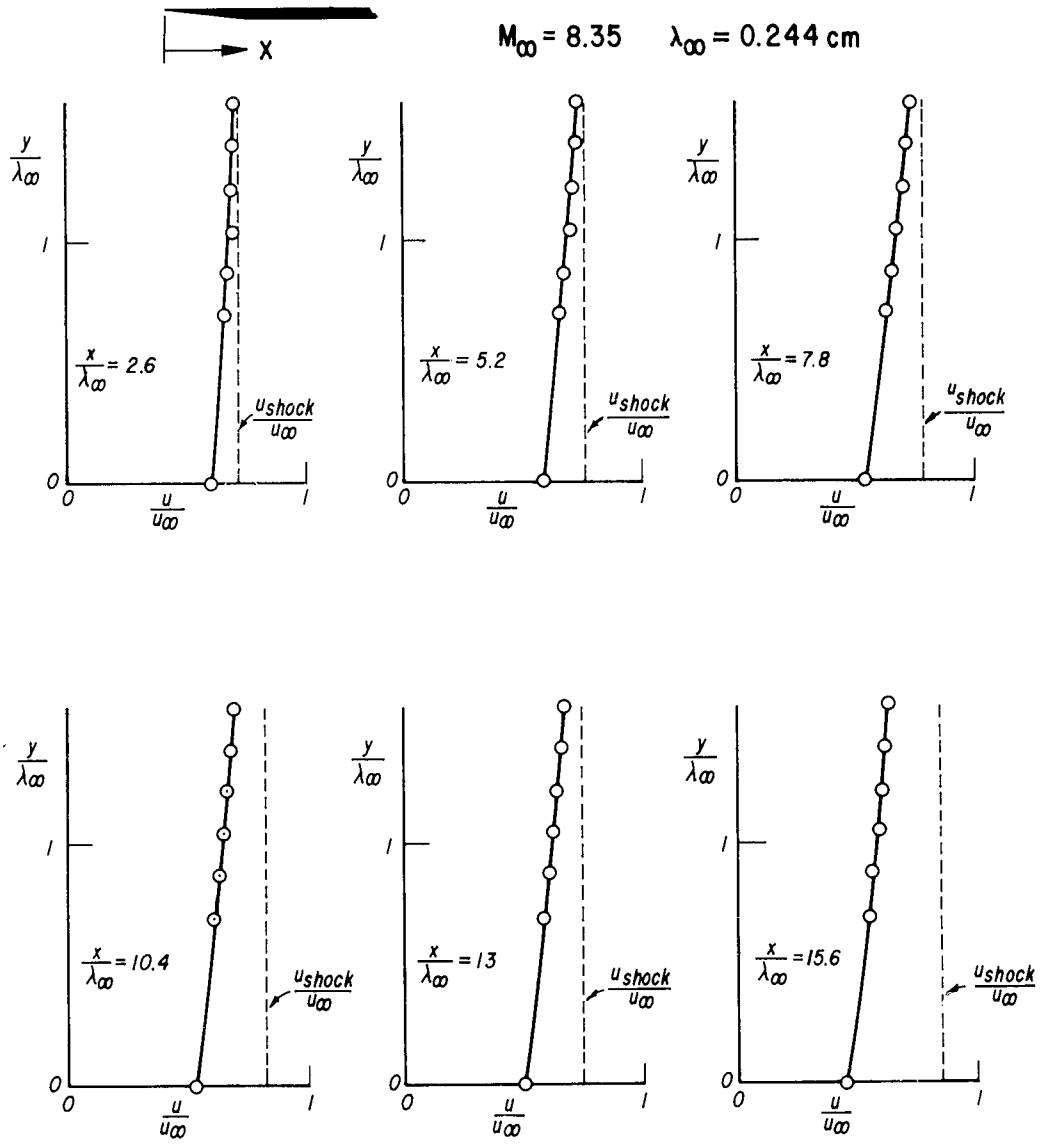

Figure 6 Velocity Distribution Near The Surface At Mach Number 8 And Low Density.

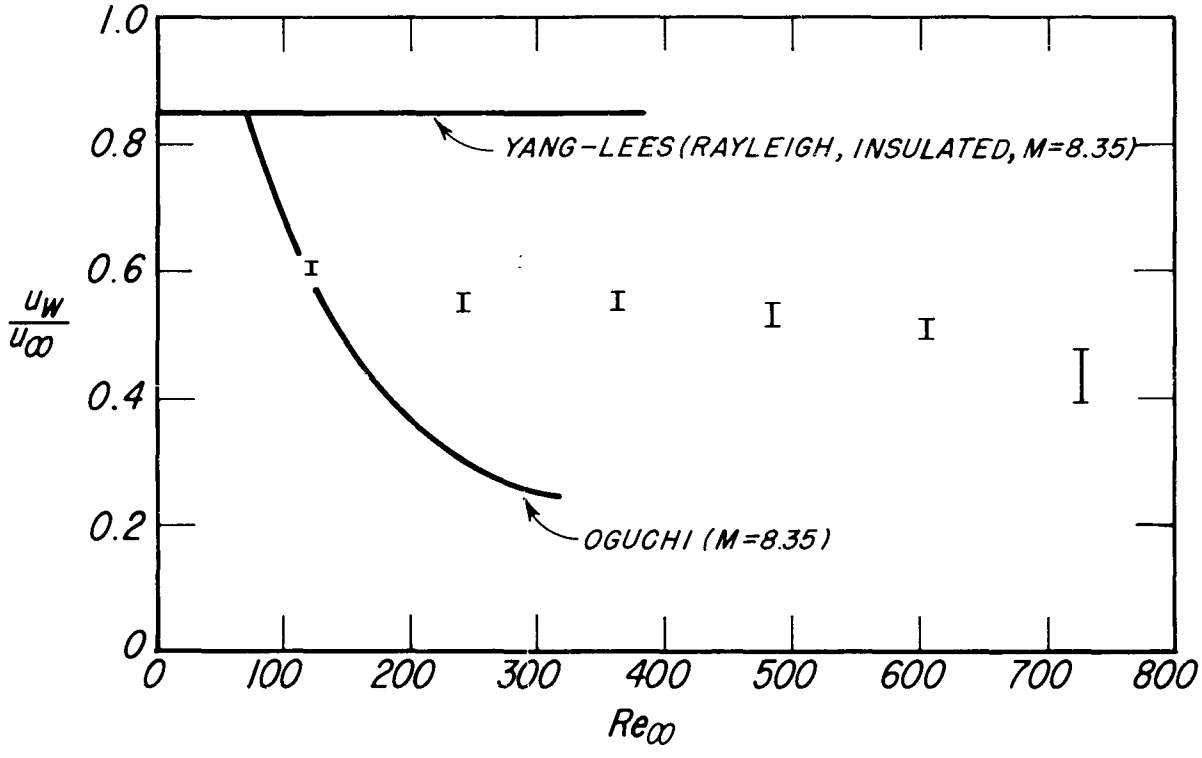

Figure 7 Slip Velocity At Mach Number 8 And Low Density.

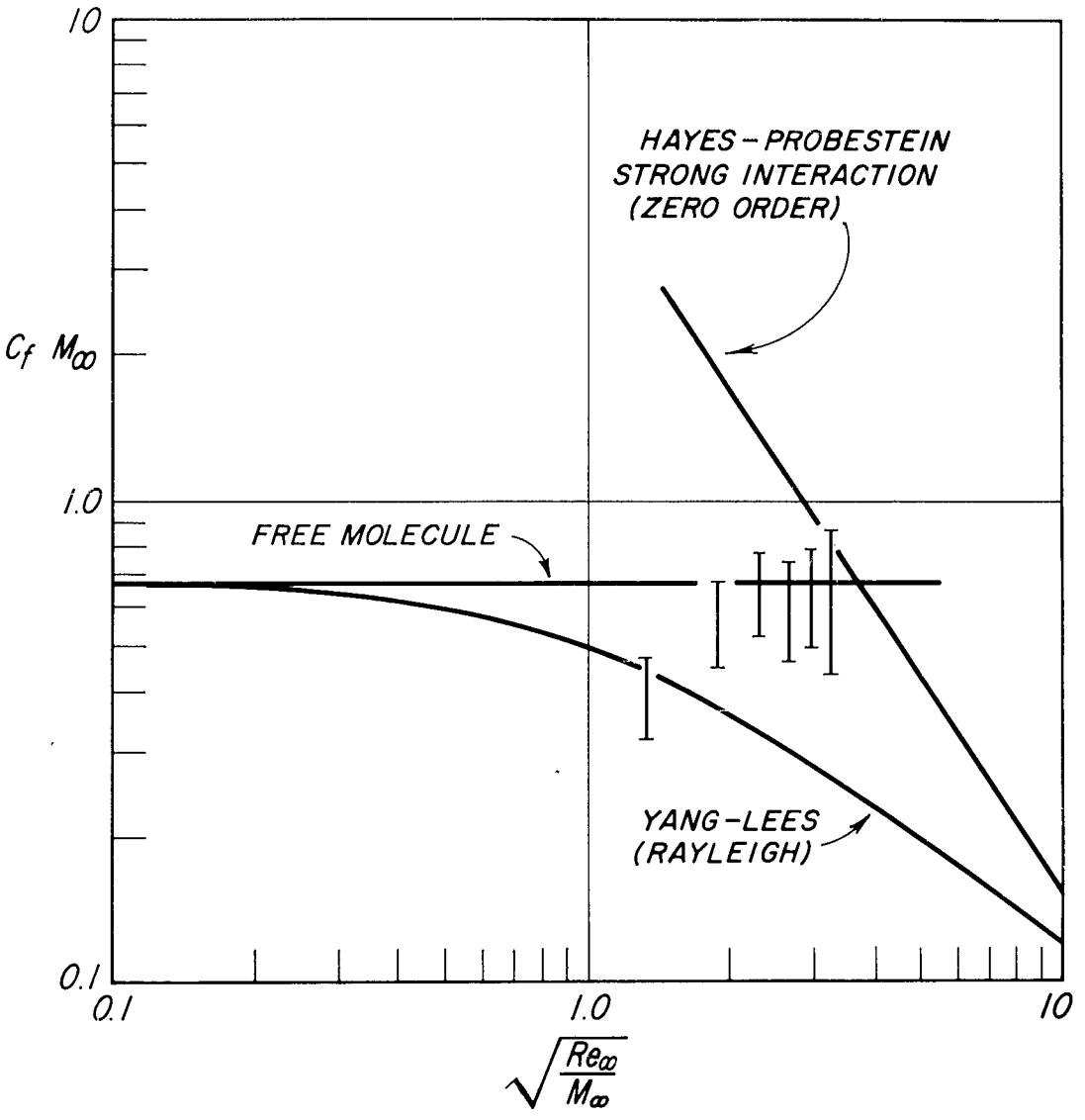

Figure 8 Skin Friction At Mach Number 8 And Low Density.

MACH 6 NOZZLE

DISTANCE FROM CENTER OF SPHERE $\frac{Z}{D}$	
1	0.93
2	1.37
3	3.5
4	5.5
5	10.5
6	25.5

$M_\infty = 5.5$
$\lambda_\infty = 0.01$ cm
D = 0.585 cm

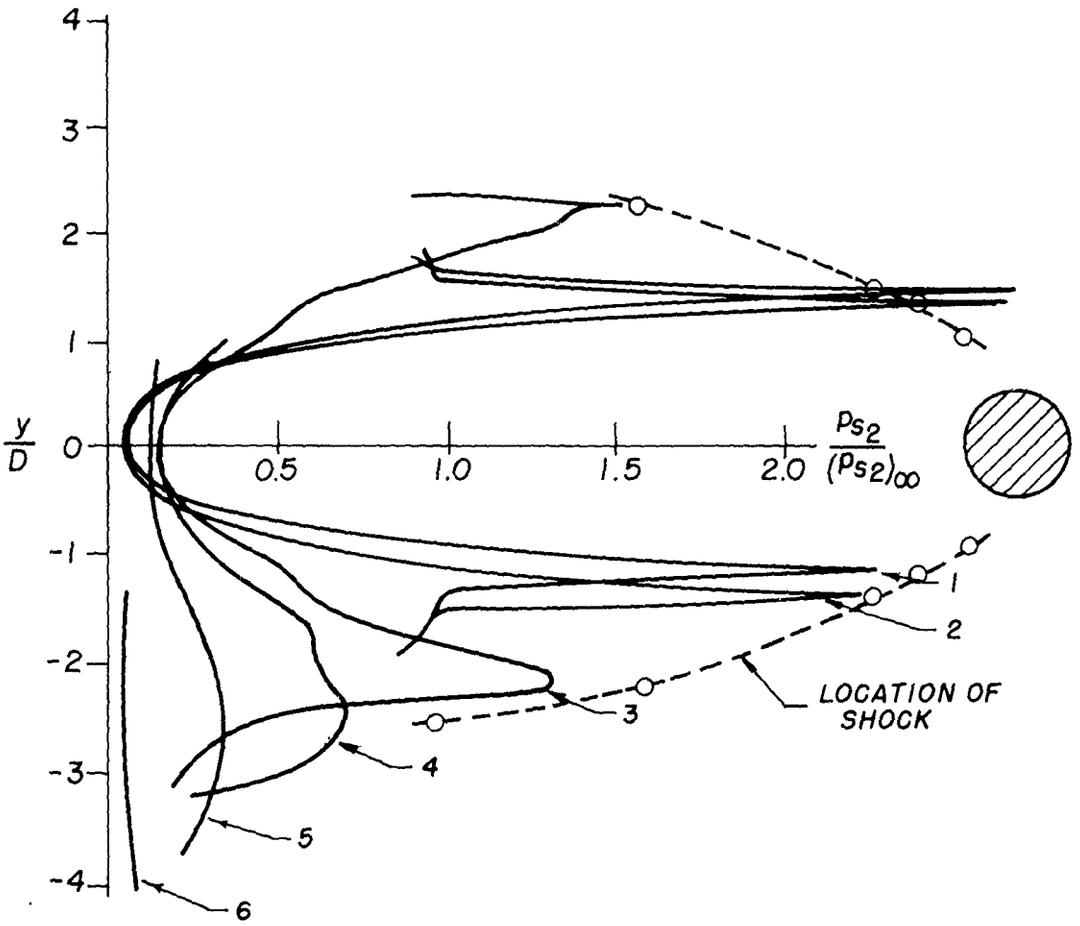

Figure 9 Pitot Pressure Profiles In The Wake Of A Sphere At Mach Number 6.

14-INCH NOZZLE

	DISTANCE FROM CENTER OF SPHERE $\frac{z}{D}$
1	0.5
2	1.5
3	2.5
4	4.5
5	8.5
6	16.5
7	32.5

$M_\infty = 8.49$
$\lambda_\infty = 0.2$ CM
$D = 0.585$ CM

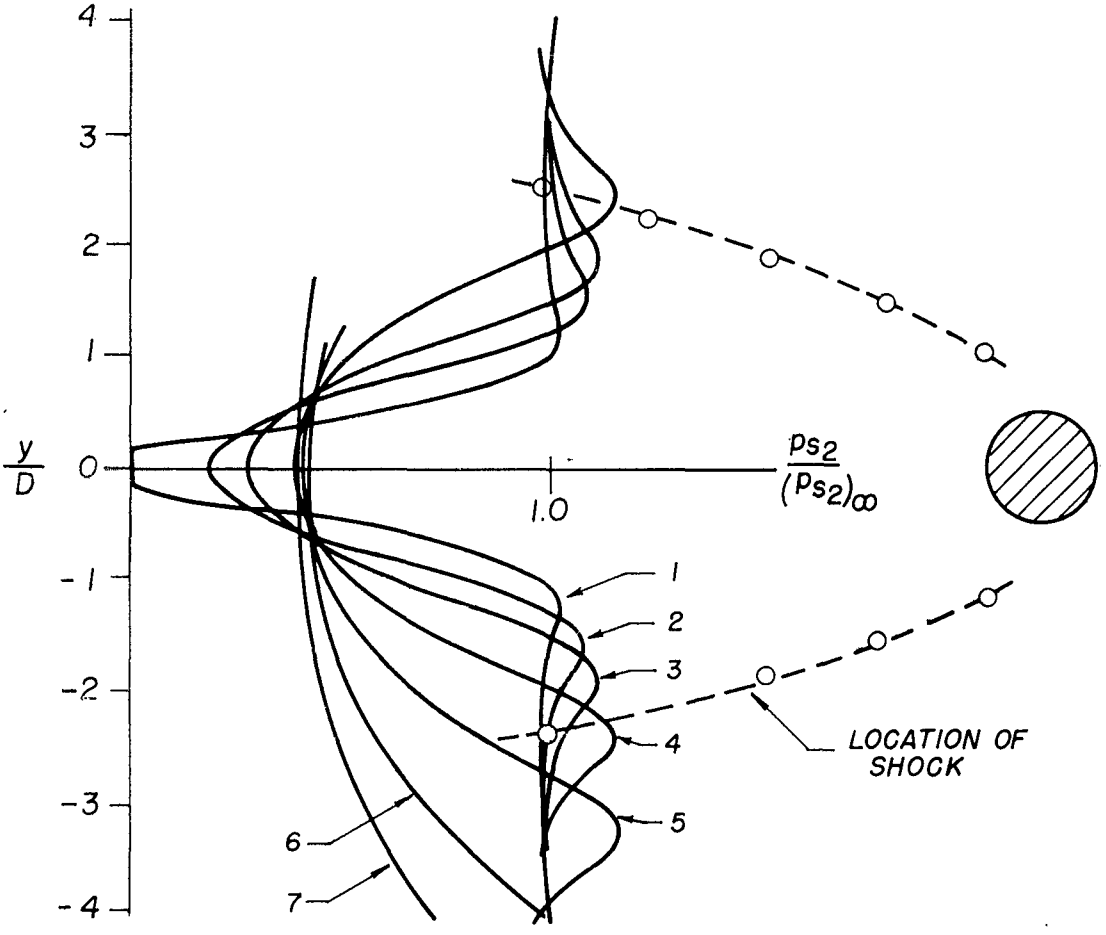

Figure 10 Pitot Pressure Profiles In The Wake Of A Sphere At Mach Number 8.

similar to those made with the flat plate, where for the low-density case the shock and the viscous layer seem to be completely merged; while for the moderate-density case there are distinct regions identifiable as shock, inviscid rotational layer and viscous layer.

Another notable feature of the low-density wake is the nearly zero pitot pressure immediately downstream of the sphere, which increases subsequently to 42 percent of the free-stream value at 16.5 diameters downstream. In contrast, the centerline pitot pressure in the moderate-density case does not decrease all the way to zero, and rises to only about 20 percent of the free-stream value.

C. NOZZLE FLOW AT LOW REYNOLDS NUMBERS (J.G. Everton)

During the early days of the operation of the low-density wind tunnel, as reported in Ref. 1, the calibration of the nozzle was accomplished with pitot-probe traverses using either a silicone oil manometer or the automatic McLeod gage (described in Ref. 9). The technique was not entirely satisfactory. Because of the lack of a rapid pressure reading system, and for lack of experience directing efforts otherwise, these traverses were not carried out too far upstream from the nozzle exit plane. It was assumed that the flow along the core was isentropic from the reservoir to the test section. With the availability of a diaphragm differential pressure transducer capable of measuring differential

pressures down to about 3 microns, with the transducer output plotted directly on a plotter, it became possible to acquire data with speeds probably two orders of magnitude greater than before, and with an order of magnitude improvement in accuracy. It was thus possible to make extensive pitot traverses into the nozzle, to within a few centimeters of the throat. This led to the realization that it is possible to measure flat profiles for a considerable distance upstream of the nozzle exit, while the flow along the core is not isentropic. Shocks originating not too far downstream of the throat became much attenuated (because of the low density) so as to be undetectable by the time the flow reaches the exit. Thus the Mach number earlier reported was higher than the real value.

It has been the conclusion of very extensive surveys of the flow in the low-density nozzle that the only way one can be sure of the flow condition in the test section is to probe the flow all the way upstream to as close to the throat as possible, making certain that there is a flat core profile and that the flow is free of shocks or compression zones. Sometimes the compression can be so diffuse, due to the low density, that it does not develop into a shock, though the flow is still dissipative through such a region. If the flow along the central portion of the nozzle

is isentropic the correct Mach number can be calculated from three measured quantities — stagnation pressure in the reservoir, static pressure in the test section, and impact pressure in the test section — by three methods. Therefore, agreement among the three calculated Mach numbers may also be considered to constitute sufficient proof that the flow is isentropic. However, the question of the static pressure is most difficult to resolve, because it is not possible to measure the local static pressure where the impact pressure is measured. This is due to the fact that it cannot be known, a priori, what the static pressure probe correction is (due to viscous interaction); and the pressure measured at some point away from the free jet may not be the same as that prevailing in the jet. The problem is further aggravated by the fact that it is difficult to measure with accuracy absolute pressures of the order of 1 micron.

It is therefore, our practice now to calculate the local static pressure from the measured local impact pressure and the reservoir pressure, once it is ascertained that the flow along the core is isentropic. Some typical impact pressure profiles are shown in Fig. 11. The measured static pressure is by a McLeod gage, and is seen to be somewhat higher than the calculated values as shown in the figure.

No.	z (inches)	p_{s_2} (microns)	M	p_∞ calculated (microns)
1	0	167	8.54	1.77
2	1	160	8.62	1.66
3	2	153	8.70	1.56
4	3	147	8.78	1.47
5	4	141	8.86	1.39
6	5	135	8.94	1.31

z = Distance Downstream From Nozzle Exit Plane

p_{s_2} = Impact Pressure

M = Mach Number Calculated From p_{s_2} And p_{s_1}

p_∞ = Calculated Local Static Pressure

p_{s_1} = 26.4 mm Hg (Reservoir Pressure)

T_{s_1} = 300 °K (Reservoir Temperature)

p_∞ = 2.1 microns (Test Section Pressure)

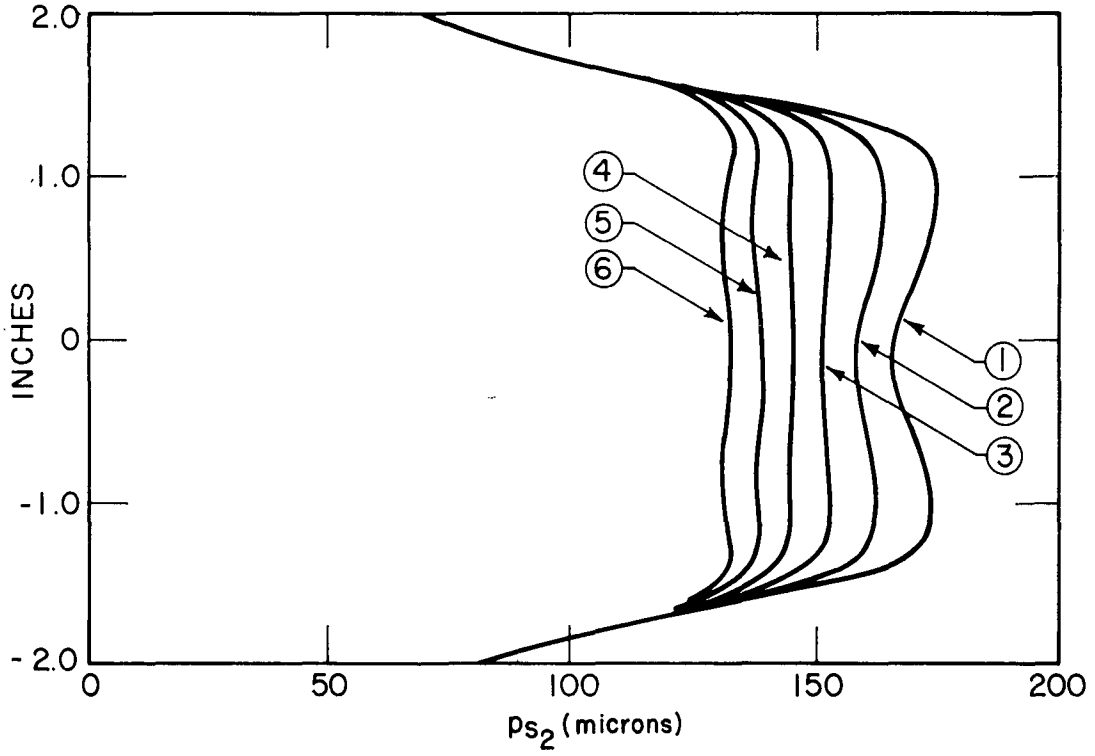

Figure 11 Impact Pressure Profiles At Low Density.

It is to be noted that the flow is supersaturated, with a stagnation temperature of 300°K. It has been found, by operating over a range of stagnation temperatures, that condensation apparently does not occur, presumably because of the very low gas density and consequent relaxation in condensation. Relaxation is particularly likely here because, the very pure test gas, being vaporized from liquid nitrogen, is free of condensation nuclei.

It was also discovered in the course of the nozzle flow surveys that the flow at the throat was far from being nearly inviscid, and was greatly affected by the manner of the contraction from the reservoir to the throat. It was found necessary to employ very rapid acceleration to the throat from a very large plenum section, the plenum diameter finally selected being 33.3 times the throat diameter. The final geometry of the Mach 8 (nominal) nozzle has a throat diameter of 0.762 cm, followed by a contoured expansion section to about Mach 3 on the centerline, after which the nozzle is a straight cone with a total included angle of 40 degrees, and an exit diameter of 35.6 cm.

Depending on the reservoir pressure various Mach numbers between about 7 and 9 can be attained in this nozzle. A plot of centerline Mach number versus reservoir pressure is shown in Fig. 12. The exit

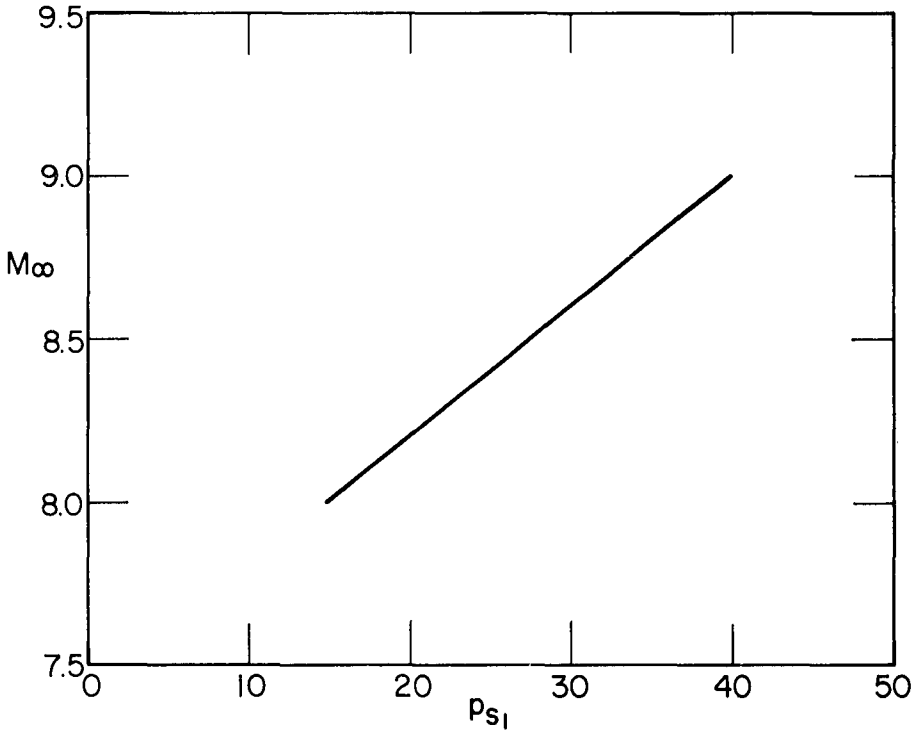

Figure 12 Effect Of Reservoir Pressure On Exit Mach Number.

static pressure varies from 1.6 to 1.9 microns. The discharge coefficient (ratio of actual mass flow to ideal mass flow through same throat with same reservoir conditions) for this nozzle varies from 0.87 to 0.93 for stagnation pressures ranging from 15 to 40 mm Hg.

The interest generated by the knowledge of the viscous flow through the throat led to additional and specific efforts directed at low density orifice flow and all-viscous flow through convergent-divergent channels. These are described in sections to follow.

The Mach 6 nozzle is designed by the conventional technique of adding viscous corrections to an inviscid core, and is completely contoured. Since this nozzle is to be operated at moderate density only, it was considered permissible to design it in a conventional manner. The resulting nozzle has an exit diameter of 5.94 cm, with a core diameter of approximately 2 cm, operating with stagnation pressure from 40 to 133 mm Hg, and exit static pressure from 50 to 84 microns. Typical results are shown in Fig. 13.

D. ORIFICE FLOW AT LOW REYNOLDS NUMBERS (F. O. Smetana)

As current technology begins to require means of generating very low density supersonic and hypersonic neutral gas streams, the fluid dynamicist naturally thinks first of the convergent-divergent nozzle. But if the operating density desired is quite low, then the question arises as

No.	p_{s_1} (mm)	p_∞ (microns)	M_∞	p_∞ calculated (microns)
1	60	24	5.61	57.2
2	80	65	5.74	66.4
3	133	7.5	6.00	84.2

p_{s_1} = Reservoir Pressure

p_∞ = Test Section Pressure

M_∞ = Center-Line Mach Number At Nozzle Exit Plane

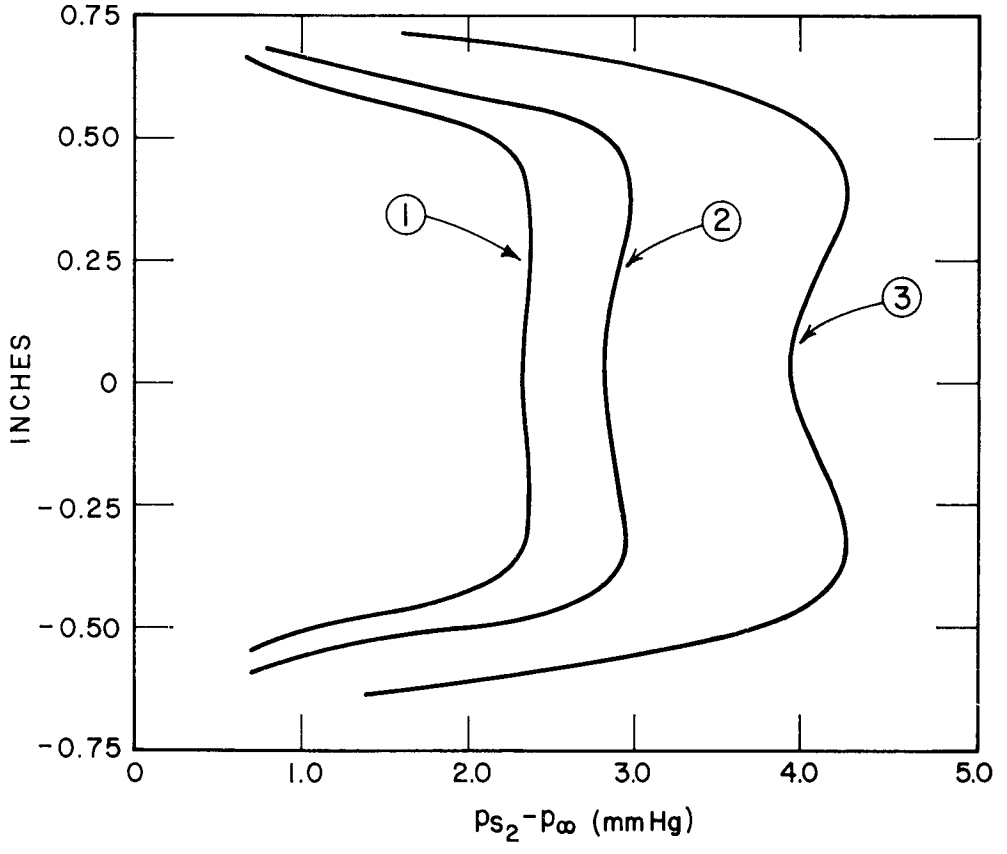

Figure 13 Impact Pressure Profiles At Moderate Density.

to whether a nozzle of the contemplated overall dimensions can actually be operated at the desired conditions, and if so, by what design procedure can this be achieved. The problem lies in the calculation of the boundary layer displacement thickness. At normal densities, this is fairly straightforward; but at low densities, because the boundary layer is quite thick and tends to fill the entire nozzle as the density is reduced, the procedure is more involved. In particular, the calculation of the density level at which a particular nozzle will completely fill with viscous flow appears to require consideration of a variety of factors and, except for the work by Williams described in a later section of the present report, is not yet well-established.

A contoured nozzle designed for use at moderate densities will usually fill with boundary layer first near the exit when the density is reduced. It is conceivable, however, that the nozzle could be so contoured that the viscous "fill-up" occurs first at the throat. In this event it seems improbable that the flow could accelerate uniformly to supersonic velocities.

The nozzle used in the experiments is shown in Fig. 14. The throat to upstream diameter ratio is made small enough so that P_1 may be considered the stagnation pressure. The contraction to the throat is chosen arbitrarily but with the idea of avoiding both excessive boundary-layer growths and flow separation.

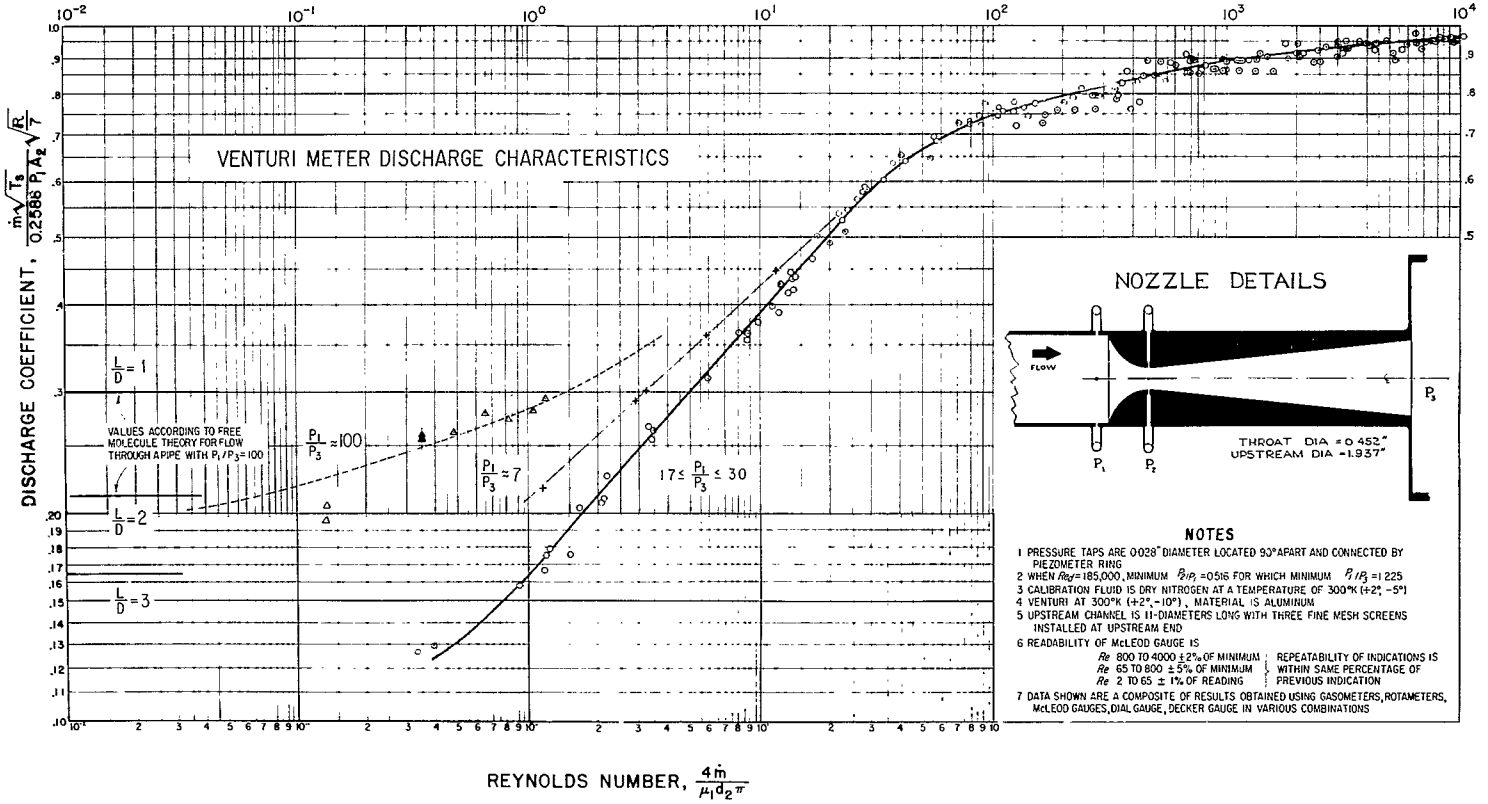

Figure 14 Venturi Meter Discharge Characteristics.

The discharge coefficient is defined as the ratio of the measured mass flow to the ideal one-dimensional mass flow assuming critical flow through the throat; for nitrogen this is

$$C_d = \frac{\dot{m}}{\frac{\pi}{4} d_2^2 \frac{P_1}{\sqrt{T_1}} 0.2588 \sqrt{\frac{7}{R}}}$$

where $\dot{m}$, d_2, P_1, T_1 and R are in compatible units.

The Reynolds number is based on throat diameter and is computed according to the relation

$$Re_d = \frac{\dot{m}}{\frac{\pi}{4} d_2 \mu_1}$$

The variation of the discharge coefficient with Reynolds number is shown in Fig. 14. Above a Reynolds number of about 200, the results can be fitted very well by the equation*

$$C_d = \frac{1}{1 + \frac{3.9}{\sqrt{R_e}}} \qquad \text{(II-1)}$$

This equation is apparently valid up to a Reynolds number of about 6.8×10^5. Although it appears to be fortuitious, Eq.(II-1) also agrees fairly well with the $P_1/P_3 \approx 100$ data for $3 \leq Re \leq 200$.

---

*The development of this form and the approximate value of the numerical constant as determined from a simple, incompressible flow laminar boundary-layer analysis are given in Ref. 10.

Under free molecule flow conditions one would expect that the discharge coefficient as used here would be reduced from its maximum value by the factor $(1 - P_3/P_1)$ at any given P_1; the data below Re $\approx$ 0.5 appear to agree with the expected result. This would indicate that this point could be taken as the onset of free molecule flow condition. The Knudsen number based on throat diameter corresponding to this condition is about 1.0. This is in fact a slightly higher value of the Knudsen number for the onset of free molecule flow conditions than is reported by researchers studying flow in short pipes; it is about the same, however, as found by Liepmann (Ref. 11) for orifice flow.

Unfortunately the data obtained to date have not made it possible to define clearly the Reynolds number at which the free molecule limit is attained. It has proven difficult to separate the effects of outgassing from the flow pressure at station ① for pressures below 10 microns. This, combined with the extensive pumping required for large pressure ratios at these conditions and the care and time required to make the mass flow and pressure measurements, served to limit the amount of data which was taken. It is hoped that with improved techniques the free molecule limit can be defined more satisfactorily. It should then be possible to compare the results with those for equal length pipes of the same diameter as the nozzle throat to determine the effects of nozzle contraction and divergence on molecular reflection and the onset of true free molecule flow.

Other than assume that the curve fairs more or less smoothly between the free molecule limit and viscous, continuum flow result, one has little theory available upon which to base a more definite curve except when $P_2/P_3 \approx 1.0$. In this case, the flow can be expected to follow the well-known behavior of water flow at low Reynolds numbers through nozzles (i.e., $C_d = B/\sqrt{Re_d}$ where B is a constant), at least for Reynolds numbers from 0.3 to 30. It will be noted in this connection that on Fig. 14 all the curves in transition regime have more positive slopes than -1/2, the steepest slope being that of the curve for the lowest value of P_1/P_3. It is to be hoped that a quantitative analysis of this phenomenon will soon be available.

The Reynolds number at which the curves begin to diverge as the density is reduced is also a point of interest. This seems to be between 30 and 40. The Knudsen number for this condition is about 0.03 and this agrees with the findings of other researchers as to the Knudsen number at which rarefaction effects begin to appear. This Reynolds number also appears to be the point at which the boundary layer completely fills the throat. This view is supported by boundary-layer calculations and by the fact that the data begin to depart at this point from the characteristic behavior of what at higher Reynolds numbers is obviously an isentropic core flow with small boundary layer and to approach behavior characteristic of classical Hagen-Poiseuille flow. Further details of this investigation may be found in Ref. 12.

E. VACUUM GAGE CALIBRATION SYSTEM (J.G. Everton and F.O. Smetana)

The vacuum gage calibrator is developed in response to the need for more consistently accurate pressure measurements primarily in the range of 10^{-3} to 25 torr. Its design is based on the system described in Ref. 13 and consists, in essence, of a system in which a large vacuum reference chamber is evacuated to a negligible pressure level and then calculable amounts of gas mass are admitted to this chamber to allow discrete calibration points. Since a number of changes have been incorporated, and since the general equation given in Ref. 13 leads to an incorrect value in the limit, it seems desirable to review the theory of this device in detail.

A schematic diagram of the system is shown in Fig. 15. In operation V_a is initially pumped down to a pressure of 10^{-5} torr or less and V_c is at some higher pressure P_{c0}. By operating either valve 12 or 13, V_b is filled with gas from V_c and the valve is closed; next, either valve 10 or 11 is opened to inject this gas into V_a. At this point the indication on the gage being calibrated is recorded (the gage is connected to the system at the coupling below valve 7, or valves 6 and 7 in the case of differential gages) and V_b is ready to transfer an additional mass of gas from V_c to V_a for the next step.

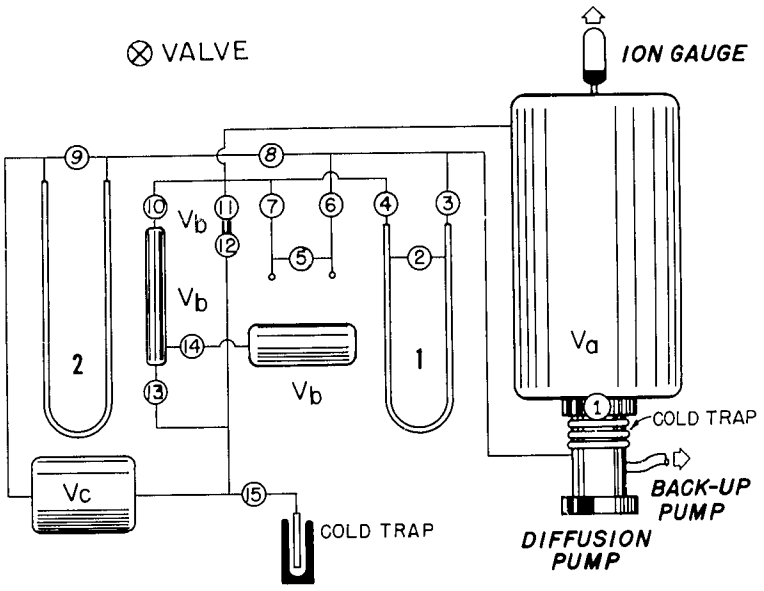

Figure 15 Vacuum Gauge Calibrator.

The mass initially available for transfer to V_a is $V_c(P_{c0}/RT)$. If one transfers $V_c(P_{c0} - P_{c1})/RT$ to V_a, the pressure in V_a will increase by $\Delta P_a = V_c(P_{c0} - P_{c1})/V_a$. If the initial pressure in V_a is assumed 0, then this is P_{a1}. At the end of any step the pressure available to fill V_b for the next step is $P_{c(n-1)} = P_{c0} - P_{a(n-1)} V_a/V_c$, and the mass which is transferred to V_b during the next step is $V_c(P_{c(n-1)} - P_{cn})/RT$, where:

$$P_{cn} = P_{bn} = \frac{P_{a(n-1)} + P_{c(n-1)}(V_c/V_b)}{1 + (V_c/V_b)} \qquad \text{(II-2)}$$

Substituting for $P_{c(n-1)}$ from above this becomes:

$$P_{bn} = \frac{P_{c0}(V_c/V_b) - P_{a(n-1)}(V_a/V_b - 1)}{1 + (V_c/V_b)} \qquad \text{(II-3)}$$

Since $P_{an} = P_{a(n-1)} + (P_{bn} - P_{an})V_b/V_a$, solving for $P_{a(n-1)}$ and substituting in (II-3) gives:

$$P_{bn} = \frac{P_{c0}(V_c/V_b) - P_{an}(V_a/V_b - V_b/V_a)}{V_c/V_b + V_b/V_a} \qquad \text{(II-4)}$$

Since $dP/dn = (P_{bn} - P_{an})V_b/V_a$, substituting for P_{bn} from (II-4) gives:

$$\frac{dP}{dn} = \frac{P_{c0} - P_{an}(1 + V_a/V_c)}{V_a/V_b + V_b/V_c} \qquad \text{(II-5)}$$

Integrating (II-5) and solving for P_{an} results in the general equation:

$$P_{an} = \frac{P_{c0}}{1 + V_a/V_c} \left[1 - \exp\left(-n \frac{1 + V_a/V_c}{V_a/V_b + V_b/V_c}\right)\right] \qquad \text{(II-6)}$$

The simplest form of this equation (the one most often used in practice) is the one that results when valve 15 is left open to atmospheric pressure P_0. In this case P_{cn} is always P_0 and V_c becomes, effectively, infinite so that all ratios containing V_c in the denominator disappear. This results in the special equation:

$$P_{an} = P_0 \left(1 - \epsilon^{-n \frac{V_b}{V_a}}\right) \qquad \text{(II-7)}$$

V_a/V_b is determined most easily by venting V_c to atmospheric pressure, and then measuring the pressure at each step using the silicone oil manometer 1, and solving Eq. (II-7) for V_b/V_a. To reduce reading and other errors, an average of the results of a number of steps should be used. V_a/V_c can be determined by transferring mass from V_c to V_a, observing the oil manometer on V_a and the mercury manometer 2 on V_c, and fitting the results into the expression for P_{cn}. V_b/V_c is then determined by multiplying V_b/V_a by V_a/V_c.

The use of Eqs. (II-6) or (II-7) with the volume ratios as determined above is preferable to using the indications of the oil manometer directly because calibration pressures below 100 μ which are too small to be read conveniently can easily be supplied, and because the errors in reading the manometers are practically eliminated.

By proper selection of volume ratios it is possible to attain linear relationships which are accurate to, say, 1% over a given range of pressures. For instance, if the quantity

$$n \frac{1 + V_a/V_c}{V_a/V_b + V_b/V_c}$$

is small and V_b/V_c is small compared to V_a/V_b, then for all practical purposes Eq. (II-6) can be written as $P_{an} = P_{c0}\, n\, V_b/V_a$. This simple linear relation will be accurate to within 1% for values of $n\, V_b/V_a$ up to the order of 0.02. For larger values, graphs or tables of n vs P_{an} can be drawn up to simplify the data reduction.

The calibrator currently in use is equipped with an electric timer for timing the opening and closing of the appropriate valves and a counter to count the number of steps, so it is only necessary to push a button and record the appropriate readings for each calibration point.

III. THEORETICAL STUDIES IN RAREFIED GASDYNAMICS

A. VISCOUS COMPRESSIBLE AND INCOMPRESSIBLE FLOW IN SLENDER CHANNELS (James C. Williams III)

The problem at hand is to determine the motion of a viscous, compressible, heat-conducting gas in a channel bounded by two walls (two-dimensional channel), or by a surface of revolution (axisymmetric channel). The flow configurations are shown in Fig. 16. The motion of

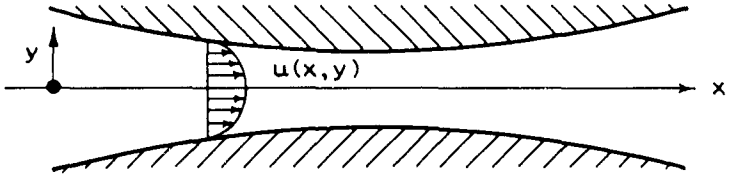

(A) FLOW IN A TWO-DIMENSIONAL CHANNEL.

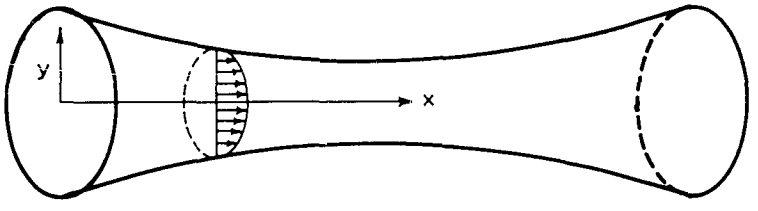

(B) FLOW IN AN AXISYMMETRIC CHANNEL.

Figure 16 Geometries For Flow In Two-Dimensional And Axisymmetric Channels.

such a gas is governed by the Navier-Stokes Equations. In most practical cases the channels under consideration are slender, i.e., the length of the channel, ℓ is much greater than the radius (or half height) r, so that $r << \ell$. The approximate equations of motion describing the flow in slender channels at moderate or high Reynolds numbers are identical in form with the boundary-layer equations. This fact was alluded to in Ref. 14. The detailed order of magnitude analysis which leads to the conclusion was carried out in Ref. 15.

Complete details of this work may be found in Ref. 16. An abbreviated version of it may also be found in Ref. 17. For flow in slender channels then the approximate equations of motion for steady two-dimensional or axisymmetric flow are:

$$\frac{\partial \rho u}{\partial x} + \frac{\partial \rho v}{\partial y} + \frac{\epsilon \rho v}{y} = 0 \qquad \text{continuity} \qquad \text{(III-1)}$$

$$\rho u \frac{\partial u}{\partial x} + \rho v \frac{\partial u}{\partial y} + \frac{\partial p}{\partial x} = + \frac{\partial}{\partial y}\left(\mu \frac{\partial u}{\partial y}\right) + \frac{\epsilon \mu}{y} \frac{\partial u}{\partial y}$$

x momentum equation (III-2)

$$\frac{\partial p}{\partial y} = 0 \qquad \text{y momentum equation} \qquad \text{(III-3)}$$

$$\rho u\, cp \frac{\partial T}{\partial x} + \rho v\, cp \frac{\partial T}{\partial y} - u \frac{\partial p}{\partial x} = \frac{\partial}{\partial y}\left(k \frac{\partial T}{\partial y}\right) + \epsilon \frac{k}{y} \frac{\partial T}{\partial y} + \mu \left(\frac{\partial u}{\partial y}\right)^2$$

energy equation (III-4)

$p = \rho RT$ equation of state (III-5)

Here $\epsilon = 0$ for two-dimensional flow and $\epsilon = 1$ for axisymmetric flow.

Although the equations of motion for flow in slender channels at moderate or high Reynolds numbers are identical in form with the boundary-layer equations, the present problem differs from the boundary-layer problem in two important respects. First, the pressure distribution in the thin boundary layer is generally known at the outset from a solution to the inviscid problem outside the boundary layer; in the channel-flow problem, the pressure distribution must be obtained as part of the solution. Second, the temperature and velocity are known at the upper edge of the boundary layer, again from a solution to the inviscid problem, and may be used as boundary conditions in the boundary-layer problem; in the channel-flow problem, velocity and temperature distributions are not known in any part of the flow field so that other boundary conditions must be sought.

For incompressible flows with no body force similar solutions may be found from the ordinary differential equation

$$\left(\frac{f'}{\eta^{\epsilon}}\right)'' + \frac{\epsilon}{\eta}\left(\frac{f'}{\eta^{\epsilon}}\right)' - 1 + \frac{(1+\epsilon)}{2}\,\beta f'^{2} = 0 \qquad \text{(III-6)}$$

where f is the dimensionless stream function defined by

$$f \equiv \frac{\psi}{a},$$

and

$$\xi \equiv \frac{x}{L}$$

$$\eta \equiv \frac{y}{r} \quad \text{(where r is the height of the channel from the centerline)}$$

The two parameters α and β, related to the wall shape and pressure gradient, must be constants and defined by

$$\alpha \equiv \frac{r^{3+\epsilon}}{\mu} \frac{dp}{dx}$$

$$\beta \equiv \frac{\rho \alpha}{\mu r^{\epsilon}} \frac{dr}{dx}$$

To assess the validity of the present method solutions are obtained for the two-dimensional convergent and divergent channels with plane walls, and the results compared in Figs. 17 and 18 with exact solution by Millsaps and Pohlhausen (Ref. 18). The close agreement between the approximate and the exact solutions leads one to conclude that the present method does accurately describe the flow in slender channels.

For axisymmetric channels, similar solutions are possible for exponential wall shapes. Some examples for a divergent channel with positive pressure gradient are shown in Fig. 19.

It is found that the two-dimensional compressible flow can be transformed to an equivalent incompressible flow by the Stewartson transformation

$$X = \int_0^x \frac{p}{p_o} dx \qquad Y = \int_0^y \frac{\rho}{\rho_o} dy$$

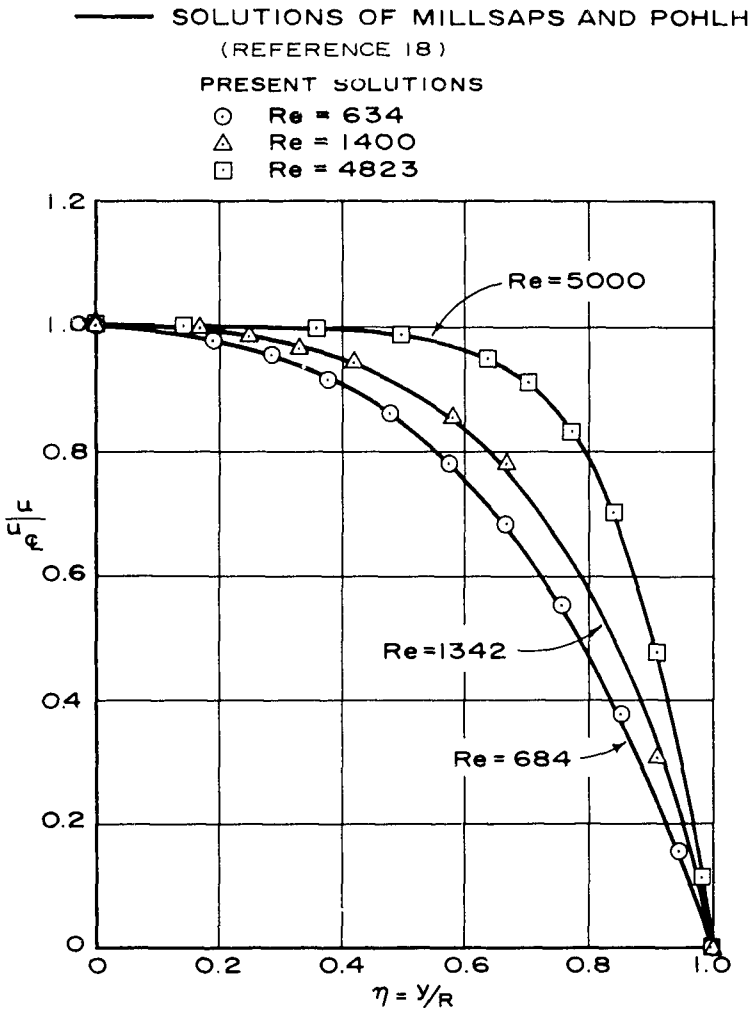

Figure 17 Convergent Channel With 5° Half Angle.

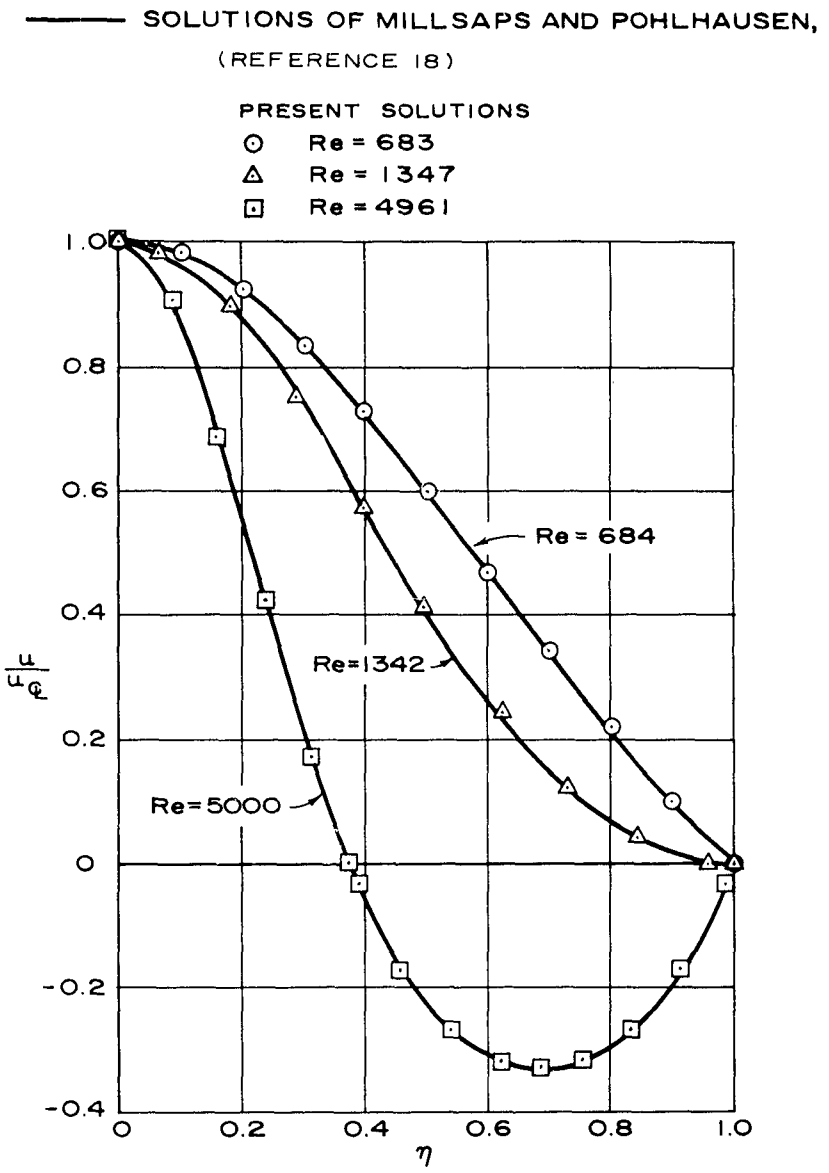

Figure 18 Divergent Channel With 5^{o} Half Angle.

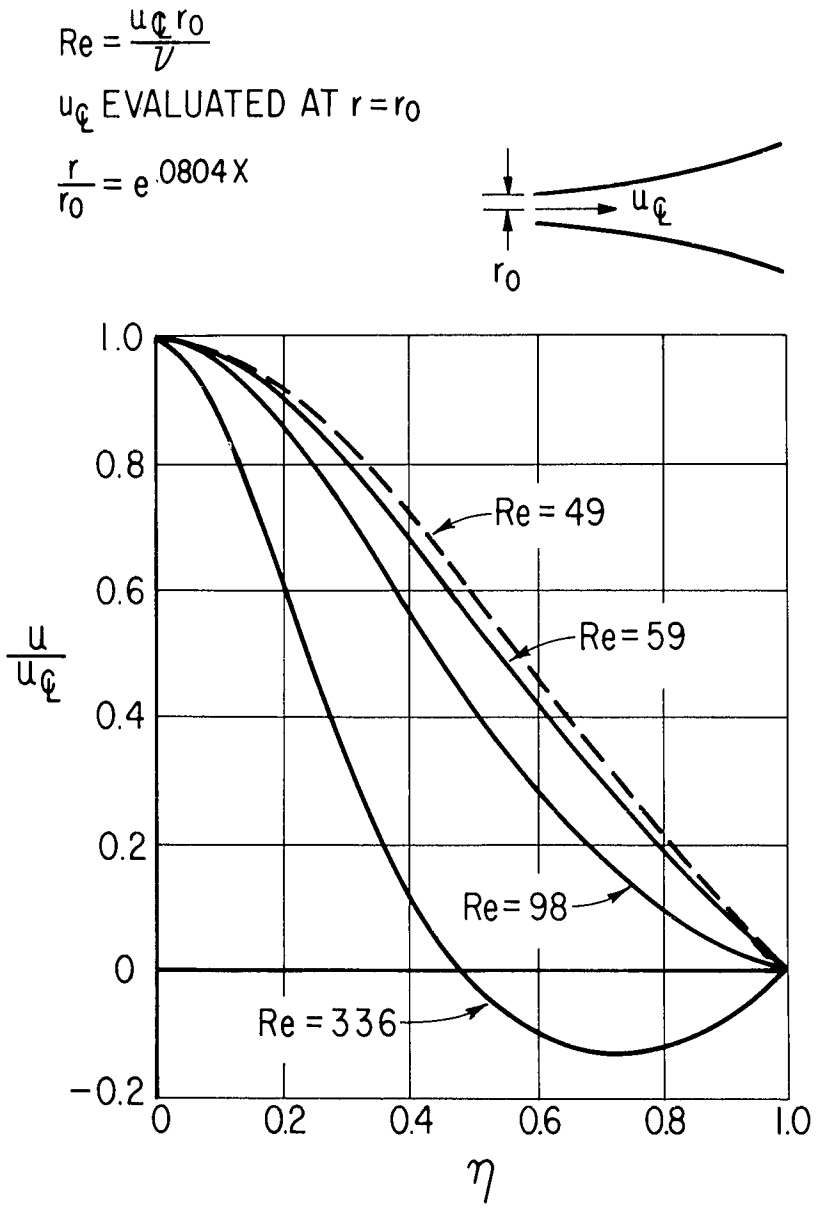

Figure 19 Divergent Axisymmetric Channel.

An ordinary differential equation then results, after applying the usual nondimensional transformations

$$f''' - 1 + \beta f'^2 = 0 \qquad \text{(III-7)}$$

where

$$f \equiv \frac{\psi(X, Y)}{a}$$

is the dimensionless stream function in the transformed coordinate, and

$$a \equiv \frac{RT_o}{\nu_o} \quad Y_o^3 \quad \frac{d\,\ell np}{dX}$$

$$\beta \equiv \frac{a^2}{2c_p Y_o^2 T_o} + \frac{a}{\nu_o} \frac{d Y_o}{dX}$$

with Y_o = height of channel in transformed coordinate.

Similar solutions are possible for wall shapes defined by

$$\frac{d Y_o^*}{dX} = \left(1 - \frac{a}{Y_o^{*2}}\right) \qquad \text{(III-8)}$$

and pressure gradient defined by

$$\frac{1}{p^*} \frac{dp^*}{dx} = \frac{2\nu ab}{(\nu - 1) Y_o^{*3}} \qquad \text{(III-9)}$$

where

$$Y_o^* \equiv \frac{Y_o}{Y_{o_1}}, \quad p^* \equiv \frac{p}{p_1}, \quad a \equiv \frac{a^2}{2c_p T_o Y_{o_1}^2 \beta}, \quad b \equiv \frac{\nu_o \beta}{a Y_{o_1}}$$

A typical solution for a divergent channel is shown in Fig. 20, with $a = 0.1$, $\beta = 467$, $f'(o) = 0.0913$, $p_o = 10^{-3}$atm., $T_o = 800^oK$, and $r(x=o) = 5$ cm. This flow field is interesting since it shows a reversal of the flow next to the wall similar to that found in the incompressible solution (as, for example, Fig. 18).

The most interesting class of solutions is that for convergent-divergent channels with negative pressure gradient. A typical solution of this class is computed for the case where $a = 10^{-3}$, $\beta = 205.3$, $f'(o) = 0.06896$, $p_o = 10^{-3}$ atm., $T_o = 400^oK$, and $r(x=o) = 5$ cm. This corresponds to the flow in a convergent-divergent channel with an initial Mach number of 0.07 and a Reynolds number* of 87.3. The results are shown in Fig. 21. Mach number distribution in the immediate vicinity of the geometric throat is shown in Fig. 22. It is seen that the sonic line

---

*The Reynolds number is based on the mass flow per unit channel width, $\dot{m} = 2\rho_o a f(1)$, and expressed as $Re = \frac{\dot{m}}{\mu_o} = \frac{2af(1)}{\nu_o} = \frac{2\beta f(1)}{bY_{o1}}$. The quantities b and Y_{o_1} are scale factors determining the size of the channel. Since each solution corresponds to a channel of slightly different geometry from others of comparable values of Re, it is impossible to determine the effect of viscosity for a single geometry over a large range of Reynolds numbers. For this reason it is convenient to ignore the factor bY_{o_1} and take the parameter $\beta f(1)$ as representative of Reynolds number.

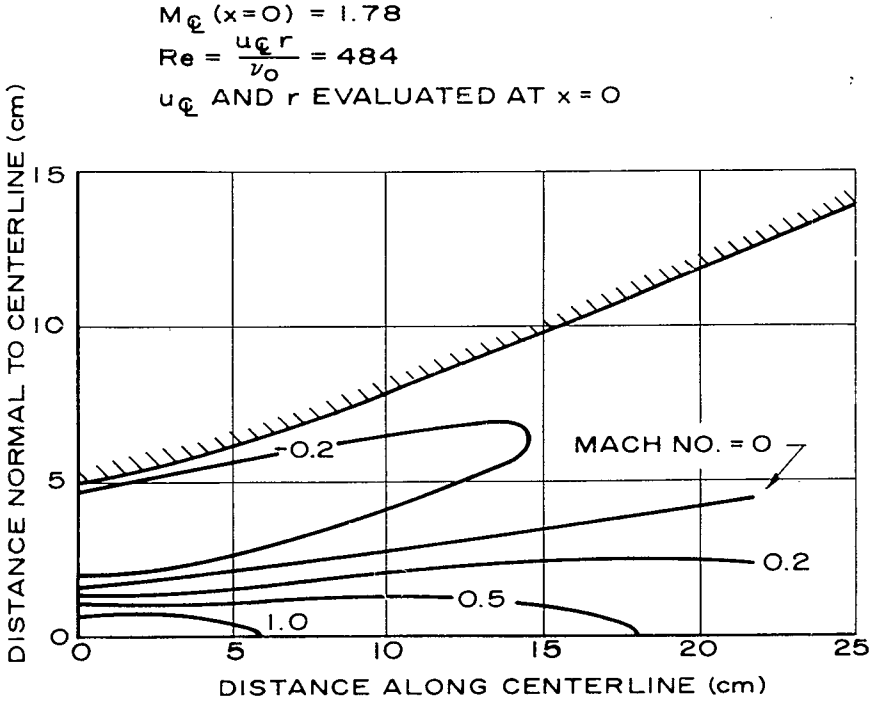

Figure 20 Commpressible Flow In Divergent Channel.

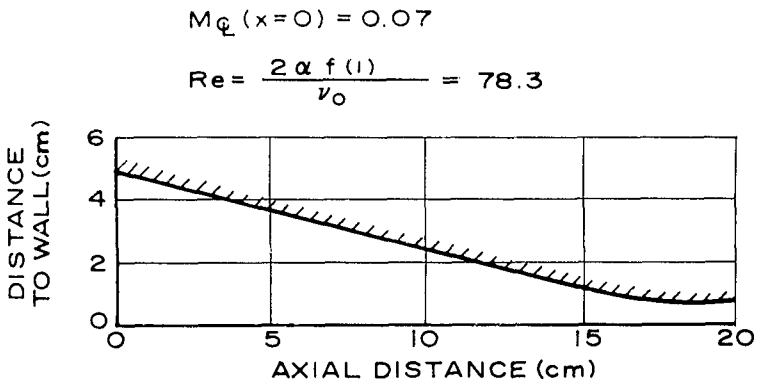

(a) WALL SHAPE

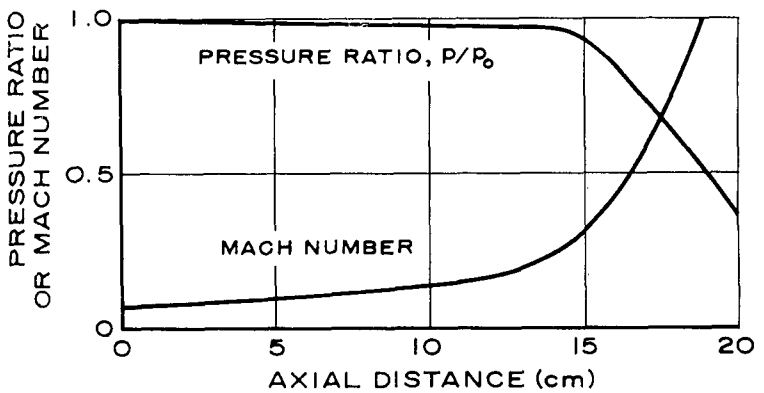

(b) PRESSURE RATIO AND CENTERLINE MACH NUMBER.

Figure 21 Compressible Flow In Convergent-Divergent Channel.

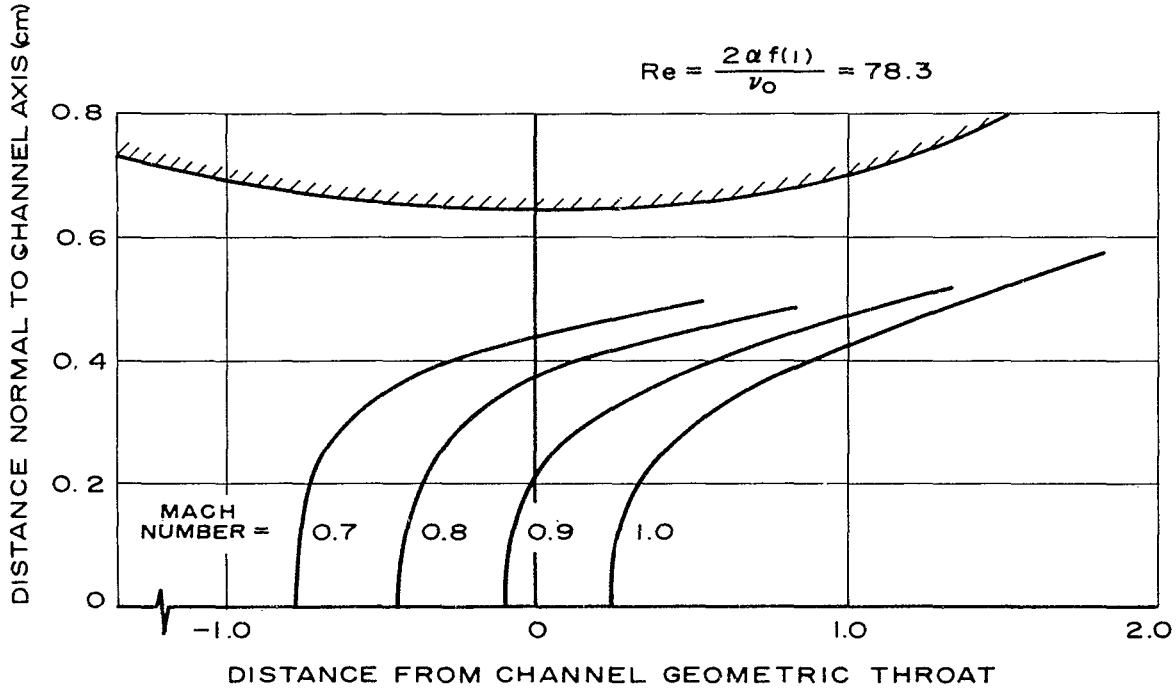

Figure 22 Mach Number Distributions Near Throat.

lies downstream of the geometric throat. Correspondingly, one would expect the pressure ratio at the throat to be greater than the inviscid value of $\left(\frac{2}{\gamma+1}\right)^{\gamma/\gamma-1}$. This effect is shown in Fig. 23. In the same manner, one can also compute the discharge coefficient as a function of the Reynolds number. The result is shown in Fig. 24. This may be compared with Fig. 14, with the appropriate adjustment for the difference in the Reynolds number definition.

B. FREE-MOLECULE FLOW FIELD ABOUT A FLAT PLATE (H. T. Yang)

In connection with the experimental studies of R. L. Chuan on a thin flat plate (Ref. 8), theoretical investigation has been undertaken. The first phase treats the free-molecule flow field over a finite plate shorter than the free-stream mean free path. This study is now completed.

Most conventional free-molecule flow results are limited to the body surface. For real understanding and comparison with experiments, the flow field must be known in detail. Furthermore, this phase of work is a first step toward the gas-kinetic study of the flow near the leading edge of a semi-infinite flat plate.

The discontinuous two-stream molecular distribution function and the line-of-sight principle are employed (Ref. 19). In the particular case of no free-stream motion, any circular arc subtending the plate as its

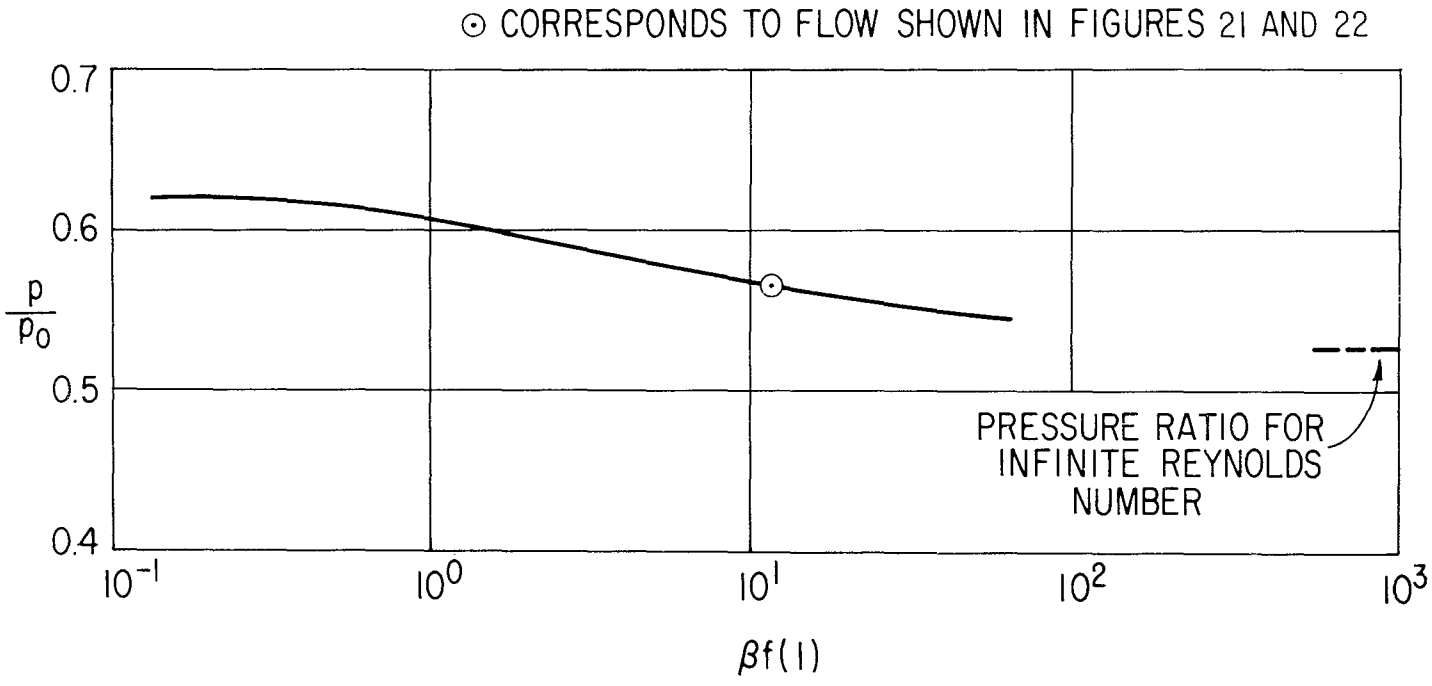

Figure 23 Pressure Ratio At Geometries Throat.

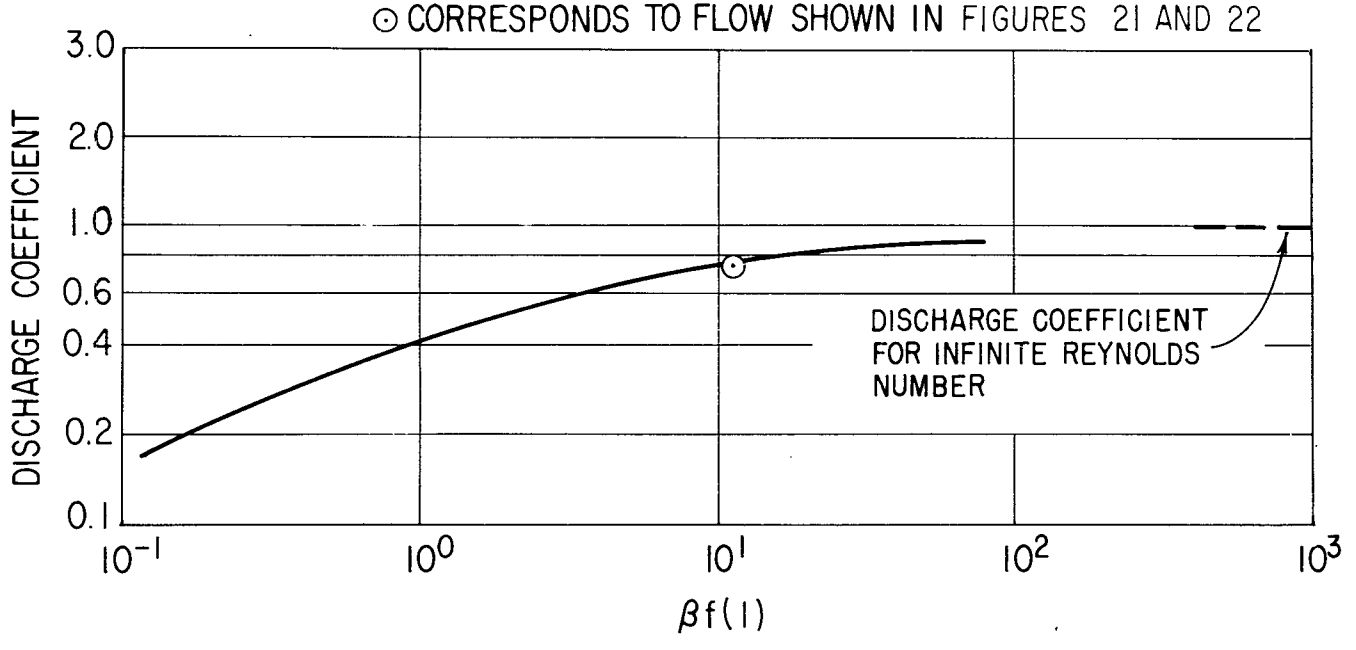

Figure 24 Discharge Coefficient.

chord is a constant-density line. This result is independent of the form of the distribution function and in principle may be verified experimentally by density visualization (Ref. 20) over a thin film heated or cooled in a low-density chamber.

Assuming two-stream Maxwellian distribution, one obtains density, velocities, stresses, temperature, and heat fluxes for the entire flow field. They are expressed, with free-stream speed ratio, S, (Mach number) and plate to free-stream temperature ratio, $\frac{T_b}{T_\infty}$ as parameters, in the form of infinite series. These flow quantities reduce to conventional free-molecule results on the plate and approach correct free-stream values away from the plate. For example, the density of the flow field is given by

$$\frac{\rho}{\rho_\infty} = 1 + \left[1 - \left(\frac{T_\infty}{T_b}\right)^{\frac{1}{2}}\right] \frac{\theta - \phi}{2\pi}$$

$$+ \frac{1}{2\sqrt{\pi}} S \sum_{n=1}^{\infty} \left[e^{-\frac{1}{2}S^2} I_{\frac{n-1}{2}}\left(\frac{1}{2}S^2\right) + e^{-\frac{1}{2}S^2} I_{\frac{n+1}{2}}\left(\frac{1}{2}S^2\right)\right] \frac{1}{n} (\sin n\theta - \sin n\phi) \tag{III-10}$$

where I_n's are the modified Bessel functions of the first kind and the angles θ and ϕ are those shown in Fig. 25.

Numerical results have been obtained by Mr. David Stadelman from IBM 7090 digital computers. More computation is underway.

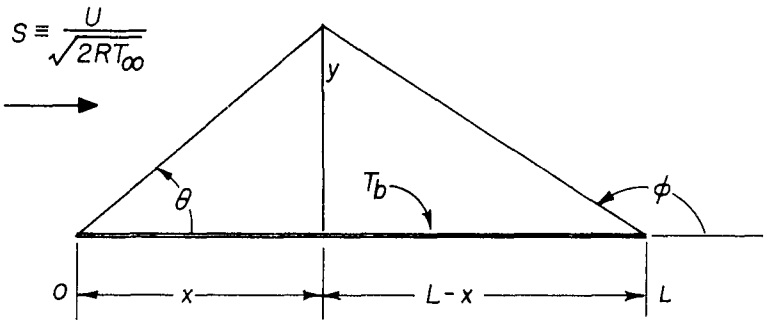

Figure 25 Free-Molecule Flow Configuration Of A Flat Plate.

As can be seen from Eq. (III-10), the free-molecule result is already very complicated. For the transition flow regime from free molecule to continuum, much more complication can be expected. The first attempt for this very difficult leading-edge problem will be limited to the low Mach number case, where $\frac{\rho}{\rho_\infty} = 1$ from Eq. (III-10) with $S \longrightarrow 0$. The other quantities simplify accordingly. The continuum end is given by the well-established Blasius solution. It is hoped that Lees' moment method (Ref. 19) will yield an approximate transition solution to bridge the two.

Details of the above described study will appear in a forthcoming USCEC report (Ref. 7).

C. SHOCK WAVE STRUCTURE (H. T. Yang)

The Navier-Stokes equations yield formally solution for the shock wave structure without any limit on the upstream Mach number. The thirteen-moment equations, which are higher order approximations to the Boltzmann equation than the Navier-Stokes, break down (Ref. 21) at Mach numbers greater than 1.65. Later Grad attributed this remarkable difference between the two solutions to the types of their respective equations (Ref. 22). He proposed to modify his hyperbolic thirteen-moment equations into a parabolic system by interpolatory cutoff at fourth moments. The present investigator carries out the actual solution of this problem based on Grad's modification. However, no profile of the shock has been obtained. Closer examination reveals the system suggested by Grad is not genuinely parabolic.

The interest of this work was renewed recently by the work of Lawrence Sirovich of New York University (Ref. 23). Through a series of correspondence, a parabolic system of moment equations was finally given by Sirovich (Ref. 24). For the plane shock wave problem they take the following form:

mass	$\rho u = m$	(III-11)
momentum	$\rho u^2 + p + p_{xx} = P$	(III-12)
energy	$\rho u^3 + 5pu + 2p_{xx}u + 2q_x = Q$	(III-13)
state	$p = \rho RT$	(III-14)

The above are the usual conservation equations. Sirovich's constitutive equations are

$$\text{stress} \quad \frac{4}{3} p \frac{du}{dx} + \frac{8}{15} \frac{d q_x}{dx} = - \frac{p}{\mu} p_{xx} \tag{III-15}$$

$$\text{heat flux} \quad \frac{d}{dx}(u q_x) + \frac{4}{3} \frac{dq}{dx} + \frac{4}{3} p \frac{dRT}{dx} + \frac{9}{2} \frac{d}{dx}\left(\frac{\mu}{\rho} \frac{d q_x}{dx}\right) + \frac{35}{8} \frac{d}{dx}\left(\frac{\mu}{\rho\sqrt{RT}} \frac{dq}{dx}\right)$$

$$= - \frac{16}{45} \frac{p}{\mu} q_x \tag{III-16}$$

$$\text{compound pressure} \quad \frac{d}{dx}(uq) + RT \frac{d q_x}{dx} + \frac{35}{8} \frac{d}{dx}\left(\frac{\mu}{\rho} \frac{dq}{dx}\right) = - \frac{16}{45} \frac{p}{\mu} q \tag{III-17}$$

The singularities of this system upstream and downstream of the shock are now under study. They are governed by a five-dimensional phase space. The characteristic exponents are being solved from a quintic equation by David Stadelman on a Honeywell 800 digital computer. Preliminary results indicate the singularities are not stable (Ref. 25).

IV. THEORETICAL STUDIES IN PLASMADYNAMICS

A. FUNDAMENTAL EQUATIONS OF THE DYNAMICS OF AN IONIZED GAS (T. Koga)

Considering the long-range character of the Coulomb interactions amond charged particles, it is conceivable that the kinetic equations for plasmas may be much more complex than the Boltzmann equation for gases of neutral particles. Emphasizing the effect of weak encounters which occur between two particles at distances shorter than the Debye distance and longer than the Landau distance, and neglecting the effect of strong encounters between two particles at distances shorter than the Landau distance, kinetic equations of the Fokker-Planck type have been derived and recommended by many authors.

In the present study it was first assumed that the effect of "strong encounters" is not negligible. In a kinetic equation, the effect of "strong encounters" may be represented by a collision term of the Boltzmann type, while the effect of "weak encounters" by the terms of the Fokker-Planck type

$$\frac{df}{dt} = \left(\frac{\partial f}{\partial t}\right)_{coll} + \frac{\partial}{\partial p} \cdot \vec{A}f + \frac{\partial^2}{\partial \vec{p}^2} \cdot \vec{B}f$$

It was concluded during an early phase of the study that the effect of strong encounters is much larger than that of weak encounters in most practical cases (Refs. 26-29). Recently, after a more careful consideration

of the process of deriving kinetic equations and after an analysis of multiple interactions by the method of Holtsmark and Chandrasekhar, it is believed that the effect of strong encounters and that of weak encounters are comparable with each other in most practical cases. Further it is concluded that the effect of weak encounters is predominantly due to encounters which occur with interparticle distances equal to and/or shorter than the average distance of nearest neighbors (and longer than the Landau distance) (Ref. 30). The convergence of the weak interaction effect is not the result of the Debye shielding effect but the result of the mutual cancellation of multiple interactions.

Considering comparatively short interparticle distances of effective encounters, it is expected that a collision term of the Boltzmann type may represent the encounters (including weak and strong ones) in a good and simple approximation.

B. INTERACTION BETWEEN ELECTROMAGNETIC WAVES AND A PARTIALLY IONIZED GAS IN THE PRESENCE OF AN EXTERNAL MAGNETIC FIELD (T. Koga)

Considering a plausible model of plasmas where molecules are partly ionized, Boltzmann-type equations are derived for ions and electrons. By introducing "generalized moments" of the distribution functions of electrons and of ions, it is easy to solve the equations, obtaining the conductivity of a plasma to an oscillating field in the

presence of a static magnetic field. According to the conductivity, the propagation of a radio wave in the plasma is investigated (Refs. 31, 32). There are seven frequencies which characterize the phenomena: Larmor frequencies of electrons and of ions, frequency of radio wave, plasma frequency and a similar one defined with respect to ions, and collision frequencies of electrons and of ions. For the first approximation, the plasma frequencies are assumed to be negligibly small compared with the radio frequency. In other words, the electric field induced by the group displacements of electrons and of ions is neglected. At this stage of approximation, as special cases, Alfvén's theory of hydromagnetic waves and Margenau's theory of radio waves in plasmas with no imposed magnetic field are included in the theory.

For the second approximation, the field induced by the group displacements of electrons and of ions is taken into account (Ref. 33). Under the conditions of practical cases, the correction in the second approximation is not significant.

C. BLAST WAVES IN ELECTROGASDYNAMICS (K. Oshima)

By adding the Poisson equation to the set of equations used in conventional blast-wave analysis the effects of the presence of charged particles in a gas are examined. Two similarity parameters result, one of which corresponds to the usual parameter, and the other contains the effects of the electric charge. Due to the low mass of the electrons as

compared with that of the ions a charge separation takes place at the shock front, resulting in a body force which tends to weaken the shock. The energy of the blast wave, which is constant for similar solutions in the conventional theory, is no longer constant in the present theory. However, a pseudosimilar solution is possible which yields constant energy.

The basic equations, in dimensionless form, are the following:

$$h(f-x)\frac{\partial f}{\partial x} + \frac{1}{\gamma}\frac{\partial g}{\partial x} + (af - A\psi)h = -hy\frac{\partial f}{\partial y} \qquad \text{(IV-1)}$$

$$(f-x)\frac{\partial g}{\partial x} + \gamma g\left(\frac{\partial f}{\partial x} + \delta\frac{f}{x}\right) + 2ag = -y\frac{\partial g}{\partial y} \qquad \text{(IV-2)}$$

$$h\frac{\partial f}{\partial x} + (f-x)\frac{\partial h}{\partial x} + \delta\frac{hf}{x} = -y\frac{\partial h}{\partial y} \qquad \text{(IV-3)}$$

$$\frac{\partial \psi}{\partial x} = h \qquad \text{(IV-4)}$$

in which the dependent variables are

$$f = \frac{u}{U}$$

$$g = \frac{c^2}{U^2}\frac{p}{p_\infty}$$

$$h = \frac{\rho}{\rho_\infty}$$

$$\psi = \frac{K\, m\phi}{\rho_\infty \mathcal{E} eR}$$

where $U = \frac{dR}{dt}$ is the speed of the wave front, c is the local speed of sound, ϕ is the electric field strength, K is the permittivity of the ionized gas, e is the charge, and m the mass of the electron. The degree of ionization is defined by $\mathcal{E} = \frac{n^+}{n^o + n^+}$.

The independent variables are

$$x = \frac{r}{R}$$

$$y = \frac{R}{R_o}$$

where R_o is a characteristic length related to the energy of the blast.

The quantities

$$a = \frac{y}{U} \frac{dU}{dy}$$

$$A = \frac{\rho_\infty}{K} \left(\frac{R\mathcal{E}e}{Um}\right)^2$$

are similarity parameters whose constancy reduces the above equations to ordinary differential equations in x.

The equations apply to plane, cylindrically symmetric and spherically symmetric flows for $\delta = 0, 1, 2$, respectively.

The boundary conditions are

$$f(1, y) = \frac{2}{\gamma + 1} (1 - \eta) \qquad \left(\eta = \frac{1}{M^2}\right)$$

$$g(1, y) = \frac{2\gamma}{\gamma + 1} - \frac{\gamma - 1}{\gamma + 1} \eta$$

$$h(1, y) = \frac{\gamma + 1}{\gamma - 1 + 2\eta}$$

$$\psi(1, y) = 0$$

$$f(x_o, y) = x_o \qquad (x_o = \text{is the location of the edge of the core})$$

The first three conditions are the Hugoniot relations across the wave.

The energy of the blast wave is

$$E = p_\infty R M^2 J \left[1 - \frac{\eta}{(\gamma - 1) J}\right] \qquad \text{for } \delta = 0$$

$$E = 2\pi p_\infty R^2 M^2 J \left[1 - \frac{\eta}{2(\gamma - 1) J}\right] \qquad \text{for } \delta = 1 \qquad \text{(IV-5)}$$

$$E = 4\pi p_\infty R^3 M^2 J \left[1 - \frac{\eta}{3(\gamma - 1) J}\right] \qquad \text{for } \delta = 2$$

where $J = \int_{x_o}^{1} \left(\frac{\gamma}{2} hf^2 + \frac{g}{\gamma - 1} + \frac{\gamma A}{2} \psi^2 \right) x^\delta dx$

The characteristic length, if the energy is constant, is defined as

$$R_o = \frac{E}{p_\infty} \qquad \text{for } \delta = 0$$

$$R_o = \left(\frac{E}{2\pi p_\infty}\right)^{1/2} \qquad \text{for } \delta = 1$$

$$R_o = \left(\frac{E}{4\pi p_\infty}\right)^{1/3} \qquad \text{for } \delta = 2$$

Another characteristic length, related to the electric force, is defined as

$$R_e = \frac{\sqrt{\gamma K\, p_\infty}}{p_\infty} \frac{m}{\mathcal{E}_e} = \frac{\sqrt{\gamma}}{\mathcal{E}} \lambda_D$$

where λ_D is the Debye shielding length.

In terms of R_o and R_e, the parameter A may be written as

$$A = \left(\frac{R_o}{R_e}\right)^2 \frac{y^2}{M^2} = A_o \frac{y^2}{M^2}$$

For A and a constant, similar solutions are found. Typical results, expressing the locations of the wave front and the inner core, are shown in Fig. 26, for the planar case with monatomic gas. The case for A = 0 corresponds, of course, to the conventional blast wave in a neutral gas.

The energy in the blast may be made dimensionless as

$$\tilde{E} = R^{1+\delta} U^2 J \left[1 - \frac{1}{(\delta+1)(\gamma-1)J}\right]$$

which, for the strong blast case, can be approximated as

$$\tilde{E} = R^{1+\delta} U^2 J$$

This quantity is not necessarily constant in time for the general case of similar solutions. But, by making E constant and solving, with constant A, a posteriori, for the value of "a", pseudosimilar solutions are found for which "a" does not vary much for a wide range of values

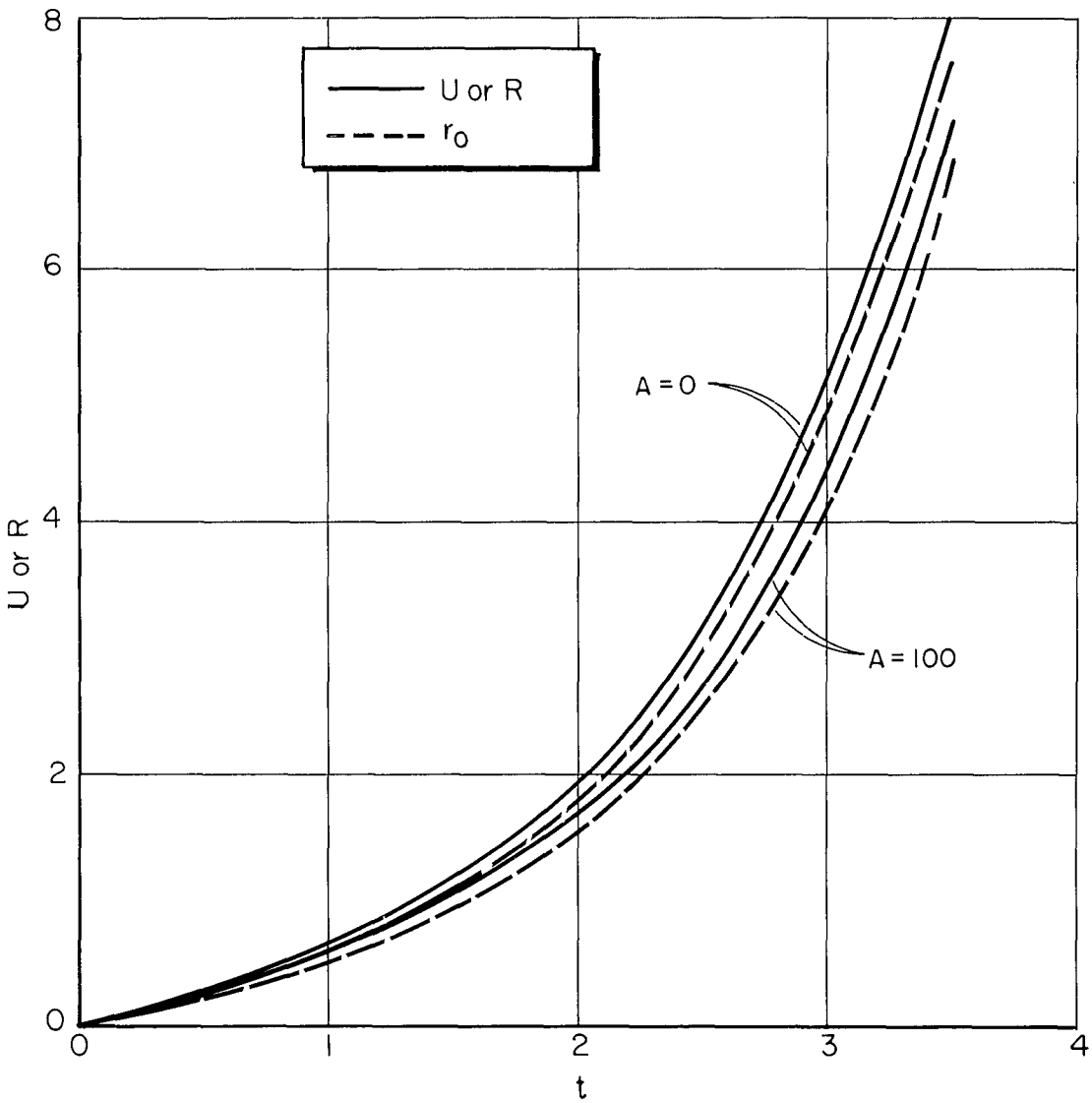

Figure 26 Propagation Of Blast Wave For $\delta = 0$, $\gamma = 5/3$.

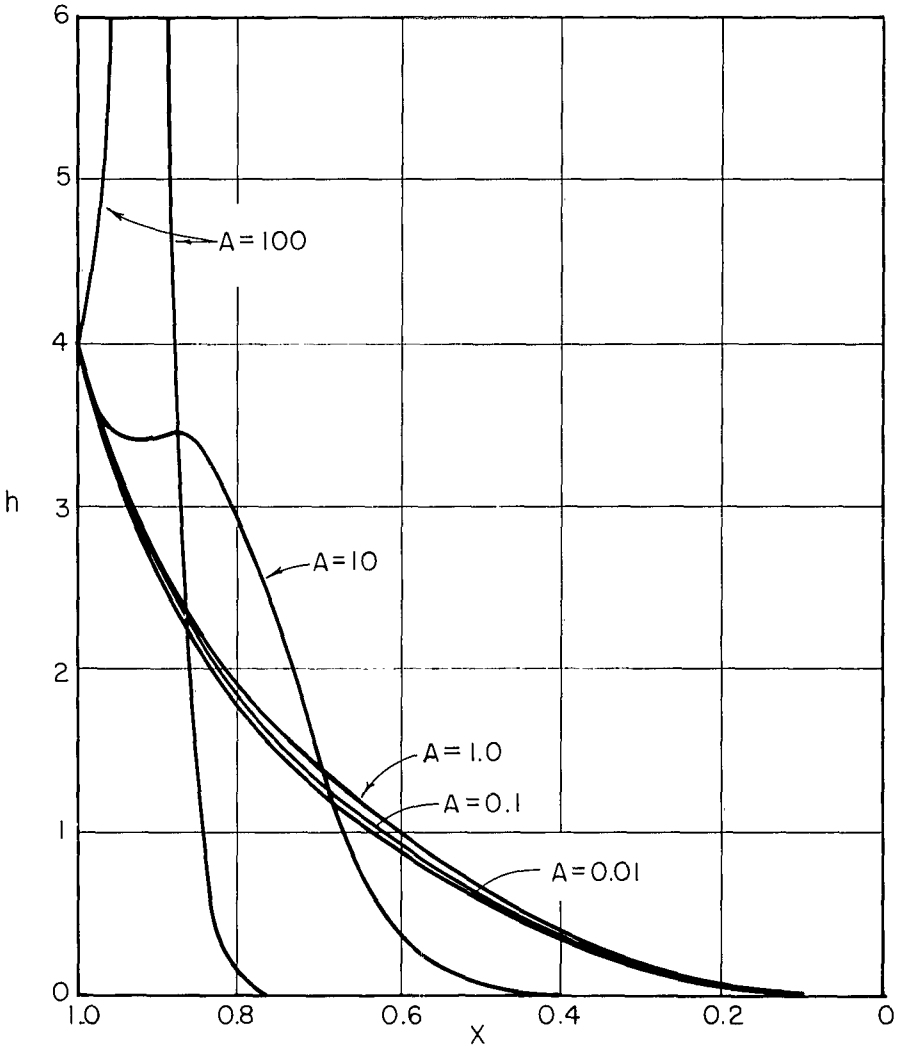

Figure 27 Density Distribution In Pseudosimilar Solution At $\delta = 0$, $\gamma = 5/3$.

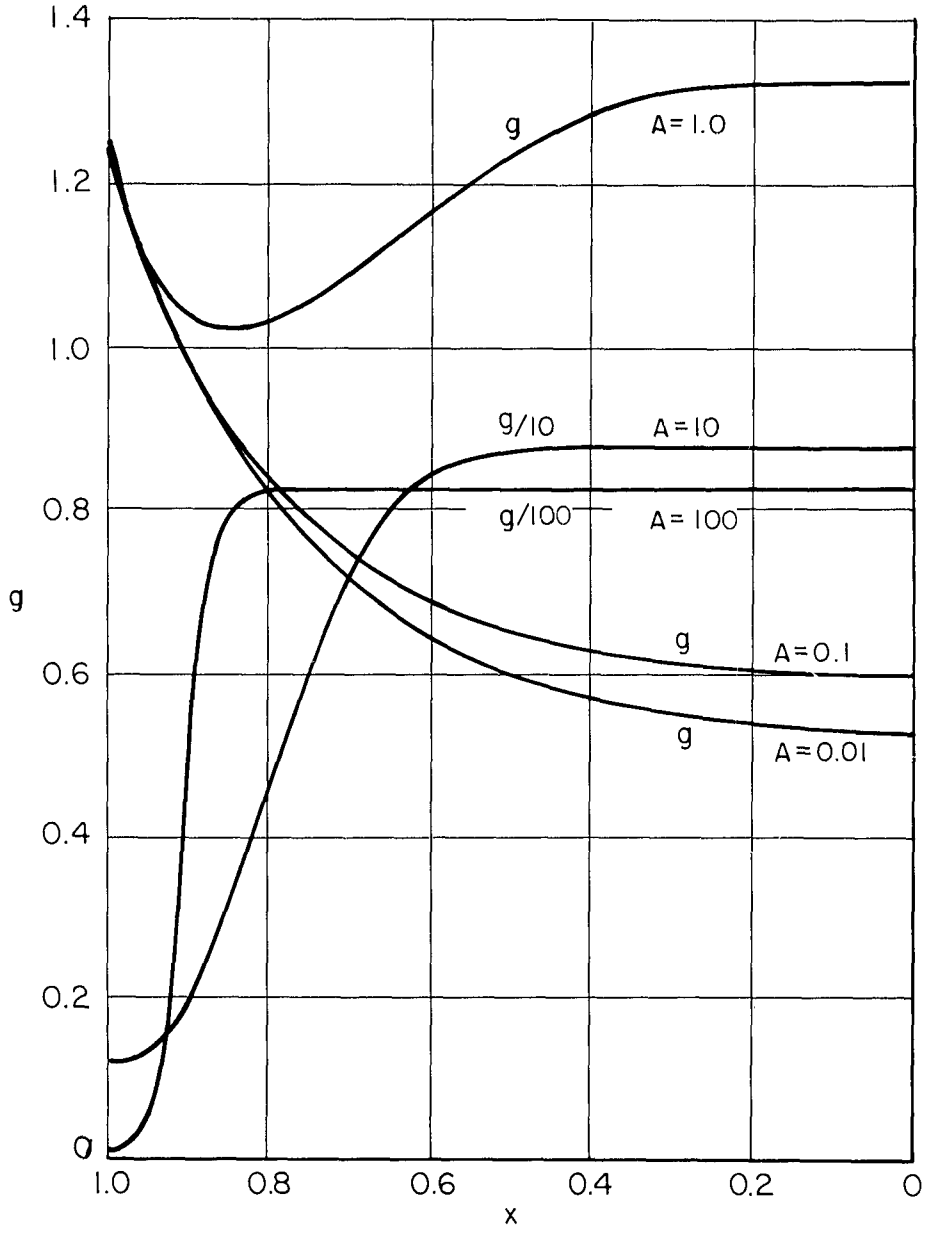

Figure 28 Pressure Distribution In Pseudosimilar Solution At $\delta = 0$, $\gamma = 5/3$.

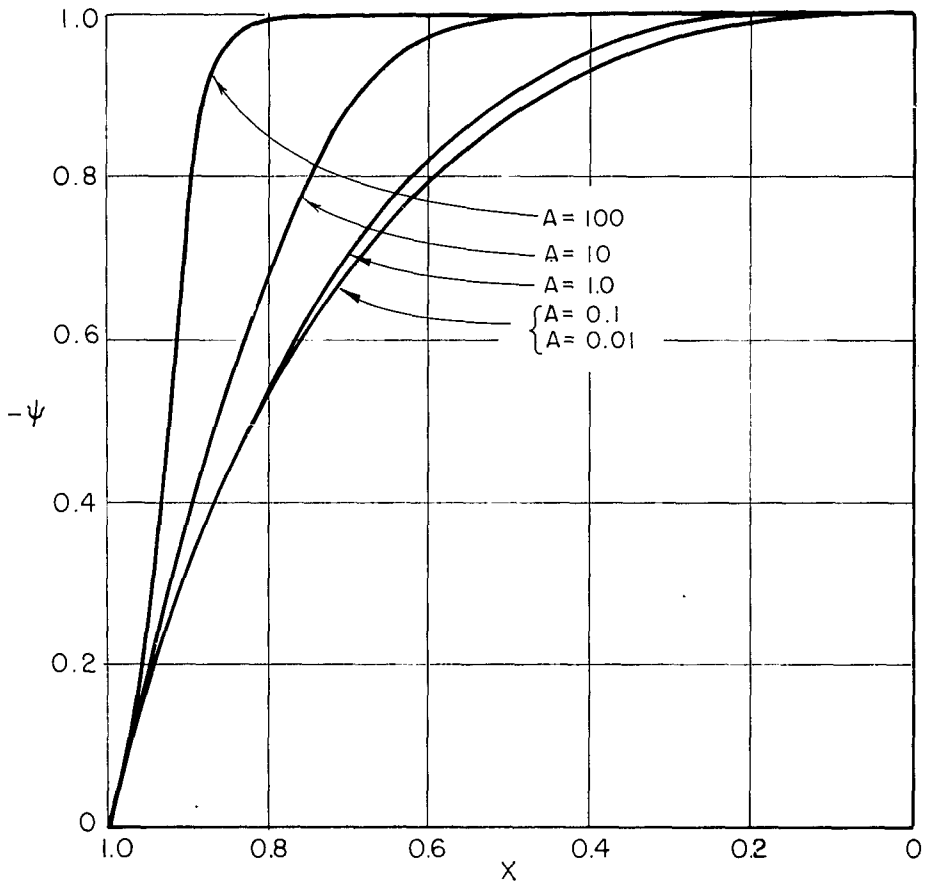

Figure 29 Electrical Potential Distribution In Pseudosimilar Solution At $\delta = 0$, $\gamma = 5/3$.

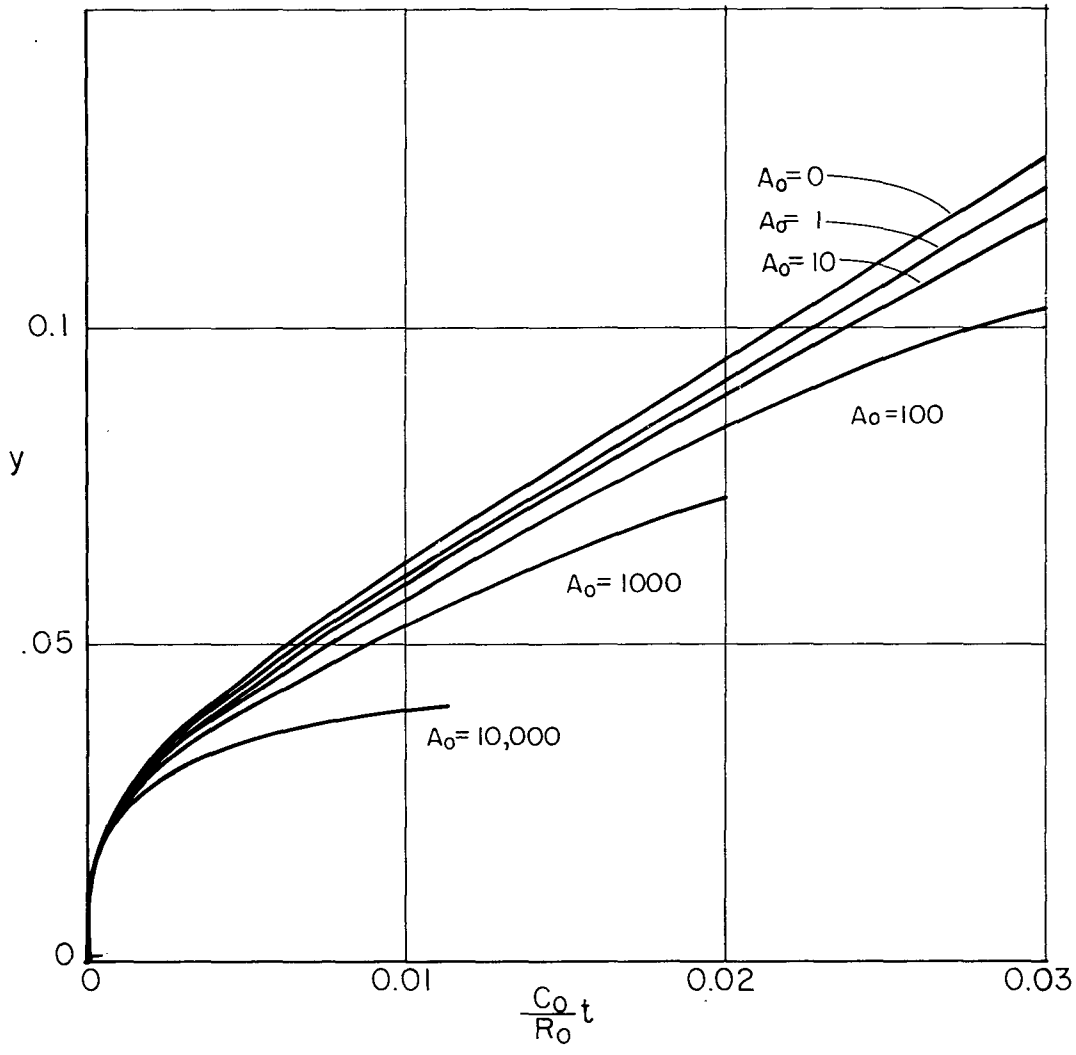

Figure 30 Blast Wave Propagation In Pseudosimilar Solution At $\delta = 0$, $\gamma = 5/3$.

of A. Typical results are shown in Figs. 27 to 30 for the density, pressure and electric potential distributions and the propagation of the wave front. It is seen that for a strong blast wave with significant ionization (large values of A) the mass of the gas is concentrated in a relatively thin layer near the shock front; and behind it there is a large space filled with low density gas of high static temperature accompanied by strong electrostatic potential. The speed of propagation is seen to be significantly reduced at large values of A_o (large values of ϵ).

Further details of the study may be found in Ref. 34.

D. FREE MOLECULE ELECTROSTATIC PROBE THEORY (F. O. Smetana)

The conventional Langmuir probe can be applied only to measurements in a macroscopically stationary plasma; while for plasmadynamic research purposes it is necessary to develop a probe which can measure the local charged particle density in a flowing plasma. The present study is an attempt at combining an approximate Poisson Equation with the free molecule flux equation to yield results relating the current in a cylindrical probe to the charged particle density in a rarefied high speed plasma flow.

The following basic assumptions are made:

1. The plasma is composed of three species: singly ionized positive ions, electrons and neutral molecules.

2. Each of these species is in local thermodynamic equilibrium, although the electron temperature may not be the same as the ion or neutral temperature. The ions and neutrals have the same temperature.

3. The number densities of ions and electrons are equal and small compared with the number density of neutrals.

4. Collisions between charged particles are neglected in comparison with collisions between charged particles and neutrals.

5. The stream is moving with a uniform velocity, U_o.

6. The cylinder diameter is small compared with the electron-neutral free path length or the ion-neutral path length.

7. The field of the cylinder does not perturb the plasma significantly beyond one electron-neutral or ion-neutral path length. Consequently, there are no collisions involving charged particles in the region where the cylinder potential is significant.

8. The change in the potential field of the cylinder in the circumferential direction may be neglected. The field is therefore a central force field.

With a central attractive force field it can be established that there is a maximum tangential charged particle velocity for each initial radial velocity for which the particle will be captured by the probe. It is thus possible to calculate the flux to the cylinder as

$$N = \int_{-\infty}^{\infty} \int_{-\xi_{2max}}^{\xi_{2max}} \int_{0}^{\infty} \xi_1 \, f \, d\xi_1 \, d\xi_2 \, d\xi_3 \qquad \text{(IV-6)}$$

where ξ_1, ξ_2, ξ_3 are the absolute radial, tangential and axial velocity components, respectively; f, the distribution, is Maxwellian; and $\xi_{2_{max}}$ is the maximum tangential velocity described above. The value of $\xi_{2_{max}}$ depends, of course, on the imposed potential of the probe. To make the integration of (IV-6) possible, the finite limits of integration are established by means of a simplified picture wherein the central force field of infinite extent through which a charged particle is assumed to traverse without collision is given a finite "cut-off". The result is a flux to the cylindrical probe of radius r_c given by

$$N = n_o \left(\frac{2\pi kT}{m}\right)^{-3/2} \frac{r_e}{r_c} \int_{-U_o \sin\theta}^{\infty} (c_1 + U_o \sin\theta) \exp(-\beta^2 c_1^2)$$

$$\left[\operatorname{erf}\left(S\cos\theta + \frac{r_c}{r_e} Z\right) - \operatorname{erf}\left(S\cos\theta - \frac{r_c}{r_e} Z\right)\right] dc_1 \qquad \text{(IV-7)}$$

where n_o = charged particle density

r_e = cut-off radius

U_o = mean mass motion of plasma

$\beta = \sqrt{\frac{m}{2kT}}$

$S = U_o \beta$ = speed ratio

$$Z^2 = \frac{r_e^2}{r_e^2 - r_c^2} \left[(\beta c_1 + S \sin\theta)^2 + \eta_o \right]$$

$$\eta_o = \frac{e V_o}{kT}$$

and V_o = potential of probe.

Equation (IV-7) reduces to well-known results for free molecule neutral particle flux incident on a cylinder and charged particle flux on a cylinder without mean motion for $\eta_o = 0$ and $S = 0$ respectively.

The establishment of a cut-off radius that will give results with a tolerable error depends on the solution of a simplified one-dimensional Poisson equation of the form

$$\frac{d^2\eta}{d\left(\frac{r}{r_c}\right)^2} + \frac{r_c}{r} \frac{d\eta}{d\left(\frac{r}{r_c}\right)} - \frac{2 r_c^2}{\lambda_D^2} \sinh \eta = 0 \qquad \text{(IV-8)}$$

where η is the dimensionless potential $\frac{eV}{kT}$ and λ_D is the Debye distance.

Extensive numerical calculations have established that the above approximations result in errors no greater than 10% in the worst cases. Details of the discussions on such error estimates may be found in Ref. 35.

The results of integrating (IV-7) numerically, expressed in practical terms of current collected per unit probe length for several values of the free-stream neutral density n_N and electron density n_o, as well as two widely spaced values of the electron temperature T_e and the ion speed ratio S_o, are shown in Fig. 31.

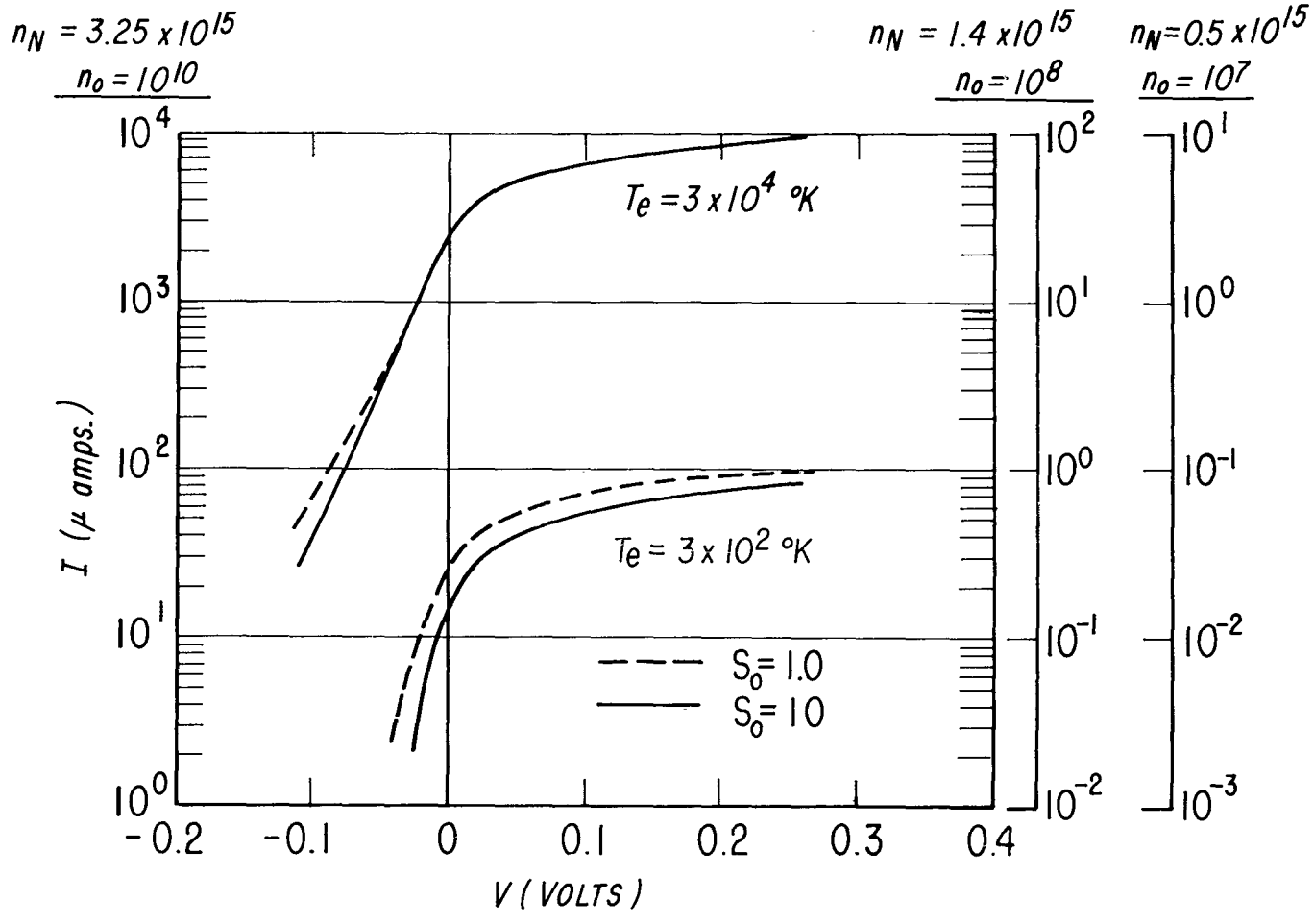

Figure 31 Current Collected By Cylindrical Probe.

From the figure it appears that one should observe the following behavior experimentally:

(1) When $S_o > 10$ the current collected is virtually independent of cylinder potential except for a small range around the plasma potential. In this range the electron current disappears rapidly below the plasma potential and the ion current disappears rapidly above.

(2) For large values of S_o, the electron current is also virtually independent of S_o and the ion current varies directly with S_o.

(3) When $S_o \approx 0$, the ion current at negative cylinder potentials is approximately independent of potential when the charged particle density is high; for relatively small charged particle densities, the current will be quite sensitive to potential. A similar situation exists with regard to the electron current at positive potentials.

V. EXPERIMENTAL STUDIES IN PLASMADYNAMICS

A. PROPAGATION OF MICROWAVES THROUGH A FLOWING PLASMA IN THE PRESENCE OF A MAGNETIC FIELD (K. Oshima)

The propagation of microwaves through the partially ionized gas flowing in a small two-dimensional supersonic wind tunnel is studied experimentally and the results compared with theoretical predictions based on the conventional tensor conductivity of a plasma such as

discussed by Koga in Ref. 31. Quantities measured are: attenuation, phase shift, and rotation of plane of polarization. Details of the analysis and the experiments may be found in Ref. 36.

The calculation of the propagation characteristics begins with expressing the complex refractive index of the plasma in the following:

Real part of refractive index:

$$n_1' = \frac{1}{\sqrt{2}}\left[\left[\left\{1-\frac{(1+\gamma)\eta}{(1+\gamma)^2+\beta^2}\right\}+\left\{\frac{\beta\eta}{(1+\gamma)^2+\beta^2}\right\}^2\right]^{1/2}+\left\{1-\frac{(1+\gamma)\eta}{(1+\gamma)^2+\beta^2}\right\}\right]^{1/2} \qquad \text{(V-1)}$$

$$n_2' = \frac{1}{\sqrt{2}}\left[\left[\left\{1-\frac{(1-\gamma)\eta}{(1-\gamma)^2+\beta^2}\right\}^2+\left\{\frac{\beta\eta}{(1-\gamma)^2+\beta^2}\right\}^2\right]^{1/2}+\left\{1-\frac{(1-\gamma)\eta}{(1-\gamma)^2+\beta^2}\right\}\right]^{1/2} \qquad \text{(V-2)}$$

where subscripts 1 and 2 refer to the ordinary and extraordinary parts of the transmitting wave.

Imaginary part:

$$n_1'' = \frac{1}{\sqrt{2}}\left[\left[\left\{1-\frac{(1+\gamma)\eta}{(1+\gamma)^2+\beta^2}\right\}^2+\left\{\frac{\beta\eta}{(1+\gamma)^2+\beta^2}\right\}^2\right]^{1/2}-\left\{1-\frac{(1+\gamma)\eta}{(1+\gamma)^2+\beta^2}\right\}\right]^{1/2} \qquad \text{(V-3)}$$

$$n_2'' = \frac{1}{\sqrt{2}}\left[\left[\left\{1-\frac{(1-\gamma)\eta}{(1-\gamma)^2+\beta^2}\right\}^2+\left\{\frac{\beta\eta}{(1-\gamma)^2+\beta^2}\right\}^2\right]^{1/2}-\left\{1-\frac{(1-\gamma)\eta}{(1-\gamma)^2+\beta^2}\right\}\right]^{1/2} \qquad \text{(V-4)}$$

In the above η, β and γ are dimensionless characteristic frequencies of the problem defined as follows:

$\eta = \left(\frac{\omega_p}{\omega}\right)^2$ where ω_p is the circular plasma frequency and ω is the circular microwave frequency

$\beta = \frac{\nu}{\omega}$ where ν is the electron-heavy particle collision frequency

$$\gamma = \frac{\omega_c}{\omega}$$ where ω_c is the electron cyclotron frequency

The phase shift and attenuation, Ⓗ and A, are related to the complex refractive index by

$$\exp(-i\,Ⓗ - A) = \frac{(1+n_o)^2 - (1-n_o)^2 \exp(2i\tilde{d})}{(n+n_o)^2 - (n-n_o)^2 \exp(2in\tilde{d})} n \exp\left[-i(1-n)\tilde{d}\right] \tag{V-5}$$

$$= \exp\left[-i(1-N)\tilde{d}\right]$$

where the second equality defines an effective refractive index N which includes the effects of the plasma thickness d and the total refractive index n_o of the walls bounding the plasma.

For an infinite plane slab of plasma of thickness d and uniform refractive index n the normalized phase shift θ and attenuation α are, in terms of (V-1) to (V-4):

$$\theta = 1 - \frac{N_1' + N_2'}{2} + \frac{1}{\tilde{d}} \tan^{-1}\left\{\tanh\frac{N_1'' - N_2''}{2}\tilde{d} \cdot \tan\left(\frac{N_1' - N_2}{2}\tilde{d} + \delta\right)\right\} \tag{V-6}$$

$$\alpha = \frac{N_1'' + N_2''}{2} - \frac{1}{2\tilde{d}} \ln\left[\frac{1}{2}\cosh(N_1'' - N_2'')\tilde{d} + \frac{1}{2}\cos\left\{(N_1' - N_2')\tilde{d} + 2\delta\right\}\right] \tag{V-7}$$

where $\theta = \frac{Ⓗ\lambda}{2\pi d}$ with Ⓗ in radians, and λ = wavelength

$\alpha = \frac{A\lambda}{2\pi d}$ with A in nepers

$\tilde{d} = \frac{2\pi d}{\lambda}$ is the normalized plasma thickness and δ is the orientation of the receiving horn with respect to the incident microwave plane of polarization.

The expressions (V-6) and (V-7) each contains two terms, the first of which is the linear term relating the total effect to the plasma thickness, while the second term represents the nonlinear effects of the thickness. It is thus seen that any application of laboratory experimental results to actual flight conditions in problems dealing with re-entry communications, for example, must be treated with great caution, taking into consideration the nonlinear effects.

Figure 32 shows a general view of the experimental apparatus. Schematic layouts of the wind tunnel – microwave – magnetic coil combination, and the microwave system are shown in Figs. 33 and 34. Two frequencies are used: 9.2 KMC (X-band) and 24 KMC (K-band). At the wavelength of K-band, 1.25 cm, the infinite slab plasma assumption appears to be adequate in relation to the actual size of plasma used, in that there is negligible interference of the microwave by the tunnel walls. The same is not true of the X-band experiments, so that the rotation of the receiving horn produces effects even without magnetic field.

In the experiments the basic properties of the plasma – the electron density and collision frequency – are determined by using K-band interferometry without any magnetic field. These are then used to calculate phase shift and attenuation as functions of rotation angle (δ) by Eqs. (V-6) and (V-7). Typical results are presented in Figs. 35, 36 and 37.

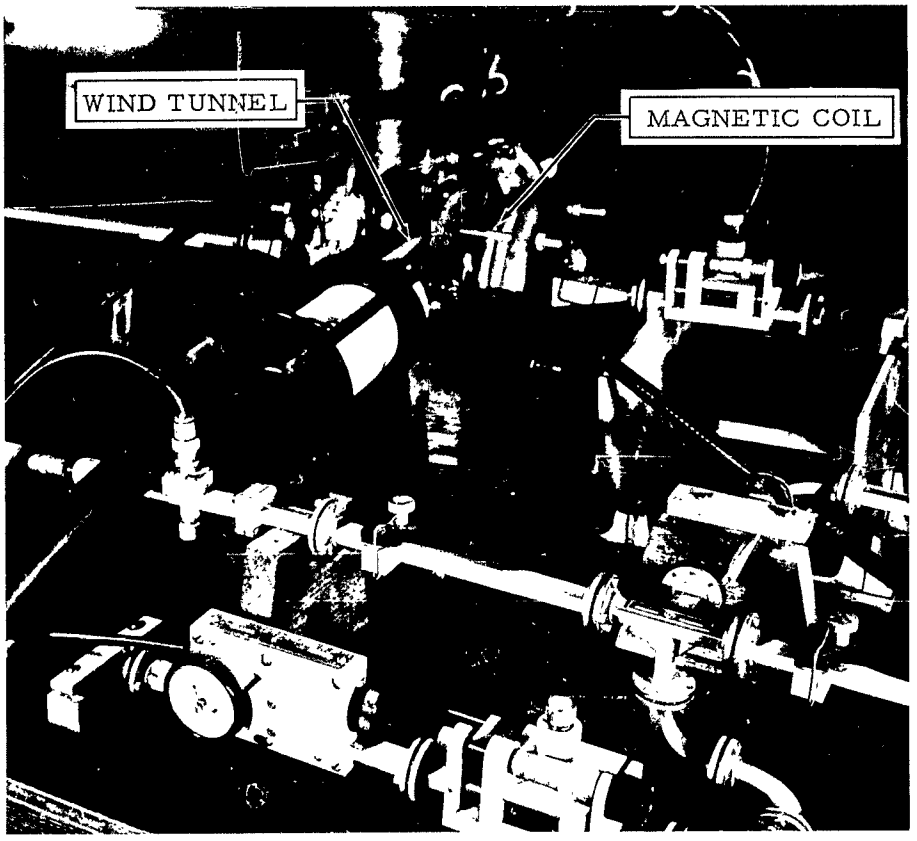

Figure 32 Experimental Apparatus.

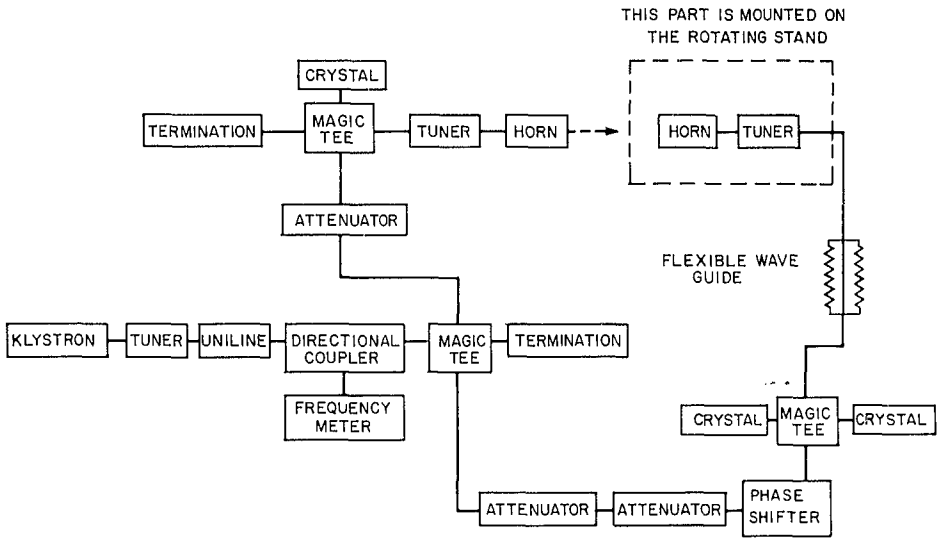

Figure 33 Schematic Diagram Of The Interferometer.

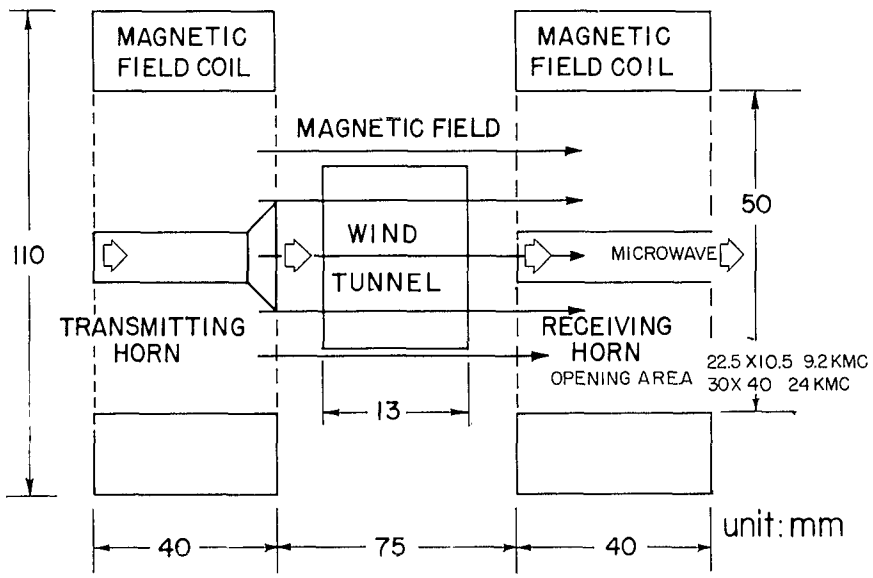

Figure 34 Arrangement Of The Wind-Tunnel, Magnetic Field Coils and Microwave System.

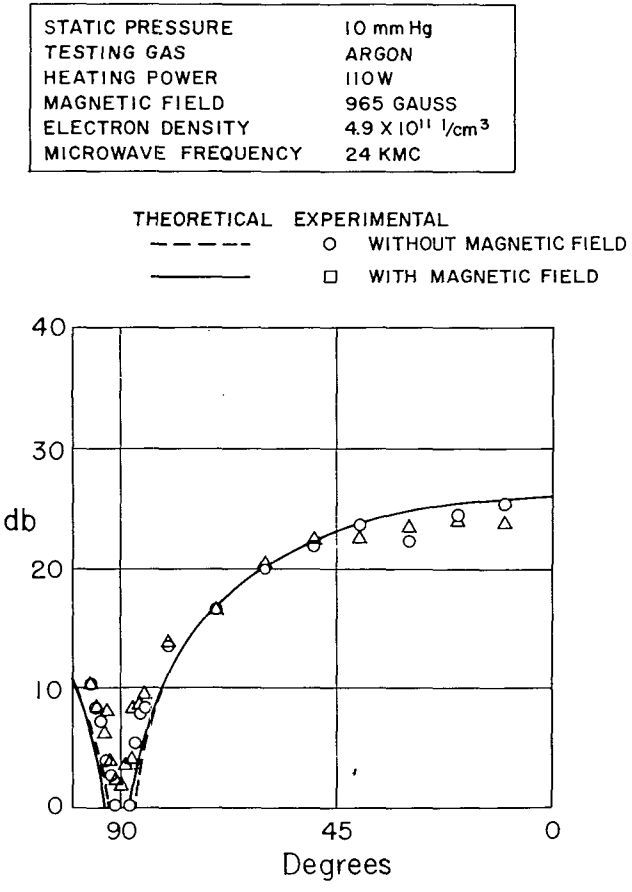

Figure 35 Attenuation At K-Band.

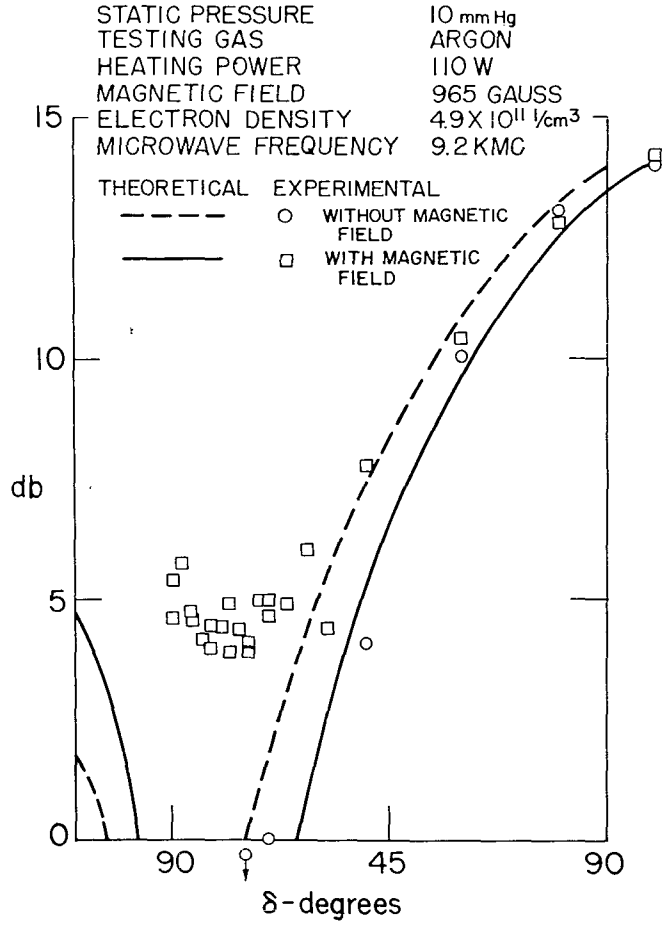

Figure 36 Attenuation At X-Band.

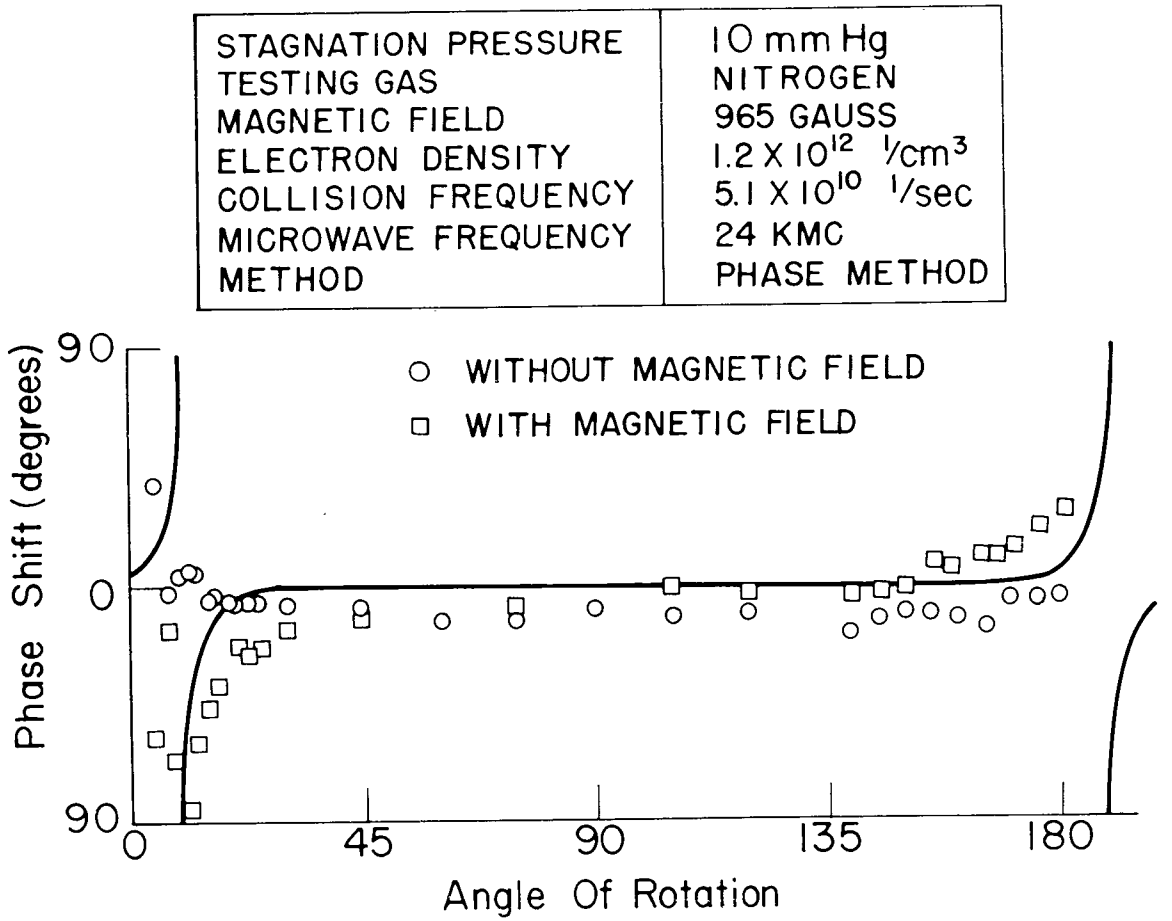

Figure 37 Phase Shift At K-Band.

The angular dependence of attenuation at K-band with and without magnetic field is shown in Fig. 35. It is seen that with the fairly low electron density, resulting in a value of η of about 0.1, the magnetic field has little effect. The agreement between theory and experiment at 24 KMC is seen to be quite good. For X-band work the interference effects of the tunnel walls are significant, such that there is considerable discrepancy between theory and experiments at δ between 45 and 90 degrees, as shown in Fig. 36. The phase shift with and without magnetic field is shown in Fig. 37. It should be recalled that, without magnetic field, the phase shift should be independent of δ, so that the no-field theoretical curve is not shown in the figure. The experimental results as shown do show good agreement with the theoretical prediction.

B. FLOW OVER A BLUNT LEADING EDGE IN A SUPERSONIC PARTIALLY IONIZED FLOW (Y. Oshima)

The electrogasdynamic blast wave theory developed by K. Oshima (see IV-C above) is applied to the steady two-dimensional flow over a blunt body. The general equations of K. Oshima are reduced to first order equations for small values of the similarity parameter A (which, it may be recalled, contains the degree of ionization of the gas) and constant energy.

The first order solutions are

$$M = \frac{1}{\sqrt{J_o y}} \left(1 - \frac{1}{2} \lambda_1 J_o A_o y^3 \right) \qquad \text{(V-8)}$$

$$y = \left(\frac{3}{2} \frac{1}{\sqrt{J_o}} \frac{c_\infty}{R_o} t \right)^{2/3} \left[1 - \frac{1}{4} \lambda_1 A_o \left(\frac{c_\infty}{R_o} t \right)^2 \right] \qquad \text{(V-9)}$$

with $J_o = 1.3$, $\lambda_1 = 0.14$ calculated by numerical integration. Details of the analysis may be found in Ref. 37.

It will be noted that the first term in each of the above represents the classical blast wave solution (for $A_o = 0$). The propagation of the blast wave is shown in Fig. 38, where the first order solution is compared with the pseudosimilar solution of Ref. 37. It is seen that at small values of t the two solutions agree well for a wide range of values of A_o. At larger values of t the first order solution agrees well with the pseudo-similar solution for small values of A_o (as is the condition underlying the first order approximation).

The experimental study is intended only as a qualitative verification of the theory, because the large Mach number condition of the theory cannot be realized in the particular apparatus used. A sketch showing the setup is shown in Fig. 39. The flow and plasma conditions are listed below:

Mach number = 2

static pressure = 10 mm Hg

electron density = 3×10^{11} $1/cm^3$ (measured by microwave)

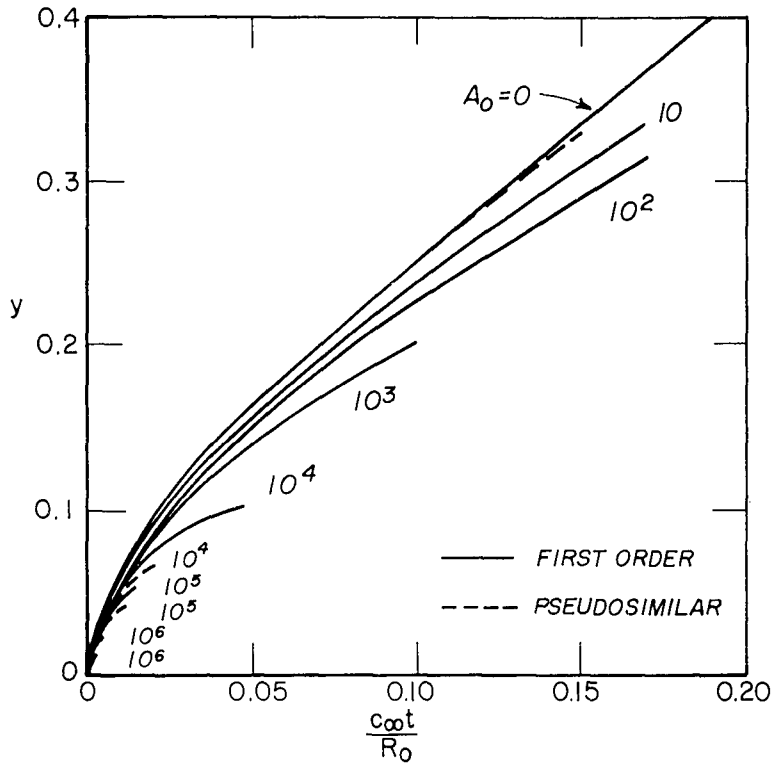

Figure 38 Propagation Of The Electrogasdynamic Blast Wave, First Order Solution.

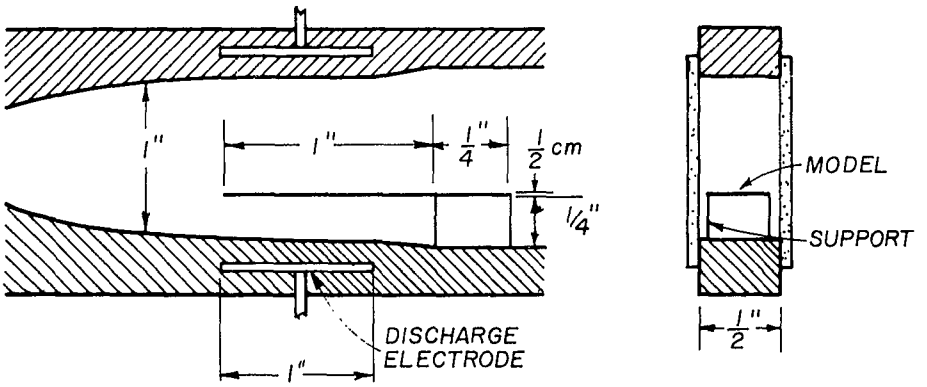

MACH NO. 2 NOZZLE (Not To Scale)

Figure 39 Sketch Of The Test Section And The Model.

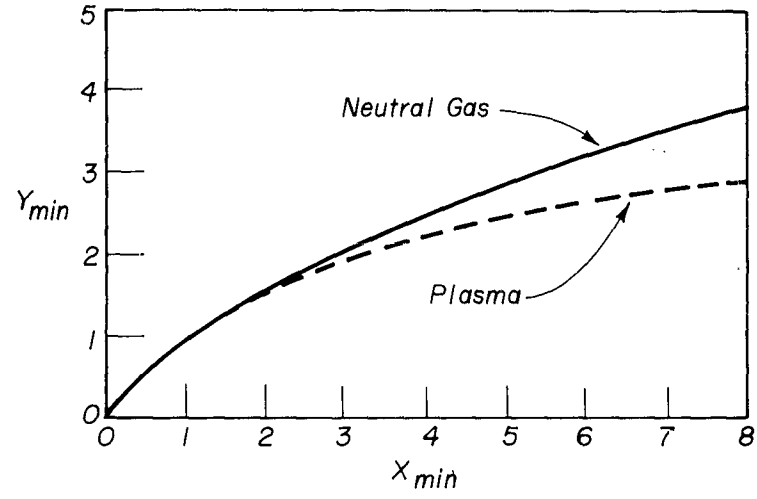

Figure 40(a) Shock Forms Around The Flat Plate (Theoretical).

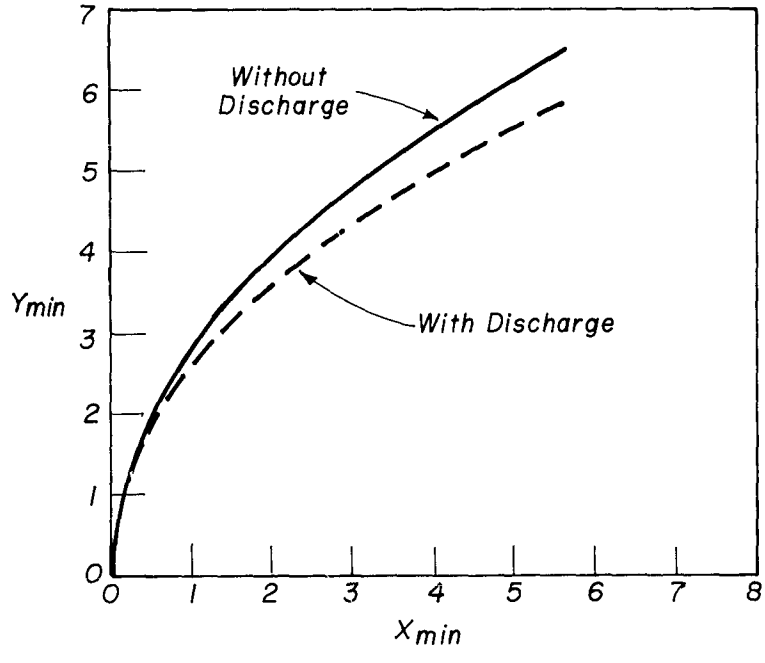

Figure 40(b) Shock Forms Around The Flat Plate (Experimental).

electron temperature $\cong$ 3 ev

gas temperature $\cong 300^{\circ}K$

degree of ionization $= 10^{-6}$

From the above the following parameters are calculated:

$R_e = 0.2$ cm

$R_o = 0.2$ cm

$A_o = 1$

The bow shock shape calculated by the first order theory, using the above data, is shown in Fig. 40(a); and the experimentally obtained shock shape is shown in Fig. 40(b)

VI. HIGH-FREQUENCY ELECTRICAL BREAKDOWN IN LOW-DENSITY GAS (P. C. Wilber)

A pressure measuring system must satisfy a number of criteria if it is to be a generally useful tool in low-density fluid-dynamic research. The more important of these requirements include adequate accuracy, precision and response over the desired pressure range, operational stability, ruggedness, and sufficient smallness of sensor relative to characteristic dimensions of the flow system.

Several gage types which provide measurements in the range of interest are available. Among these are the manometer, radiometer, ionization, and thermal conductivity pressure gages. The first two types measure pressure directly whereas the latter two provide only indirect observations. In addition the last two, as shown by various comments in the literature, fail to satisfy most of the above listed criteria to a degree deemed satisfactory for fluid-dynamic research. The primary gage types also leave much to be desired when it comes to satisfying simultaneously both the size and response-time requirements; which, for these systems, are mutually contradictory.

In an attempt to better satisfy the above requirements for pressure instrumentation a secondary gage based on the high-frequency breakdown of a gas has been proposed and is currently under development. This chapter provides a complete summary of this project to date. A more detailed discussion is available. *

For given electrode geometry, types of gas and its temperature; the field strength (E) at which discharge takes place is a unique function of gas density, ** known as the Paschen curve. When the discharge results

---

*High-Frequency Breakdown of Gases as a Means of Measuring Low Pressures, USCEC Report in preparation.

**For a fixed temperature the pressure (p) is equal to a constant times the density (as shown by the equation of state) and therefore also uniquely related to the breakdown field strength by the Paschen curve.

from application of a high-frequency electric field there is a range of conditions which also produce a Paschen curve and for which the breakdown field strength is much lower than that required for the corresponding d.c. case. Within this range the phenomenon is known as a diffusion-controlled high-frequency breakdown (Ref. 38) and is easily produced and measured in the laboratory without elaborate equipment. A study of the literature has shown that it is essential that all breakdown be of the diffusion-controlled type if ambiguity is to be minimized in interpreting the measurements.

Two basic requirements must be met if the breakdown is to be of the right type. One is that the electron mean free path must be less than the characteristic dimension of the breakdown region. For most research apparatus this occurs at about 10^{-2} mm Hg. The other is that the oscillation amplitude of the average electron is less than the dimension of the discharge region in the direction of the applied field. This limitation for air and a coaxial cylinder geometry having a characteristic diffusion length of 3 cm is shown in Fig. 41 as $f_{min.} = f(p)$.

To verify these limits, become acquainted with the techniques for production and measurement of breakdown, and study the problem of extending the region of diffusion-controlled breakdown to lower pressures ($\sim 10^{-4}$ mm Hg) breakdown of air by a 10 Mc/s field was measured as a function of pressure for the sensors described in Fig. 42. The results are shown in Fig. 43.

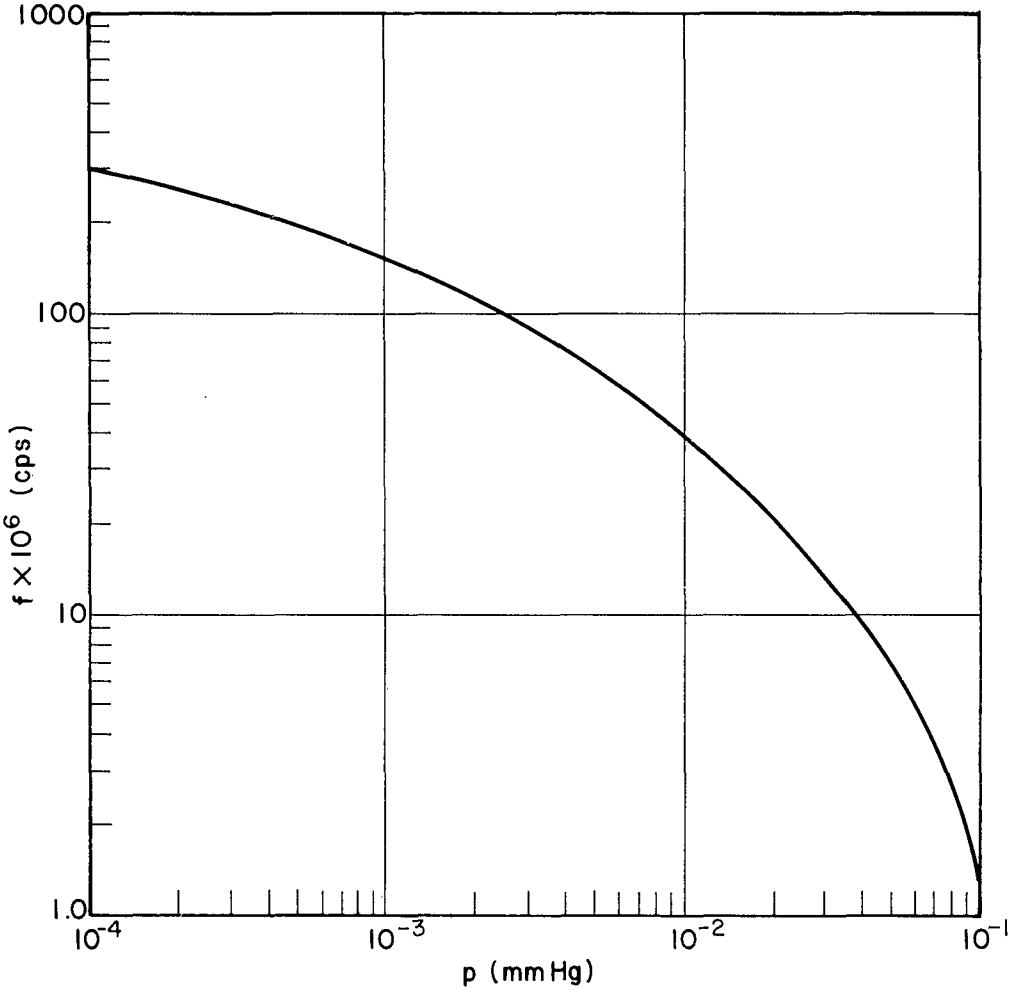

Figure 41 Oscillation Amplitude Limit Expressed As $f_{min.} = f(p)$ For A Coaxial Cylinder Geometry Having Λ = 3 cm. And In Air*.

(Based on data contained in AEDC TR 59-23, Figure 3.)

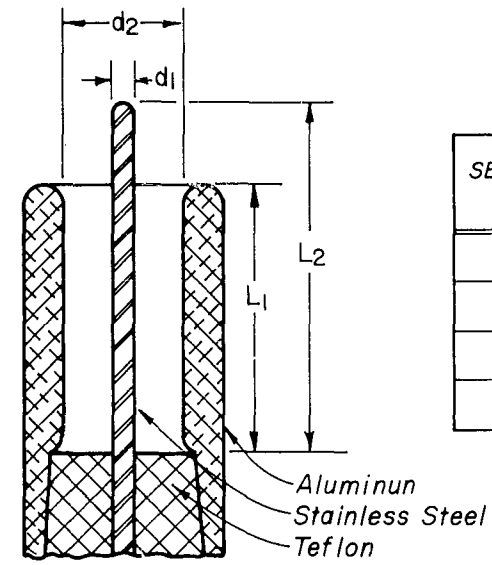

SENSOR NO.	d_1 in.	d_2 in.	L_1 in.	L_2 in.
1	0.125	0.75	1.0	1.4
2	0.125	0.75	2.0	2.4
2S	0.125	0.75	2.0	1.6
3	0.125	0.45	2.0	2.4

SENSORS 1-3

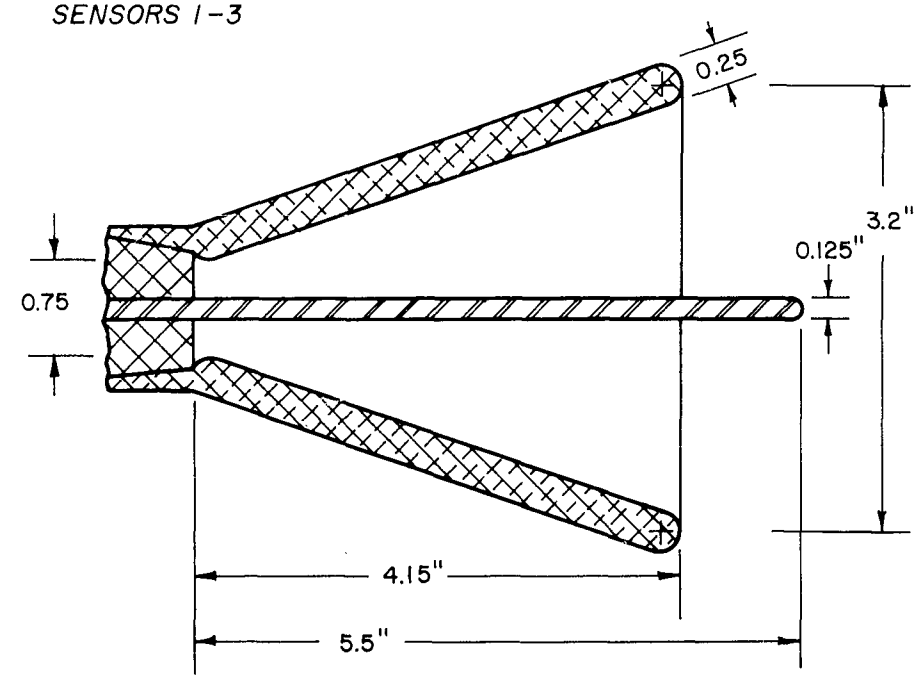

SENSOR 4

Figure 42 Preliminary Sensor Configurations.

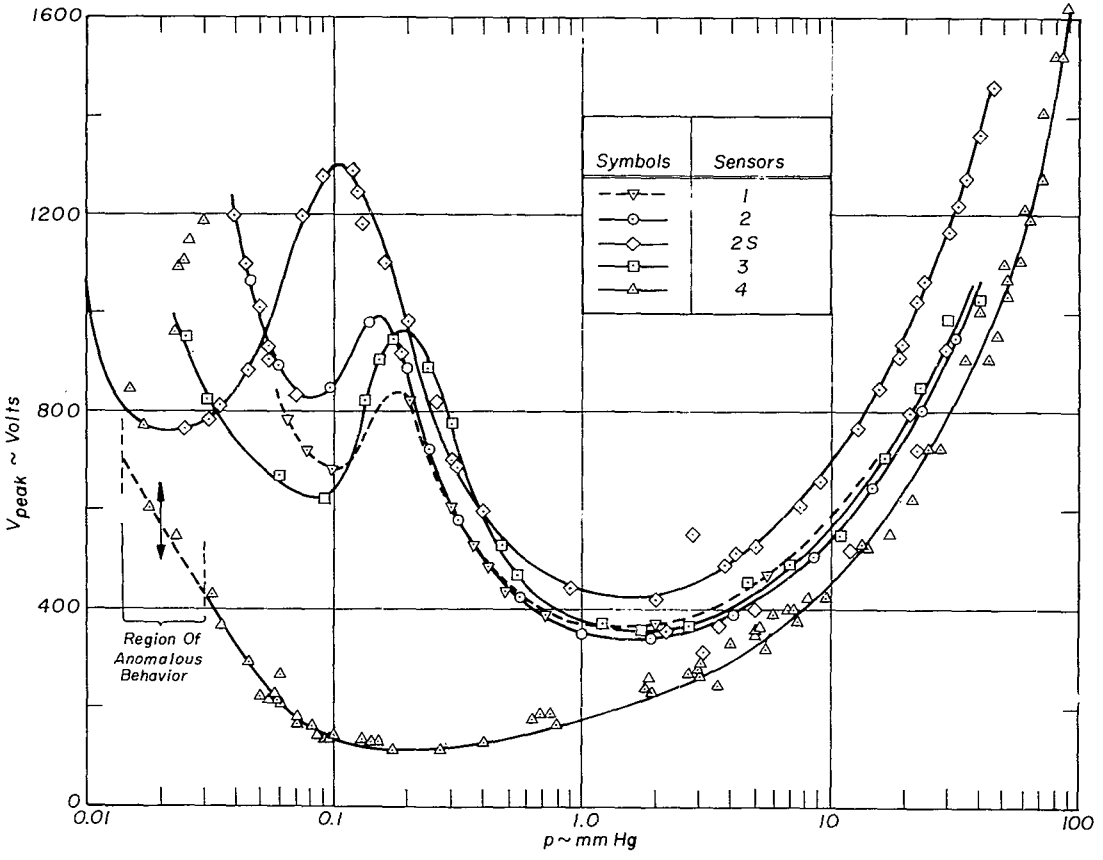

Figure 43 Breakdown Characteristics For Various Sensors
At 10 Mc./sec.

The results are in good qualitative agreement with diffusion-controlled breakdown theory for all pressures in the range considered down to about 2×10^{-1} mm Hg. Comparison of the curves for sensors 1 and 2 shows the effect of reduction of the characteristic diffusion length and increase in relative importance of end effects on the breakdown voltage. Analysis of the data from sensors 2 and 3 confirms the theoretical conclusion that the field strength to initiate breakdown increases as the characteristic diffusion length decreases and the gap between electrodes approaches the amplitude of oscillation of the electrons. The results for sensor 2S, which included a copper screen over its open end to produce a basic change in the field boundary condition as an end effect, when studied relative to those for number 2 again show the effect of increased losses by diffusion and drift but indicate very little change due to end effects except in the region of lower pressure. The curve for sensor 4 again shows the diffusion-controlled nature of the breakdown by displaying the drop in breakdown voltage which accompanies an increase in the characteristic diffusion length.

The shift in the minimum of the breakdown characteristic for sensor 4 can be explained by an inexact but plausible argument based on results from dimensional analysis of breakdown systems. It has been shown (Ref. 38) that those high-frequency breakdown systems for which the parameters

$$E\Lambda, \; p\Lambda$$

Λ = characteristic diffusion length

remain constant produce similar discharges. Thus for similar systems corresponding points on the breakdown curves are related by the similarity rules:

$$E_I \Lambda_I = E_{II} \Lambda_{II}$$

$$p_I \Lambda_I = p_{II} \Lambda_{II}$$

If $\Lambda_I < \Lambda_{II}$ then $p_I > p_{II}$ and $E_I > E_{II}$. Although sensor 4 has not been designed and operated so as to be exactly similar breakdownwise to any of the other three sensors; its geometry and field configuration are such that it might not be too far from obeying the similarity rules. Obviously the characteristic length of sensor 4 is greater than that of any of the others. Hence, if Λ_{II} corresponds to sensor 4 and Λ_I to one of the other three; then the above equalities indicate that the minimum of the Paschen curve for sensor 4 should be displaced to the left and down in Fig. 43 relative to the corresponding point for the other sensor. This is exactly what is observed experimentally.

The anomalous behavior of all the breakdown characteristics at pressures below 0.2 mm Hg appears to be the result of exceeding the oscillation amplitude limit. In addition the mean free path of electrons which are sufficiently energetic to cause ionization in N_2 is roughly 3 cm at a pressure of 10^{-2} mm Hg. Hence, if pressures less than 10^{-2} mm Hg are to be measured without ambiguity with sensors whose dimensions are of the same order as those discussed above; then the frequency of the

breakdown field must be such that the amplitude of the electrons if oscillating in free space would be considerably less than 1 cm. If the amplitude is taken as 0.1 cm and the field strength required for breakdown as 100 volts (peak)/cm (Ref. 39) then the frequency should be about 300 Mc/s. This analysis has not considered what the overall effect of exceeding the mean free path limit might be.

With the results of the previous analysis in mind a pressure-sensing system has been designed which uses a 240 Mc/s signal generator. A schematic of the system is shown in Fig. 44. Although an automatic system is shown, only a manual arrangement with a single sensing element has been assembled to date. However no excessive difficulty is envisioned in preparing the automatic version. The control unit replaces the human operator in making the measurements and provides for recycling the system at regular intervals. From the statistical time lags observed in the breakdowns at 10 Mc/s it appears that a cycle with a 3-minute period would be satisfactory for measuring pressures down to 10^{-2} mm Hg if no artificial source of initial ionization is to be used. For lower pressures it appears that such a source is essential if a measurement is to be made within a reasonable time. In the manual system voltage is measured using a commercial RF VTVM. For automatic operation a specifically designed diode rectifier network which provides peak voltage and a continuous recorder with good response appear to be needed. Two sensors with different breakdown characteristics

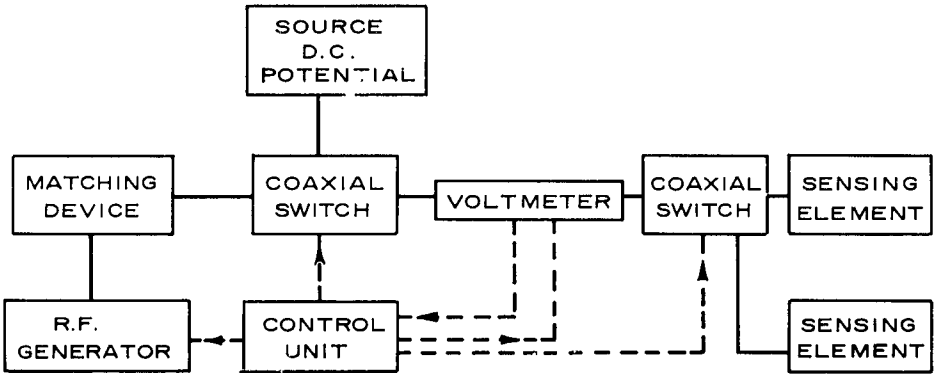

Figure 44 Schematic Of High-Frequency Breakdown Vacuum Gauge.

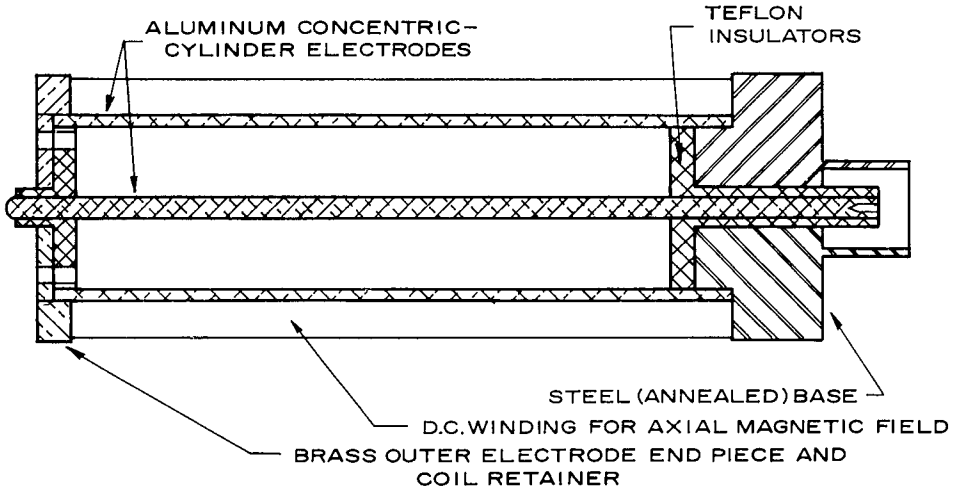

Figure 45 Extended Low Range Pressure Sensor.

but which operate over the same pressure range are used to eliminate the ambiguity in the measurement due to the double-valued nature of pressure as a function of breakdown voltage.

At the time the above system was proposed, it was anticipated that it might be possible to operate it down to between 10^{-4} and 10^{-3} mm Hg depending upon what took place when the mean free path limit was violated. Since the sensor would have its principal emitting surface made out of aluminum, which has a secondary emission coefficient δ such that $\delta < 1.05$ for all electron energies (Ref. 40), it was felt that the only result of violating the m.f.p. limit would be decreased efficiency and a corresponding increase in the breakdown field strength. However, while the 240 Mc/s system was being prepared, further study of the anomalous region in Fig. 43 and the literature (Refs. 41, 42 and 43) indicated that even though electron resonance breakdown was prevented the electron loss by scattering out of the breakdown region would be so large that it would be impossible to produce a diffusion-controlled breakdown. Later attempts to make measurements in the low-pressure region at 240 Mc/s bore out this indication.

This impasse has led to a considerable delay in the development of the HF breakdown vacuum gage. Although an axial magnetic field had been considered early in the study of the problem it was considered inadequate since electrons could still drift out of the breakdown region along the lines of force. Recently, however, further literature study

(Refs. 44 and 45) has suggested the configuration shown in Fig. 45. The winding insures that the oscillation-amplitude limit is not violated and that a minimum number of electrons are lost to the walls in the radial direction regardless of the size of their mean free path. In addition, the construction of the outer electrode is such that electrons traveling axially are deflected back from the ends during half of each cycle. Design of such a sensor is presently in progress and the actual hardware should be available for testing in the very near future. If the tests are successful, it is anticipated that the development of a high-frequency breakdown vacuum gage will be completed within the next year.

VII. ELASTIC SCATTERING OF NEUTRAL MASS-POINT PARTICLES BY A TWO-DIMENSIONAL PERFECT CRYSTAL (Earl Beder)

The elastic scattering of neutral mass-point particles by a two-dimensional semi-infinite dielectric crystal has been studied to determine what effect low-energy elastic collisions might have on surface forces in rarefied gasdynamics. The gas-solid interaction potential normal to the surface is the weak Van der Waal's one of physical adsorption. Along the surface there is a small periodic perturbation potential, representing crystal nuclei, in the absence of which the scattering is specular. A uniform beam of noninteracting particles is

scattered by the fixed potential field of the crystal surface. Forces are determined from the rate of change of momentum of the beam. The scattering problem is solved classically and quantum mechanically. By comparison, the validity of the classical theory is examined. The analysis may at best be applied to monatomic gas particles with energies below 0.1 ev.

For simplicity a square-well potential normal to the wall is assumed. This square well approximates the Morse type of Van der Wall's potential used by Lennard-Jones (Ref. 46) in a complicated approximate analysis of elastic scattering. The Lennard-Jones analysis was not considered suitable for the present investigation in which simple concepts are primarily of interest, rather than quantitative accuracy.

Some numerical cases have been carried out in the present work for helium incident on LiF. The physical constants of the square-well potential, chosen to approximate the Morse potential of Leannard-Jones, are: Average depth of well, .00825 ev; overall perturbation, one-sixth of depth of well; width of well, 2.73 Å; lattice spacing, 2.85 Å. A number of helium particle energies up to .06 ev were considered.

In the classical mechanical analysis, the trajectory of a single incident particle is found as it moves from the potential-free region through the square well and back out again after an impact with the wall. For a given potential field and particle mass, the trajectory depends upon the particle energy, angle of incidence, and the point of impact with the

square well. The angle of reflection is obtained in equations with elliptic integrals of the first kind. The change in momentum of the scattered beam follows directly from the reflection angles. The beam is scattered into a limited angular region centered near the specular reflection angle. At the angular extreme of the scattered beam, the particle density becomes infinite. The details of the classical scattering solution are thus seen to be unrealistic. The surface forces, however, depend upon an integrated effect of the scattering distribution, and are the more important criterion of the present study. In Fig. 46, for helium incident on LiF, we show classical tangential surface forces for several values of particle energy.* We observe the following characteristics: For a given angle of incidence, the scattering becomes more specular as particle energy is increased, and more diffuse as particle energy is decreased. It also seems that for a given energy the scattering becomes more specular as incidence angle is decreased, and more diffuse as it is decreased.

The normal forces deviate from specular values by very little, but show trends similar to those of the tangential forces. For example, the deviations are less than 1 percent for .06 ev, and about 3 percent for .0005 ev.

---

* The very low energy cases, .001 and .0005 ev, which are very difficult to compute, were carried out for one angle of incidence only.

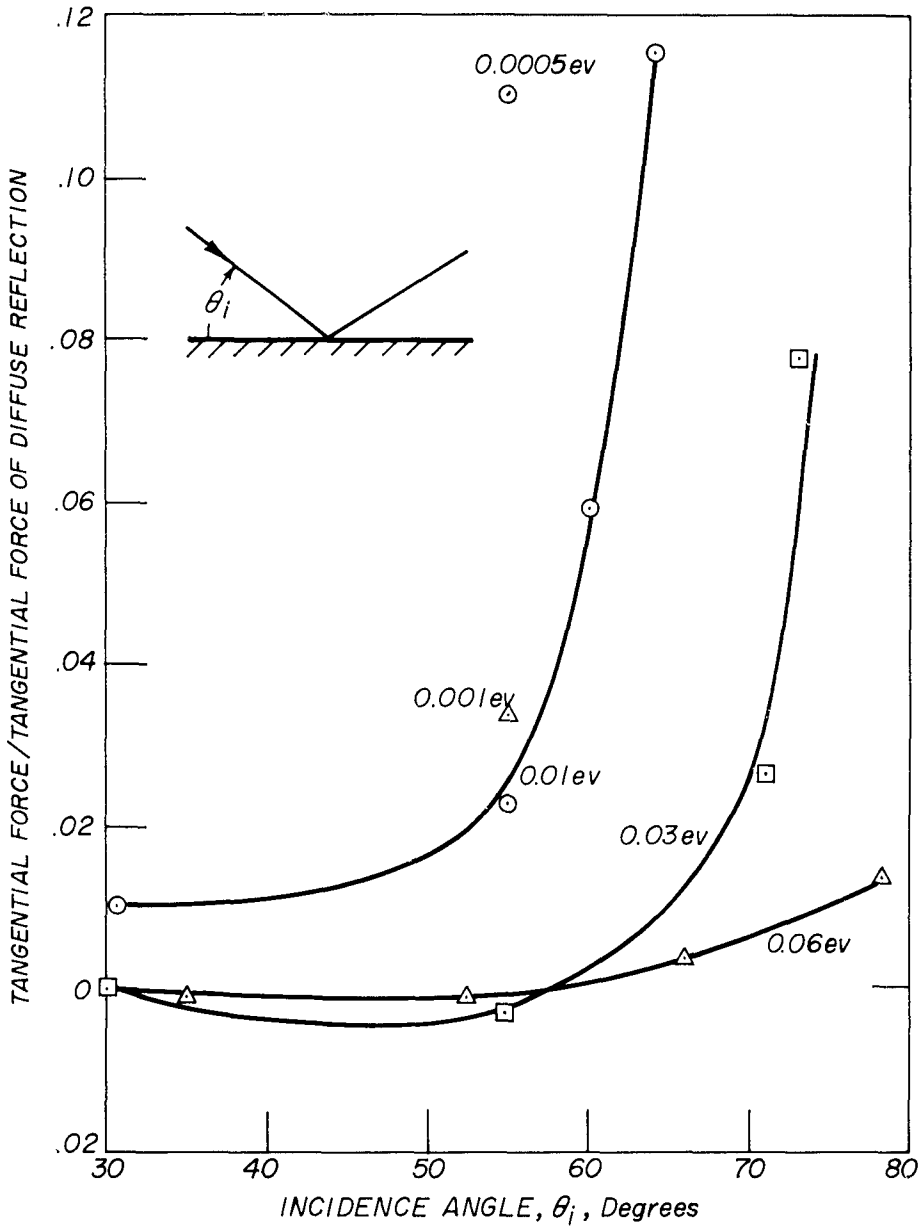

Figure 46 Tangential Forces On Surface, Classical Scattering.

In the quantum-mechanical scattering a stationary state solution of Schroedinger's equation of motion is obtained for a plane wave incident upon the potential square well. The solution may be applied to a beam of noninteracting particles. The solution, or wave function, is bounded everywhere and reduces to specular reflection for vanishing perturbation potential. The wave function is continuous at potential discontinuities and its first derivatives are continuous at the finite potential discontinuity separating the square well from the potential-free region. In the potential-free region the solutions are simple exponential functions; in the periodic region of the square well they contain Mathieu functions of integral or nonintegral order, and in the wall they are identically zero. Since the particle density must be periodic with the lattice everywhere, the wave function can only be a discrete sum of terms and not an integral. With the above restrictions a determinate solution for Schroedinger's equation may be found for a given particle energy and incidence angle. It is assumed that this solution is unique.

The forces on the surface are found by means of approximate expansions of the wave function in momentum eigenfunctions applicable to distinguished regions of space. From these expansions, fluxes of mass and momentum may be approximated; and for regions which extend to infinity, the approximations approach certainty. For the present case of a semi-infinite crystal, only fluxes through planes parallel to the surface and at a great distance from it contribute to the net forces. Through these surfaces a finite number of reflected plane waves propagate.

One very interesting result of the quantum-mechanical theory is the following: Pure specular reflection occurs for beams with particle energies and incidence angles satisfying the inequality

$$0 \leq \cos\theta_i < \frac{\lambda}{d} - 1$$

where θ_i is the angle of incidence measured from the surface, λ is the wavelength of the incident particle, and d is the crystal lattice spacing. This low energy domain of specular reflection is shown in Fig. 47. For $\lambda > 2d$ the reflection is specular independent of incidence angle. We note that the classical theory fails in this region.

Several numerical solutions are being carried out for the quantum-mechanical case, for helium incident on LiF. Particle energies are .01, .03, .06 ev. The solutions are restricted to those incidence angles which permit the use of Mathieu functions with period π, purely for convenience. It is hoped that these cases will provide evidence of the trends of the quantum-mechanical scattering, and a basis for further evaluation of the classical theory.

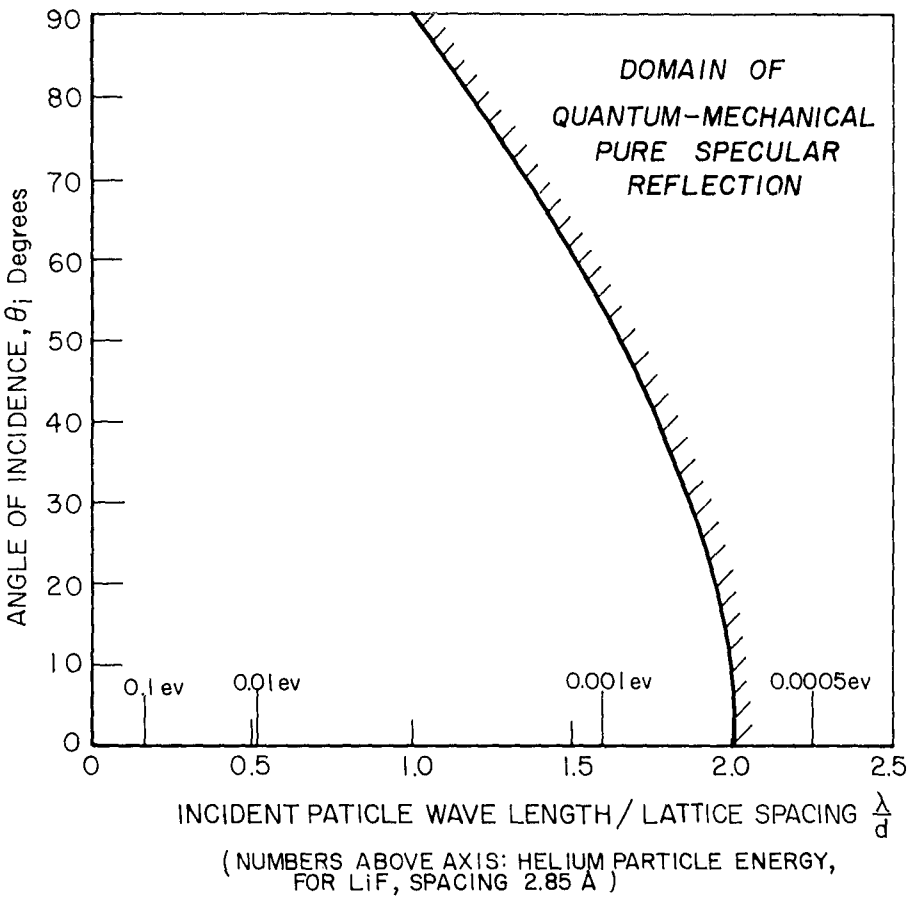

Figure 47 Specular Reflection By Quantum-Mechanical Solution.

VIII. IMPROVEMENT OF CRYOPUMP (J.G. Everton)

The cryopump of the USC Low-Density Wind Tunnel in its original form was described in Ref. 1. Its operating characteristics are shown in Table I. From these data several things became apparent regarding

TABLE I

CHARACTERISTICS OF ORIGINAL CRYOPUMP

MINIMUM CONDENSING SURFACE TEMPERATURE	20°K
MINIMUM CRYOPUMP PRESSURE	5×10^{-6} mm Hg
MINIMUM TANK PRESSURE	5×10^{-5} mm Hg
MAXIMUM CRYOPUMP CONDENSING LOAD	106 watts
MAXIMUM VOLUME FLOW INSIDE CRYOPUMP	133,000 liters/sec.
MAXIMUM VOLUME FLOW THROUGH CRYOPUMP VALVE	25,000 liters/sec.
TANK PRESSURE WITH MAXIMUM VOLUME FLOW	5.3×10^{-3} mm Hg

the cryopump. First, since the vapor pressure of nitrogen at 20°K is several decades below the minimum pressure listed, this pressure would represent the contribution of the noncondensable gases present (hydrogen, helium, neon) plus the small load imposed by outgassing. Second, the amount of usable condensing power was less than 30 percent of the total power available, indicating excessive radiation losses and a severe limitation on total pumping capacity. Third, the low volume flow through the valve imposed critical limitations from the standpoint of mass flow

versus desired tank pressure. The third limitation was further complicated by an unexpected, and as yet not fully understood, characteristic in the operation of the valve. It was found that when the valve was closed partially in order to throttle the flow and increase the pressure in the tank test section (and, incidentally, decrease the radiation loss through the valve), instead of the cryopump pressure decreasing, as might be expected intuitively, it actually increased in an apparent effort to follow the increasing tank pressure. This increase in cryopump pressure naturally gave rise to an increase in free-convection heat transfer which was accompanied by a readjustment of the temperature distribution on the radiation shields.

In order to circumvent the above listed limitations so as to achieve the full potential of the basic refrigeration system, a number of modifications have been effected. These consist principally of increasing the valve opening area leading to the cryopump and replacing the dry radiation shields with liquid nitrogen cooled shields. The new arrangement is shown in Fig. 48. The condenser plates are surrounded by a cylindrical liquid nitrogen (LIN) shield, a bottom shield and a top shield which is attached to the valve. When the valve is open it is obvious that the condensing surfaces are able to "see" the warm walls of the main wind-tunnel tank. However, the geometry of the entire setup makes it extremely difficult to accomplish complete optically dense shielding of the condenser. An approximate calculation of the radiation load entering through the open valve indicated values that were considered tolerable.

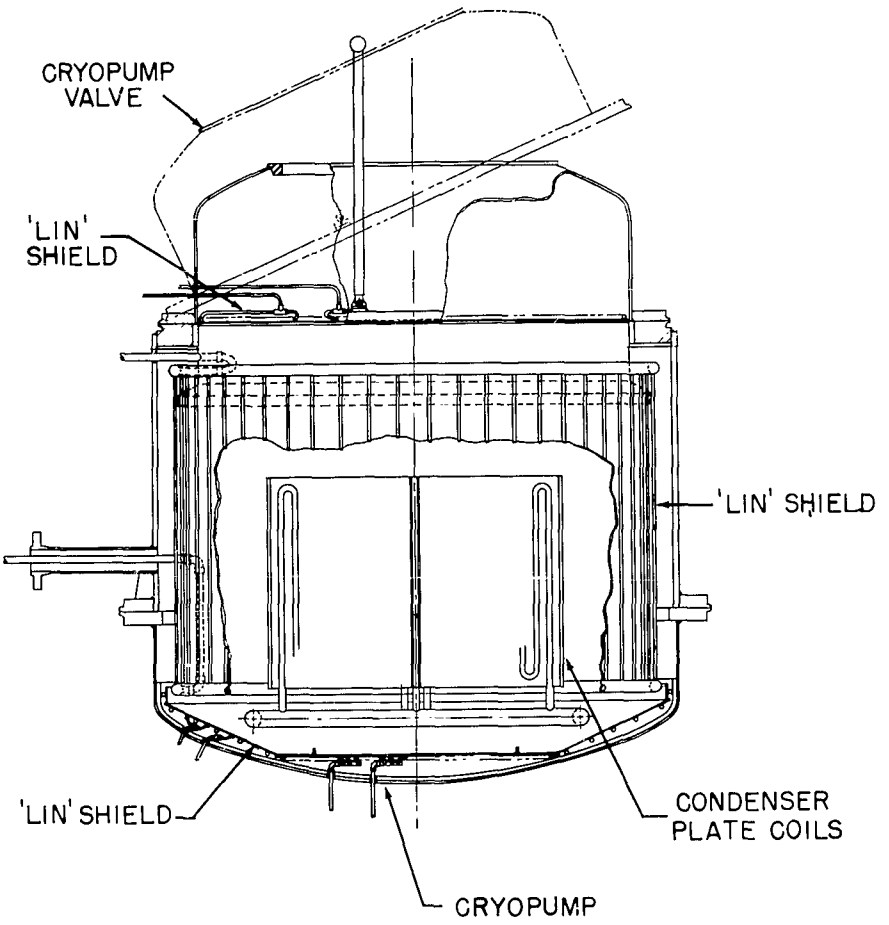

Figure 48 Schematic Drawing Of The Modified Cryopump.

Different surface treatments were given the entire radiation shielding array so as to establish the optimum as far as radiant load on the condenser was concerned. The results are shown in Fig. 49, from which it is seen that a high emissivity resulted in the least radiant load, since this reduced substantially the reflected radiation from the 300°K tunnel walls. In addition, to minimize the liquid nitrogen consumption, superinsulation (consisting of alternate layers of aluminum foil and fiber glass, totaling 30 layers) has been wrapped around the outside of the shield to reduce the radiant load from the 300°K external wall to the 80°K shield.

Table II shows some of the typical operation of the pump subsequent to modification. The values listed under "valve opening"

TABLE II
TYPICAL OPERATIONS OF MODIFIED CRYOPUMP

No.	VALVE OPENING	$\dot{m}$ gm/sec	$T_{C.P.}$ °K	$P_{C.P.}$ mm Hg	P_{TANK} mm Hg	$\dot{V}_{C.P.}$ ℓ/sec	$\dot{V}_{VALVE}$ ℓ/sec	W watts
1	.25	.286	26.5	9.6×10^{-4}	3×10^{-3}	194,000	62,000	152
2	.50	.286	28.5	7.4×10^{-4}	1.8×10^{-3}	251,000	99,000	152
3	.50	.397	29.5	9.2×10^{-4}	2.4×10^{-3}	281,000	111,000	211
4	.50	.467	—	9.3×10^{-4}	2.65×10^{-3}	326,000	115,000	248
5	1.0	.467	31.5	9.0×10^{-4}	2.1×10^{-3}	338,000	145,000	248
6	.75	.575	31	1.1×10^{-3}	2.75×10^{-3}	340,000	136,000	306
7	0	.80	31	—	—	—	—	426

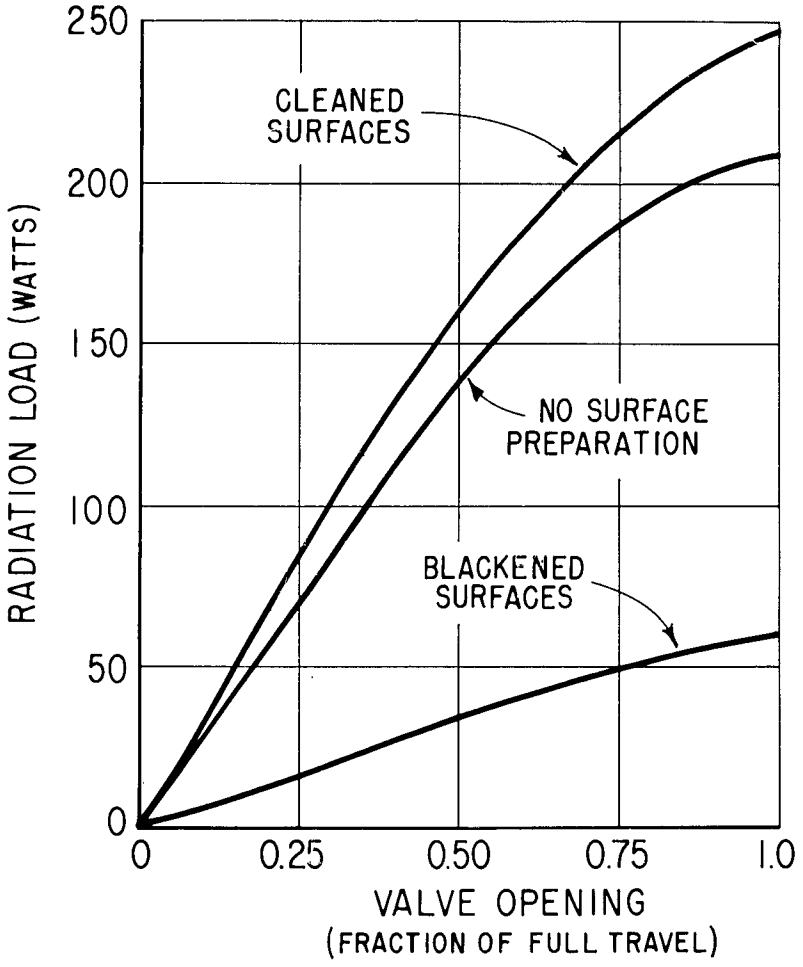

RADIATION LOSSES BEFORE AND AFTER BLACKENING INSIDE SURFACES OF THE 'LIN' COOLED SHIELDS

Figure 49 Losses Through Cryopump Valve.

represent the fraction of full travel of the valve. The first two examples given in Table II illustrate quite clearly the characteristic of $P_{C.P.}$ decreasing with increasing valve opening at constant mass flow.

The values listed for the volume flows were calculated using cryopump shell pressure for $\dot{V}_{C.P.}$ and test-section static pressure for $\dot{V}_{valve}$. Effective refrigeration, W, was calculated using the formula taken from Ref. 47:

$$W = 4.18\, C_p \dot{m} \Delta T + 4.18\, H_c \dot{m}$$

where W = condensing load (watts)

C_p = specific heat (0.25)

$\dot{m}$ = mass flow of N_2 (gms/sec)

ΔT = stagnation temperature—condenser temperature

H_c = heat of condensation (60 cal/gm, Ref. 47)

It should be mentioned that some fraction of the calculated condensing load is undoubtedly the contribution of precooling of the gas by the LIN-cooled shields. The effectiveness of this precooling, however, is not felt to be too good in the present configuration.

Further description of the modified cryopump and its operation may be found in Ref. 48.

REFERENCES

1. Chuan, R.L., "Research on Rarefied Gasdynamics," USCEC Report 56-101, AFOSR-22, November 1960.

2. Lees, L., J. Aeronaut. Sci., Vol. 23, pp. 594-600, 1956.

3. Li, T.Y. and H.T. Nagamatsu, J. Aeronaut. Sci., Vol. 20, pp. 345-355, 1953.

4. Nagakura, T. and H. Naruse, J. Phys. Soc. Japan, Vol. 12, pp. 1298-1304, 1957.

5. Oguchi, H., "The Sharp Leading Edge Problem in Hypersonic Flow," Rarefied Gas Dynamics (edited by L. Talbot), Academic Press, New York, 1961, pp. 501-524.

6. Charwat, A.F., "Molecular Flow Study of the Hypersonic Sharp Leading Edge Interaction," Rarefied Gas Dynamics (edited by L. Talbot), Academic Press, New York, 1961, pp. 553-578.

7. Yang, H.T. (University of Southern California, Engineering Center, report in preparation).

8. Chuan, R.L. and S.A. Waiter, "Experimental Study of Hypersonic Rarefied Flow Near the Leading Edge of a Thin Flat Plate," in Proceedings of Third International Symposium on Rarefied Gas Dynamics (edited by J.A. Laurmann), Academic Press, New York, 1963 (to be published).

9. Pass, H.R., "Semi-Automatic McLeod Gauge," USCEC Report 56-211, AFOSR TN 60-399, March 1960.

10. Smetana, F.O., "A Semi-Empirical Description of the Discharge Characteristics of the Converging Section of a Low Density Hypersonic Nozzle," J. Aeronaut. Sci., Vol. 28, No. 12, p. 988, 1961.

11. Liepmann, H.W., "Gas Kinetics and Gasdynamics of Orifice Flow," J. Fluid Mech., Vol. 10, pp. 65-79, 1961.

12. Smetana, F.O., "A Study of the Flow Through a Convergent-Divergent Nozzle Throughout the Range in Characteristic Gas Behavior from Near Molecule to Continuum," ASME Joint National Conference, Los Angeles, California, March 1963.

13. Flanick, A.P. and J. Ainsworth, "A Thermistor Pressure Gauge," NACA TN-D-504, November 1960.

14. Martin, D.E., "A Study of Laminar Compressible Viscous Pipe Flow Accelerated by a Body Force, with Application to Magneto-gasdynamics," NASA TN-D-855, April 1961.

15. Williams, J.C., "A Study of Compressible and Incompressible Viscous Flow in Slender Channels," Ph.D. Thesis, University of Southern California, June 1962.

16. Williams, J.C., "A Study of Compressible and Incompressible Viscous Flow in Slender Channels," USCEC Report 83-213, June 1962.

17. Williams, J.C., "Viscous Compressible and Incompressible Flow in Slender Channels," J. Aeronaut. Sci., Vol. 30, No. 1, 1963.

18. Millsaps, Knox and Karl Pohlhausen, "Thermal Distribution in Jeffery-Hamel Flows Between Nonparallel Plane Walls," J. Aeronaut. Sci., Vol. 20, No. 3, pp. 187-196, 1953.

19. Lees, L., "A Kinetic Theory Description of Rarefied Gas Flow," GALCIT Hypersonic Research Project, Memorandum No. 51, December 1959.

20. Vali, W. and G.M. Thomas, "Resonance Scattering Technique for Low Density Experiments," ARS Journal, Vol. 32, No. 7, pp. 1114-1115, July 1962.

21. Grad, H., "The Profile of a Steady, Plane Shock Wave," Communs. Pure and Appl. Math., Vol. 5, No. 3, pp. 257-300, August 1952.

22. Grad, H., "Principles of the Kinetic Theory of Gases," Encyclopedia of Physics, Springer-Verlag, 1958, Vol. 12, pp. 205-294.

23. Sirovich, L., "The Initial Problem, Sound Propagation and Modeling in Kinetic Theory," AFOSR-1380, MF-17, Mathematical Sciences, New York University, September 1961.

24. Sirovich, L., Private Communications.

25. Minorsky, N., "Nonlinear Oscillations," D. Van Nostrand Company, Inc., Princeton, New Jersey, 1962, pp. 124-127.

26. Koga, T., "On Transport Process in a Plasma (Kinetic Equations for a Plasma)," USCEC Report 83-209, AFOSR-1744, October 1961.

27. Koga, T., "The Criterion of Rarefaction of Plasmas," USCEC Report 83-212, AFOSR-2361, March 1962.

28. Koga, T., "Kinetic Equations for Plasmas," Phys. Fluids, Vol. 5, No. 6, pp. 705-711, June 1962.

29. Koga, T., "The Generalized Validity of the Boltzmann Equations for Ionized Gases," in Proceedings of Third International Symposium on Rarefied Gas Dynamics (edited by J. A. Laurmann), Academic Press, New York, 1963 (to be published).

30. Koga, T., "Multiplicity of Particle Interactions in Plasmas," Phys. Fluids (to be published).

31. Koga, T., "Interaction Between a Radio Wave and a Plasma in the Presence of a Uniform Magnetic Field," USCEC Report 83-204, AFOSR 283, January 1961.

32. Koga, T., "A Radio Wave in a Plasma in a Uniform Magnetic Field," Proceedings of the 5th International Conference on Ionization Phenomena in Gases, North Holland Publishing Co., Amsterdam, 1962, Vol. 1, pp. 507-516.

33. Oshima, K., S. A. Waiter and T. Koga, "Propagation of Microwave Through a Plasma in the Presence of a Magnetic Field, Theory and Experiments," Plasma Sheath Symposium, Boston, Mass., April 1962.

34. Oshima, K., "Self-Similar and Pseudosimilar Solutions of Blast Waves in Electrogasdynamics," USCEC Report 83-215, August 1962.

35. Smetana, F. O., "On the Current Collected by a Charged Circular Cylinder Immersed in Two-Dimensional Rarefied, Plasma Stream," in Proceedings of Third International Symposium on Rarefied Gas Dynamics (edited by J. A. Laurmann), Academic Press, New York, 1963 (to be published).

36. Oshima, K., "Measurements of Plasma Flow in a Magnetic Field with Microwave Systems," USCEC Report 93-204, December 1962.

37. Oshima, Y., "First Order Approximation of Electrogasdynamic Blast Wave, Calculation and Preliminary Experiments," USCEC Report 93-202, October 1962.

38. Brown, Sanborn C., "High-Frequency Gas-Discharge Breakdown," MIT Research Laboratory of Electronics, TR-301, July 1955.

39. Scharfman, W.E. and T. Morita, "Voltage Breakdown of Antennas at High Altitudes," AFCRC-TN-60-750, 1960.

40. Francis, Gordon, "Ionization Phenomena in Gases," Butterworths Scientific Publications, London, 1960.

41. Hatch, A.J. and H.B. Williams, "The Secondary Electron Resonance Mechanism of Low-Pressure High-Frequency Gas Breakdown," J. Appl. Mech., Vol.25, p.417, 1954.

42. Francis, G. and A. von Engel, "The Growth of the High Frequency Electrodeless Discharge," Phil. Trans. Roy. Soc. London, Vol.A246, p.143, 1953.

43. Krebs, K. and H. Meerbach, "Die Pendelvervielfachung von Schundarelektronen," Vol.15, p.189, 1955.

44. Redhead, P.A., "The Townsend Discharge in a Coaxial Diode with Axial Magnetic Field," Can. J. Phys., Vol.36, p.255, 1958.

45. Hobson, J.P. and P.A. Redhead, "Operation of an Inverted-Magnetron Gage in the Pressure Range 10^{-3} to 10^{-12} mm Hg," Can. J. Phys., Vol.36, p.271, 1958.

46. Massey, H.S.W. and E.H.S. Burhop, "Electronic and Ionic Impact Phenomena," Oxford at the Clarendon Press, 1952, pp.606-608.

47. Chuan, Raymond L., "A Study of the Condensation of Nitrogen Below the Triple Point," USCEC Report 56-201, AFOSR TN 57-19 AD-115 052, February 1957.

48. Everton, J.G., "Operational Characteristics of a Cryopump Used in a Low-Density Wind Tunnel," Paper presented at Ninth National Vacuum Symposium, American Vacuum Society, at Los Angeles, Calif., October-November 1962.

APPENDIX I

A. REPORTS ISSUED UNDER CONTRACT AF 49(638)-831

"The Structure of Strong Shock Waves of Stable Monatomic Molecules"

October 1960 — USCEC Report 83-201
Toyoki Koga — AFOSR TN 60-1344

"Interaction Between a Plasma and a Microwave"

November 1960 — USCEC Report 83-202
Toyoki Koga — AFOSR TN-3

"A Method of Analyzing the Boltzmann Equation of Electrons and Its Application to Plane Oscillations of Electrons in a Warm Plasma"

December 1960 — USCEC Report 83-203
Toyoki Koga — AFOSR 74

"Interaction Between a Radio Wave and a Plasma in the Presence of a Uniform Magnetic Field"

January 1961 — USCEC Report 83-204
Toyoki Koga — AFOSR 283

Supplement I - USCEC Report 83-204

July 1961
Toyoki Koga

"Experiments in Cryopumping CO_2"

March 1961 — USCEC Report 83-205
Raymond W. Moore, Jr. — AFOSR 561
Arthur D. Little, Inc.
Cambridge 42, Mass.
(Work performed while on temporary leave to USCEC in 1959)

"An Elastic Collision Model for the Kinetic Theory of Gases"

June 1961 — USCEC Report 83-206
Toyoki Koga — AFOSR 823

"Electric Conductivity of a High Temperature Plasma to a Radio Wave"

July 1961 — USCEC Report 83-207
Toyoki Koga — AFOSR 1184

"Microwave Measurements of Plasma Flow in a Supersonic Wind Tunnel"

September 1961 — USCEC Report 83-208
Koichi Oshima — AFOSR 1556

"On Transport Processes in a Plasma (Kinetic Equation for a Plasma)"

October 1961 — USCEC Report 83-209
Toyoki Koga — AFOSR 1744

"The Distribution of Charged Particles Near a Charged Spherical Body in Motion"

November 1961 — USCEC Report 83-210
Toyoki Koga — AFOSR 1870

"Pressure Lag Through Orifices and Short Tubes for Small Pressure Ratios and Flow Conditions from Free Molecule to Continuum"

January 1962 — USCEC Report 83-211
J.G. Everton — AFOSR 2360
F.O. Smetana

"The Criterion of Rarefaction of Plasmas"

March 1962 — USCEC Report 83-212
Toyoki Koga — AFOSR 2361

"A Study of Compressible and Incompressible Viscous Flow in Slender Channels"

June 1962 — USCEC Report 83-213
James C. Williams III

"A Calibration Facility for High Resolution Vacuum Gauges"

July 1962 — USCEC Report 83-214
Frederick O. Smetana
J. G. Everton

"Self-Similar and Pseudosimilar Solutions of Blast Waves in Electric Gasdynamics"

August 1962 — USCEC Report 83-215
Koichi Oshima

"Kinetic Equations for Plasmas"

June 1962 — USCEC Report 83-216
Toyoki Koga — AFOSR 2006

B. PUBLICATIONS IN JOURNALS AND PAPERS PRESENTED AT MEETINGS

Koga, Toyoki, "The Boltzmann-Maxwell Equation as the Fundamental Equations of Gas Dynamics," Rarefied Gasdynamics, Pergamon Press, London, 1960, p. 151.

Chuan, Raymond L., "USC Low-Density Wind Tunnel," Vacuum Facilities Conferences, University of Southern California, Los Angeles 7, Calif., April 22, 1960.

Chuan, Raymond L., "Selected Lectures on Plasma Physics," Rarefied Gasdynamics and Wind-Tunnel Technology, Two-Part Lecture at Ballistic Research Laboratories, Aberdeen Proving Ground, Maryland, September 1960.

Chuan, Raymond L., "Recent Developments in Rarefied Gasdynamics," Japan National Congress of Theoretical and Applied Mechanics, Tokyo, Japan, September 1960.

Chuan, Raymond L., "Research in Plasma Dynamics," Japan Institute of Aero-Space Sciences, Tokyo, Japan, September 1960.

Chuan, Raymond L., "Research in Rarefied Gasdynamics at USCEC," Japan National Aeronautical Laboratory, Tokyo, Japan, September 1960.

Chuan, Raymond L., "Cryopumping Applied to Low-Density Wind Tunnels," Conferences on Low-Pressure Facilities, London, England, October 1960.

Koga, Toyoki, "Conductivity of a Plasma to High Frequency Electric Fields," Second Annual Meeting of Plasma Physics, Division of American Physical Society, Gatlinburg, Tenn., November 1960.

Chuan, Raymond L. and Donald A. Wallace, "Present Status of Cryopumping," USCEC Memorandum Number 1, University of Southern California, Los Angeles 7, California, November 1961.

Smetana, Frederick O., "Measurement of Electron Density in Rarefied Gas Streams by Microwave Interferometry," American Physical Society Meeting, Johns Hopkins University, New York, N.Y., November 21, 1960.

Yang, Hsun-Tiao, "Low Speed Plane Couette Flow of a Rarefied Conducting Gas in a Uniform Transverse Magnetic Field," American Rocket Society, Washington, D.C., Preprint No. 1457-60, December 1960.

Yang, Hsun-Tiao, "Magnetogasdynamics of Low-Speed Rarefied Couette Flow," Department of Mechanical Engineering, Rice University, Houston, Texas, December 16, 1960.

Chuan, Raymond L., "RF Plasma Heating of Wind-Tunnel Flow," AD Hoc Committee on High Temperature Wind Tunnels, Scientific Advisory Board, Headquarters, USAF, December28, 1960.

Chuan, Raymond L., "Heating of Supersonic Stream by Radio Frequency Discharge," Japan Society for Aeronautical and Space Engineering, Tokyo, Japan, Vol. 9, No. 92, pp. 282-284, 1961.

Chuan, Raymond L., "Microwave-Plasma Interaction," Seminar at Thermodynamic Division, National Bureau of Standards, Washington, D.C., April 1961.

Chuan, Raymond L., "Review of Research in Rarefied Gasdynamics and Plasma Physics at USCEC," Fourth AFOSR Contractors' Meeting in Hypersonic Flows and Aerophysics, University of Toronto, Toronto, Canada, June 7-9, 1961.

Chuan, Raymond L., Donald Wallace, Kenneth Rogers and J.G. Everton, "The Cryopump First and Second Generation: A Report on the Operational History of the University of Southern California Cryopump and the Design of a New Facility," Second Annual Symposium on Space Vacuum Simulation, Arthur D. Little, Inc., Cambridge, Mass., June 16, 1961.

Chuan, Raymond L., "Laboratory Experimental Techniques," Hypervelocity Flight in the Upper Atmosphere, University of California at Los Angeles, Engineering Extension, March 6-July 15, 1961.

Koga, Toyoki, "Transport Phenomena in a Fully Ionized Gas Confined in a Strong Magnetic Field," Phys. Fluids, Vol. 4, No. 7, July 1961.

Koga, Toyoki, Paul Wilber and J.G. Everton, "Electron-Heavy Particle Collision Model in a Plasma," Phys. Fluids, Vol. 4, No. 8, pp. 105-107, August 1961.

Koga, Toyoki, "A Radio Wave in a Plasma in a Uniform Magnetic Field," Proceedings Fifth International Conference on Ionization Phenomena in Gases, Munich, 1961, North-Holland Publishing Company, Amsterdam, Vol. 1, p. 507.

Chuan, Raymond L., "The Current Equation for a Partially Ionized Gas," Seminar, Mechanical Engineering Department, Illinois Institute of Technology, Chicago, Illinois, October 1961.

Koga, Toyoki, "Interaction Between a Radio Wave and a Plasma," Phys. Fluids, Vol. 4, No. 9, pp. 1162-1166, September 1961.

Oshima, Koichi, "Blast Waves Produced by Exploding Wires," Conference on Exploding Wires, Geophysics Research Directorate, Air Force Cambridge Research Laboratories, Boston, Mass., November 13-14, 1961; Plenum Press Inc., New York, Vol. 2, 1962, pp. 159-174.

Koga, Toyoki, "On Transport Processes in Fully Ionized Gases," 3rd Annual Meeting of Plasma Physics Division, Applied Physical Society, Colorado Springs, Colorado, November 15-18, 1961.

Williams, James C. III, Raymond L. Chuan, F. O. Smetana and P. C. Wilber, "Plasma Heating of Supersonic Gas Stream," Symposium on Plasma Jet Technology, Annual Winter Meeting, New York City, November 26 - December 1, 1961.

Chuan, Raymond L., "Review of USCEC Work in Microwave-Plasma Interaction," ONR Contractors Conference, Washington, D.C., December 1961.

Oshima, K., S.A. Waiter and T. Koga, "Propagation of Microwave Through a Plasma in the Presence of a Magnetic Field Theory and Experiments," Plasma Sheath Symposium, Boston, Mass., April 10-12, 1962.

Chuan, Raymond L., "Heat Addition to Supersonic Flow by Radio Frequency Discharge," Seminar, North Carolina State College, Raleigh, N.C., April 27, 1962.

Smetana, Frederick O., "Comment on Comparison of Flow-Direction Probes at Supersonic Speeds," J. Aeronaut. Sci., Vol. 29, No. 5, pp. 625-626, May 1962.

Koga, Toyoki, "Kinetic Equations for Plasmas," Phys. Fluids, Vol. 5, No. 6, pp. 705-711, June 1962.

Chuan, Raymond L. and Serge A. Waiter, "Experimental Study of Hypersonic Rarefied Flow Near the Leading Edge of a Thin Flat Plate," 3rd International Symposium, Rarefied Gas Dynamics, University of Paris, June 26-30, 1962.

Koga, Toyoki, "The Generalized Validity of the Boltzmann Equation for Ionized Gases," 3rd International Symposium, Rarefied Gas Dynamics, University of Paris, June 26-30, 1962; Academic Press, 1963 (edited by J.A. Laurmann), to be published.

Smetana, Frederick O., "On the Current Collected by a Charged Circular Cylinder Immersed in Two-Dimensional Rarefied Plasma Stream," 3rd International Symposium, Rarefied Gas Dynamics, University of Paris, June 26-30, 1962.

Chuan, Raymond L. and James C. Williams III, "Heat Addition to Supersonic Flow by Radio Frequency Discharge," Ninth International Symposium on Combustion, The Combustion Institute, Cornell University, Ithaca, N.Y., August 27-September 1, 1962.

Everton, J.G., "Operational Characteristics of a Cryopump Used in a Low-Density Wind Tunnel," American Vacuum Society, 9th National Vacuum Symposium, Statler Hilton Hotel, Los Angeles, California, October 31-November 1, 1962.

Smetana, Frederick O., "On the Prediction of Gas Flow Rates Through Round Wire Screens," Transactions to the ASME, Paper No. 62 WA 66, Winter Annual Meeting, New York, The American Society of Mechanical Engineers, November 25-30, 1962.

Yang, H.T., "Moment Equations and Boundary Conditions for Magneto-Gas-Dynamics," Phys. Fluids, Vol. 5, No. 12, December 1962.

Koga, Toyoki, "Interaction Between a Radio Wave and a High Temperature Plasma," Phys. Fluids, Vol. 5, No. 12, December 1962.

Williams, James C. III, "Viscous Compressible and Incompressible Flow in Slender Channels," J. Aerospace Sci., Vol. 30, No. 1, 1963.